New Solution Methods for Fractional Order Systems

A Thesis
Submitted for the Degree of
Doctor of Philosophy
in the Faculty of Engineering

By
Satwinder Jit Singh

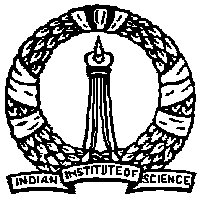

Department of Mechanical Engineering
Indian Institute of Science
Bangalore - 560 012
India

November 2007

Abstract

This thesis deals with developing Galerkin based solution strategies for several important classes of differential equations involving derivatives and integrals of various fractional orders. Fractional order calculus finds use in several areas of science and engineering. The use of fractional derivatives may arise purely from the mathematical viewpoint, as in controller design, or it may arise from the underlying physics of the material, as in the damping behavior of viscoelastic materials. The physical origins of the fractional damping motivated us to study viscoelastic behavior of disordered materials at three levels. At the first level, we review two first principles models of rubber viscoelasticity. This leads us to study, at the next two levels, two simple disordered systems. The study of these two simplified systems prompted us towards an infinite dimensional system which is mathematically equivalent to a fractional order derivative or integral. This infinite dimensional system forms the starting point for our Galerkin projection based approximation scheme.

In a simplified study of disordered viscoelastic materials, we show that the networks of springs and dash-pots can lead to fractional power law relaxation if the damping coefficients of the dash-pots follow a certain type of random distribution. Similar results are obtained when we consider a more simplified model, which involves a random system coefficient matrix.

Fractional order derivatives and integrals are infinite dimensional operators and non-local in time: the history of the state variable is needed to evaluate such operators.

This non-local nature leads to expensive long-time computations ($\mathcal{O}(t^2)$ computations for solution up to time t). A finite dimensional approximation of the fractional order derivative can alleviate this problem. We present one such approximation using a Galerkin projection. The original infinite dimensional system is replaced with an equivalent infinite dimensional system involving a partial differential equation (PDE). The Galerkin projection reduces the PDE to a finite system of ODEs. These ODEs can be solved cheaply ($\mathcal{O}(t)$ computations). The shape functions used for the Galerkin projection are important, and given attention. Calculations with both global shape functions as well as finite elements are presented. The discretization strategy is improved in a few steps until, finally, very good performance is obtained over a user-specifiable frequency range (not including zero). In particular, numerical examples are presented showing good performance for frequencies varying over more than 7 orders of magnitude. For any discretization held fixed, however, errors will be significant at sufficiently low or high frequencies. We discuss why such asymptotics may not significantly impact the engineering utility of the method.

Following this, we identify eight important classes of fractional differential equations (FDEs) and fractional integrodifferential equations (FIEs), and develop separate Galerkin based solution strategies for each of them. Distinction between these classes arises from the fact that both Riemann-Liouville as well as Caputo type derivatives used in this work *do not*, in general, follow either the law of exponents or the commutative property. Criteria used to identify these classes include; the initial conditions used, order of the highest derivative, integer or fractional order highest derivative, single or multiterm fractional derivatives and integrals. A key feature of our approximation scheme is the development of differential algebraic equations (DAEs) when the highest order derivative is fractional or the equation involves fractional integrals only. To demonstrate the effectiveness of our approximation scheme, we compare the numerical results with analytical solutions, when available, or with suitably developed series solutions. Our approximation scheme matches analytical/series solutions very well for all classes considered.

Acknowledgements

I am deeply indebted to my advisor Prof. Anindya Chatterjee, who is also a very good friend, for his comprehensive guidance throughout this doctoral work.

I sincerely thank my lab-mates, gym-partners, and other friends for providing enjoyable company.

I thank M. Pradeep for helping me with some of the calculations in Chapter 3.

Contents

List of Figures

Chapter 1

Introduction

Fractional order derivatives and integrals appear in many areas of science and engineering [1]. The viscoelastic behavior of rubber like materials is modeled using fractional order derivatives [2–10]. Fractional calculus is used in control of dynamical systems [11–15]. Some problems in fluid mechanics are also modeled using fractional calculus [2, 10, 16, 17]. Koh *et al.* [18] have suggested applications of fractional derivatives for earthquake engineering and structural dynamics. Fractional calculus also finds applications in electrical and electronics engineering [19]. Use of fractional calculus is reported in the physics literature as well, see for example [20, 21].

The content of this thesis may be divided into three parts. The first part deals with the viscoelastic behavior of rubber like disordered viscoelastic materials. In the second part of this thesis, we develop a Galerkin projection based finite dimensional approximation scheme for fractional order derivatives and integrals. The third part deals with the development of Galerkin based solution strategies for fractional differential equations (FDEs) and fractional integrodifferential equations (FIEs), and solutions of some important classes of FDEs and FIEs. These three parts are described in slightly greater detail below.

1.1 Part One

Part one of this thesis consists of Chapters 2 to 4. Observed fractional power law dominated relaxation of rubber like viscoelastic materials prompts the use of fractional order derivative damping models in the dynamical modeling of such materials. In this part of the thesis we will study the origins of this power law relaxation at three levels. At the first level, we describe two existing models of rubber viscoelasticity and view the fractional order power law relaxation behavior as a macroscopic manifestation of many parallel random microscopic processes in random networks of chains. At the second level, we study some simplified systems consisting of networks of springs and dash-pots. The dash-pots will be assumed to have randomly distributed damping coefficients. Analytical results are obtained for a particularly simple 1-D random viscoelastic chain mode. At the third level, we will further simplify the system by assuming a random system coefficient matrix. The system studied here motivates a key step in developing the numerical approximation that follows in the remainder of the thesis.

1.2 Part Two

Part two of this thesis consists of Chapters 5 to 6. Systems with fractional derivatives and integrals are infinite dimensional. A fractional derivative of order α between 0 and 1 given by the Riemann-Liouville definition [47, 48] is

$$\mathrm{D}^{\alpha}[x(t)] = \frac{1}{\Gamma(1-\alpha)}\frac{d}{dt}\left[\int_0^t \frac{x(\tau)}{(t-\tau)^{\alpha}}d\tau\right],$$

and a fractional integral of order α between 0 and 1 is given by

$$\mathrm{I}^{\alpha}[x(t)] = \frac{1}{\Gamma(\alpha)}\int_0^t \frac{x(\tau)}{(t-\tau)^{1-\alpha}}d\tau.$$

The above definitions of the fractional derivative as well as integral involve convolution integrals; these systems are non-local in time. Evaluation of such operators at time t requires the entire history of the function in the time interval $[0, t]$, which leads to increased computational costs. For example the method used in [22] requires $\mathcal{O}(t^2)$ computational cost for a numerical simulation upto time t. A finite dimensional approximation of such operators can reduce the cost of computations.

In the second part of this thesis we will develop a finite dimensional approximation for these operators. Our discretization scheme involves:

- Identifying an infinite dimensional system (IDS) which is equivalent to a fractional derivative or integral.
- Applying Galerkin projections to the partial differential equation involved in the IDS.
- Obtaining a finite set of ordinary differential equation (ODEs) from Galerkin projections, which approximate the fractional order operator.

Our Galerkin projection based approximation scheme replaces an infinite dimensional non-local system with a *finite dimensional* and *local* system. This approximation scheme shows a large reduction in computational costs; $\mathcal{O}(t^2)$ computational cost of the method used in [22] is reduced to $\mathcal{O}(t)$. At the same time this approximation scheme is accurate. Good performance of this approximation scheme can be obtained on a user specifiable frequency range, as will be discussed in detail.

1.3 Part Three

Part three of this thesis consists of Chapters 7 to 9. In the third part of this thesis we develop strategies for accurately solving some useful classes of fractional integral/differential equations using our Galerkin projection based approximation scheme. The classes of problems considered in this paper are listed in Section 1.5.

We will compare results of numerical solutions obtained using our methods with analytical closed form or series solutions to demonstrate the effectiveness of the proposed approach.

1.4 Layout of the Thesis

Chapter 2 presents a summary of some existing theoretical treatments in the literature, aimed at understanding why a power law stress relaxation is observed in rubber. The contributions of this thesis begin from Chapter 3.

Chapters 3 and 4 deal with the relaxation (transient unforced response) of systems whose mathematical models involve random matrices. In Chapter 3 we will study 1-D chains and 2-D networks of springs and random dashpots. Chapter 4 deals with a further simplified model (from the literature) where the system coefficient matrix is random, with no reference to underlying springs or dashpots. In both cases, power law relaxation is observed. The aim of these two chapters is to provide a bridge between the theoretical rubber models of Chapter 2 and the subsequent numerical solutions. The random systems studied in Chapters 3 and 4 eventually motivate the Galerkin procedure developed in subsequent chapters.

In Chapters 5 and 6 we develop a Galerkin projection based approximation scheme for fractional order derivatives. Chapter 5 deals with identifying an infinite dimensional system which is equivalent to the fractional order derivative. This infinite dimensional system involves a partial differential equation (PDE). A Galerkin projection is applied to this PDE to get a finite set of ordinary differential equations (ODEs), hence replacing a fractional order derivative with a finite set of ODEs. In Chapter 5, global shape functions are used for the Galerkin projection procedure. Finite elements are used for the Galerkin projection procedure in Chapter 6. The scheme improves in a few steps to finally give very good performance.

Chapters 7, 8 and 9 deal with using the Galerkin projection based approximation scheme to solve some useful FDEs and FIEs. In Chapter 7, we solve three classes of FDEs with fractional order derivative terms of order between 0 and 1, with the system assumed to start from rest in all cases. Chapter 8 is an extension of applications of the Galerkin approximation scheme, where we solve a broader class of possibly-nonlinear multiterm fractional integrodifferential equations (FIEs) with *nonzero* initial conditions. A key new idea here is the use of differential algebraic equations (DAEs), which are subsequently solved using commercially available Matlab routines. Chapter 9 is a further extension of the work of Chapters 7 and 8, where we solve higher order FDEs and FIEs with *nonzero*

initial conditions, and the order of the fractional derivative is now arbitrary.

Chapter 10 presents some concluding remarks.

1.5 List of FDEs and FIEs Solved in this Thesis

Several classes of FDEs and FIEs are considered in this thesis. The differences between these classes are nontrivial, because of essentially the fact that both Riemann-Louville as well as Caputo type derivatives used in this work *do not*, in general, follow either the law of exponents or the commutative property [23, 24, 25].

To help the reader navigate through the different problems solved numerically (and analytically) in this thesis, a list of these problems is supplied here.

1. Class one consists of second order FDEs with a fractional damping term of order between 0 and 1; zero initial conditions are considered. Such problems arise in the mathematical modeling of viscoelastic materials. Chapter 5 deals with solving this class of problems, linear as well as nonlinear. In particular, we solve

$$\mathrm{D}^2 x(t) + \mathrm{D}^{1/2} x(t) - x(t) + x(t)^3 = \sin(2\pi t),$$

   with $x(t) \equiv 0$ for $t \leq 0$ and $\dot{x}(0) = 0$ as a nonlinear example.

2. Class two consists of FDEs involving a fractional damping term of order between 0 and 1; zero initial conditions are assumed. The order of the FDE is more than 2. Chapter 7 deals with this class of problems. We consider steady state solutions of an infinite beam on an elastic, fractionally damped, foundation, under the action of a moving point load. Specifically, we seek steady state solutions of

$$u_{xxxx} + \frac{\bar{m}}{EI} u_{tt} + \frac{c}{EI} \mathrm{D}_t^{1/2} u + \frac{k}{EI} u = -\frac{1}{EI} \delta(x - vt)\,,$$

   The boundary conditions of interest are $u(\pm\infty) \equiv 0$.

3. Class three consists of a first order FDE with fractional derivative term of order between 0 and 1; zero initial conditions are assumed in this case also. Such FDEs

arise for example in the modeling of a sphere falling through a viscous liquid. The generalized Basset's problem of the following form is solved in Chapter 7.

$$\dot{v}(t) + \mathrm{D}^{\alpha} v(t) + v(t) = 1\,, \quad v(0) = 0 \quad \text{and} \quad 0 < \alpha < 1.$$

4. Class four consists of FDEs where the highest order derivative is fractional. Order of the derivative is taken between 0 and 1; the system starts from zero initial conditions. Our usual Galerkin method will not work here, because $\dot{x}(t)$ is required as an input to evaluate the fractional derivative. Here, we use a strategy for the adaptation of the Galerkin method through constraints that lead to differential algebraic equations (DAEs). Stress relaxation or creep phenomena are modeled using such FDEs. An example from this class is solved in Chapter 7. It is given by

$$\mathrm{D}^{\alpha} x(t) + x(t) = f(t)\,, \quad x(0) = 0 \quad \text{and} \quad 0 < \alpha < 1.$$

5. Class five consists of fractional integral equations, where the order of the fractional integral is assumed between 0 and 1. The system is allowed to start from *nonzero* initial conditions in this case. The solution strategy for this class of problems also involves DAEs. An example of this class of FIEs, considered in Chapter 8, is

$$g(x,t) + h(x,t)\,\mathrm{I}^{\alpha} x(t) = 0, \quad 0 < \alpha < 1.$$

6. Class six consists of multiterm nonlinear fractional integrodifferential equations (FIEs); order of the fractional derivatives and integrals is assumed between 0 and 1; the system starts from *nonzero* initial conditions. The solution strategy for these FIEs also involves DAEs. Linear as well as nonlinear examples are solved in Chapter 8. The form of FIEs considered is

$$\mathrm{D}^{\alpha} x(t) + f(x,t)\,\mathrm{D}^{\beta} x(t) + g(x,t)\,\mathrm{I}^{\gamma} x(t) + h(x,t) = 0, \quad x(0) = x_0\,, \text{ and } \alpha\,, \beta\,, \gamma \in (0,1).$$

7. Class seven consists of any arbitrary integer ordered FDE; order of the fractional derivative involved in the FDE is also assumed arbitrary; the system starts from *nonzero* initial conditions. As an example of this class, the Bagley-Torvik equation is solved in Chapter 9. This is a second order FDE with fractional derivative of order between 1 and 2. We solve the Bagley-Torvik equation of the following form

$$\ddot{x}(t) + \mathrm{D}^{\alpha}[x(t)] + x(t) = 0\,, \quad 1 < \alpha < 2 \quad \text{and} \quad x(0) = 1\,,\ \dot{x}(0) = 1.$$

8. Class eight is a generalization of the multiterm nonlinear FIEs to higher order fractional derivative terms; the system starts from *nonzero* initial conditions; fractional derivative terms can be of any arbitrary order, but the order of the fractional integral is between 0 and 1. An example from this class is solved in Chapter 9. The typical form considered is

$$\mathrm{D}^{\alpha}x(t) + f(x,t)\,\mathrm{D}^{\beta}x(t) + g(x,t)\,\mathrm{I}^{\gamma}x(t) + h(x,t) = 0\,, \quad \mathbf{x}(0) = \mathbf{x}_0,$$

where $n-1 < \alpha < n$, $m-1 < \beta < m$, $0 < \gamma < 1$ and $m < n$. Unlike the previously described equations, here poor numerical accuracy is obtained for a nonlinear problem. In contrast, for a linear problem, the accuracy obtained is excellent.

Chapter 2

Rubber Viscoelasticity

In this thesis we have solved several classes of differential equations involving derivatives and integrals of various fractional orders. Fractional order derivatives find use in control, viscoelasticity, fluid mechanics, structural dynamics, earth quake engineering, etc. However, the use of fractional derivatives, for example, in computing control inputs is purely from a mathematical viewpoint. On the other hand, the fractional damping behavior of viscoelastic materials arises from the underlying physics of the material. As mentioned earlier, this physical origin of the fractional damping has motivated us to study viscoelastic behavior of disordered materials at three levels. At the first level, a first principles study of viscoelasticity is presented here, and will motivate us to study two simpler disordered systems. The study of these two simplified systems will in turn prompt us towards an infinite dimensional system which is mathematically equivalent to a fractional order derivative or integral. This infinite dimensional system will form the starting point for our Galerkin projection based approximation scheme. Thus our Galerkin scheme of Chapter 5 is motivated from the three level study of viscoelasticity (of Chapters 2 to 4).

Rubber is made of long chain molecules. These molecules are randomly oriented in all directions and are cross-linked with each other to form a three dimensional network. Incorporating aspects of such networks into models for rubber viscoelasticity has been of interest for several decades. In this chapter we briefly describe some approaches developed in the literature [26, 27, 28, 29, 30] to model rubber elasticity and viscoelasticity. The aim of this chapter is to understand why a rubber like material shows a damping behavior which can be modeled well using fractional order derivative terms. In other words, the relaxation

study of a piece of rubber shows a macroscopic power law dominated decay instead of the usual exponential decay. The origin of this macroscopic power law decay seems to lie in the fact that several parallel random processes with closely spaced decay rates occur at the microscopic level. Note that the contribution of this thesis is in numerical solutions, not first-principles rubber modeling; the discussion of rubber models is included here for motivation and completeness.

This chapter is not original. Barring some changes in wording, what follows is essentially taken from [26, 28, 29, 30].

2.1 Rubber Elasticity

When a load is applied on a specimen made of rubber, it deforms and supports the load. This suggests elastic behavior in rubber. Many studies have been conducted to analyze rubber elasticity. It is evident from the literature [26] that the kinetic theory of long chain molecules explains this phenomenon very well. The chain models with fixed bond length and bond angles, the freely joined bead-rod chain model, the freely joined bead spring model and dumbbell models are some examples of simplified microstructure models which are used while applying this kinetic theory. We will explain some ideas of this theory briefly, for more details the reader can refer to [26].

One important assumption in modeling long chain molecules is that given one orientation of one link, the next consecutive link can take any arbitrary orientation, hence constructing a random walk. This assumption leads to a Gaussian distribution of the end to end vector of the molecule. Consider a molecule chain consisting of $N-1$ rigid links of length a. The length of the fully extended chain is given by $(N-1)a$ and RMS length is $\sqrt{N-1}\,a$. The probability density of the end to end vector $\mathbf{Q}$ is given by

$$p(\mathbf{Q}) = \left(\frac{3}{2\pi(N-1)a^2}\right)^{3/2} \exp\left(\frac{-3Q^2}{2(N-1)a^2}\right),$$

where $Q = |\mathbf{Q}|$. The Helmholtz free energy for absolute temperature T is given by

$$\psi = \frac{3kT}{2(N-1)a^2}Q^2 - CT,$$

where C is some constant and k is Boltzmann's constant. Thus the force in the chain obtained using the Gaussian approximation is given by

$$\mathbf{F} = \frac{\partial \psi}{\partial Q}\,\hat{\mathbf{q}} = \frac{3kT}{(N-1)a^2} Q\,\hat{\mathbf{q}} = H\,\mathbf{Q},$$

where $\hat{\mathbf{q}}$ is a unit vector in the direction of $\mathbf{Q}$ and H is the spring constant which relates force with the displacement. The spring force varies linearly with the displacement in this case. The net stress on a given cross section of the material can be obtained assuming that all the junctions of the network move affinely (see for details [26]). An interesting observation is that, by this model, rubber stiffness rises with temperature.

We now turn to models of viscoelasticity developed in the literature.

2.2 Rubber Viscoelasticity

2.2.1 Transient Networks Model

When a piece of rubber is kept at a constant stretch, the stress at any given section relaxes with time. Similarly, the creep phenomenon is also observed under constant loading conditions. It is also observed that the energy is dissipated as heat if these materials are subjected to cyclic loading. These phenomena point to the viscoelastic nature of rubber. The first theory to explain these phenomena was by Green and Tobolsky [27]. According to their theory, the stretched network chains break and new chains are reformed in a stress free state. This process of breaking and reforming of chains relaxes the stress. Networks of breaking and reforming chains are called transient networks. The following assumptions are made while studying such networks [28].

1. A crosslinked polymeric solid can be represented by a molecular network with polymer-polymer interactions occurring at some isolated points along the molecular chain. These points are called junctions.

2. The polymeric material is assumed to be incompressible.

3. The network junctions move affinely. Thermal motion of junctions is neglected.

4. The phase-space distribution function for each chain is equilibrated at all times.

5. The polymeric material is subjected to either a homogeneous deformation or a homogeneous flow.

6. Each network chain can be modeled as a Gaussian chain. The chains are assumed to be freely jointed, bead-rod chains. Thus each chain can be modeled as a Hookean spring with spring constant $H_N = 3kT/(N-1)a^2$.

7. The chains are lost and reformed during the flow. The stresses are assumed to be the sum of forces in all the chains which are connected to the network at both ends.

8. It is assumed that the distribution function for the network chains at the moment of creation is identical to the equilibrium distribution function for a freely jointed bead-rod chain with no constraints on the end points.

9. Chains are characterized on the basis of complexity of the entanglements by positive integer i, and on the basis of number of links by N, where $N-1$ is the number of links. Thus an iN-chain is a chain with $N-1$ links and has complexity i.

A study of these networks involves the following important steps [29].

- A simplified microstructure model of the actual system.
- The evolution equation (convection equation) which describes the change of the structure in time.
- The averaging procedure connecting the macroscopic stress tensor with microscopic stresses.

Simplified Microstructure Models

Some examples of simplified microstructure model are: the chain models with fixed bond length and bond angles, the freely joined bead-rod chain model, the freely joined bead spring model and dumbbell models [28].

The Evolution Equation

Define a distribution function $\Psi_{iN}(\mathbf{Q}, t)$ such that

$$\Psi_{iN}(\mathbf{Q}, t)d\mathbf{Q} = \text{number of } iN\text{-chains per unit volume at time } t \text{ with end to end vector in the region } d\mathbf{Q} \text{ centered at } \mathbf{Q}. \quad (2.1)$$

After defining the distribution function, the convection equation for the network is given by [28]

$$\frac{\partial \Psi_{iN}}{\partial t} = -\left(\frac{\partial}{\partial \mathbf{Q}} \cdot [\mathbf{L} \cdot \mathbf{Q}]\Psi_{iN}\right) + L_{iN}(Q, t) - \Psi_{iN}\lambda_{iN}(Q, t), \quad (2.2)$$

where $\mathbf{L}$ is the velocity gradient, L_{iN} is iN-chain creation rate per unit volume (of chain length Q), λ_{iN} is probability per unit time that an iN-chain will be destroyed. Equation (2.2) is a first order partial differential equation that describes how the chain distribution function Ψ_{iN} changes in time when the flow field is described by $\mathbf{L}$.

The Averaging Procedure

Now we consider the expression which relates the macroscopic stress tensor to the microscopic stresses. The contribution to the total stress tensor from iN-chains is given by

$$\mathbf{T}_{iN} = -H_N\langle \mathbf{QQ} \rangle_{iN}, \quad (2.3)$$

where H_N is the spring constant of chains with $N-1$ links, $\langle \cdot \rangle$ is the average over the entire configuration space of all types of chains, and $\mathbf{QQ}$ is the dyadic product of vector $\mathbf{Q}$. The total stress tensor is given by

$$\mathbf{T} = -\sum_i \sum_N H_N \langle \mathbf{QQ} \rangle_{iN}. \quad (2.4)$$

The quantity $\langle \mathbf{QQ} \rangle_{iN}$ is obtained by solving the ODE [28]

$$\frac{d}{dt}\langle \mathbf{QQ} \rangle_{iN} = \mathbf{L} \cdot \langle \mathbf{QQ} \rangle_{iN} + \langle \mathbf{QQ} \rangle_{iN} \cdot \mathbf{L}^T + \int L(Q, t)_{iN} \mathbf{QQ} d\mathbf{Q} - \langle \lambda_{iN}(Q, t)\mathbf{QQ} \rangle_{iN}. \quad (2.5)$$

Notice in Equation (2.4) that the total macroscopic stress tensor is a sum of several microscopic parallel random processes taking place at different rates. Each process is

represented by Equation (2.5) and the rate of the process is governed by $\mathbf{L}$ and $\lambda_{iN}(Q,t)$. It seems feasible that in some cases the rates of these many microscopic processes can be closely spaced; moreover, the combined effect of these factors might lead to a macroscopic behavior which involves a fractional order derivative (see [20]). In other words the stress relaxation of a piece of rubber kept at a constant stretch can show a power law dominated behavior instead of the usual exponential law. Analytically proving such statement is difficult because of the lack of the knowledge about λ_{iN} as a function of i and N. But it is clear from Equation (2.4) that, as per this model [28], several parallel, possibly random, microscopic relaxation processes take place inside a rubber like material, whose net effect can be a power law stress relaxation.

Another theory of viscoelasticity, namely the tube model theory, has shown that the stress relaxation follows a power law on certain time scales. In the following section we will discuss this theory briefly.

2.2.2 Tube Model

The tube model was first introduced by de Gennes [31] to discuss the motion of an unattached chain through a fixed network. Doi and Edwards [32, 33] used this concept in modeling concentrated polymer solutions and melts.

The tube model is motivated by the fact that in a network, a chain is surrounded by several other arbitrarily oriented chains, thus restricting its motion. Thus the assumption that the motion of a chain is confined within a tube like region surrounding it seems reasonable. The shape of the tube is similar to that of the chain itself. The chain can have two types of motions; one is along the longitudinal axis of the tube and other is normal to this same axis. The second type of motion is due to thermal fluctuations, and is governed by the Rouse model [34]. The first type of motion is due to the actual movement of the chain through the network, this is modeled by reptation dynamics [30]. An important result of this theory gives the relaxation modulus $G(t)$ of the rubber like material as [30]

$$G(t) = C \sum_{p=1}^{\infty} \exp(-2tp^2/\tau_R), \tag{2.6}$$

where C is a constant and

$$\tau_R = \frac{\xi N^2 b^2}{3\pi^2 kT}.$$

ξ in the above is a friction constant, N is number of segments of a chain, b is segment length, k is Boltzmann's constant and T is absolute temperature. For $t \ll \tau_R$, the sum of Equation (2.6) can be replaced by an integral to give

$$G(t) = C \int_0^\infty \exp(-2tp^2/\tau_R)dp = \bar{C}\left(\frac{\tau_R}{t}\right)^{1/2}, \tag{2.7}$$

where $\bar{C}$ is constant. Hence the relaxation modulus shows a power law decay instead of the exponential, which suggests the use of fractional order derivatives in the mathematical models involving dynamics of rubber like materials.

2.3 Discussion

We have discussed two well known models for rubber viscoelasticity, namely the transient network model and the tube model. It is observed from the transient network model that several parallel possibly random processes take place at microscopic level, whose net effect is the macroscopic stress. But due to the lack of the knowledge about λ_{iN}, using this model one can not prove that a power law relaxation occurs, although such behavior is feasible. On the other hand, the tube model predicts a power law relaxation at short time scales. In this context, a fractional order derivative model for rubber damping seems theoretically defensible. Note that experimental data does support the use of such models (see, [35] and references therein).

Chapter 3

Relaxation in Some Simple Random Chains and Networks

It was discussed in the last chapter why the power law relaxation of a rubber like substance may simply be due to the presence of several parallel random processes with closely spaced decay rates. In this chapter we perform a relaxation study of 1-D chains and 2-D networks of springs and dashpots. The damping coefficients of the dashpots are assumed random. Hence we get a system with several parallel random processes. The values of damping coefficients are chosen in such a way that the decay rates (or eigenvalues) of the system are closely spaced. We have performed a numerical study of the potential energy relaxation for 1-D and 2-D cases. Further, analytical descriptions of potential energy relaxation for the 1-D case are obtained as well. For the 2-D case such analytical results have not been obtained.

The aim of this chapter is to show that, separate from first-principles physics based models for rubber like materials, fractional order damping behavior may be expected from many disordered materials.

Several papers in the physics literature [36, 37, 38, 39] have dealt with phenomena determined by several microscopic parallel processes. The microscopic processes exhibit closely but randomly spaced rates of decay. More recent literature [20, 21] has shown that the parallel random microscopic processes lead to fractional calculus at the macroscopic level. Hence, the physical quantity under consideration follows a power law decay instead

of the usual exponential. With these thoughts, we now present studies of strain energy relaxation in some random viscoelastic chains and networks.

3.1 Relaxation of 1-D Chain: A Numerical Study

In this section we study relaxation in a 1-D chain. The chain consists of n pairs of springs and dashpots, as shown in Figure 3.1. The springs are assumed to be of a fixed stiffness $s = n$, whereas the damping coefficients of the dashpots follow a random distribution, as discussed later. In Figure 3.1 the circles between two pairs of spring and dashpots represent massless nodal points.

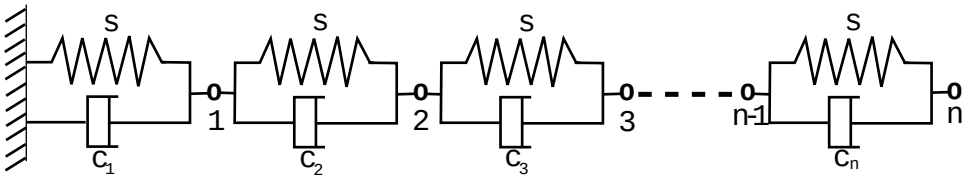

Figure 3.1: 1-D chain of springs and dashpots.

The relaxation study of the present work involves decay analysis of the averaged potential energy of the chain. In what follows we will numerically show that a chain with fixed stiffness springs and with a certain type of distribution of damping coefficients gives rise to a particular power law decay of potential energy instead of the usual exponential decay. The power law decay implies, at a macroscopic level, the presence of fractional order derivative. The damping coefficient of dashpot i is here selected as $1/v_i^{1/\alpha}$, where α is a given exponent, and v_i is uniformly distributed on $(0, A)$, for a suitable positive constant A. We will consider an ODE of the following form

$$\mathbf{C}\dot{\mathbf{x}} + \mathbf{K}\,\mathbf{x} = 0, \qquad \mathbf{x}(0) = \mathbf{x}_0, \tag{3.1}$$

where $\mathbf{C}$ and $\mathbf{K}$ are $n \times n$ damping and stiffness matrices respectively, and $\mathbf{x}$ is $n \times 1$ state vector. The matrices $\mathbf{K}$ and $\mathbf{C}$ are obtained as described below.

Stiffness and Damping Matrices

Entries of **K** and **C** are obtained by the following force balance equations:

$$x_1(s_1 + s_2) - x_2 s_2 + \dot{x}_1(c_1 + c_2) - \dot{x}_2 c_2 = 0, \tag{3.2a}$$

$$x_i(s_i + s_{i+1}) - x_{i-1}s_i - x_{i+1}s_{i+1} + \dot{x}_i(c_i + c_{i+1}) - \dot{x}_{i-1}c_i - \dot{x}_{i+1}c_{i+1} = 0, \quad \text{for} \quad 2 \leq i \leq n-1 \tag{3.2b}$$

and

$$x_n s_n - x_{n-1}s_n + \dot{x}_n c_n - \dot{x}_{n-1}c_n = 0, \tag{3.2c}$$

where s_i is stiffness of i^{th} spring, we take $s_i = n$, and c_i is damping coefficient of the i^{th} dashpot. Say we are interested in long-time power law decay like $t^{-\alpha}$, $0 < \alpha < 1$. Then c_i is chosen (numerical justification will follow) to be $\frac{1}{v_i^{1/\alpha}}$, where v_i is a random variable uniformly distributed in $(0, A)$, with $A = n^{-\alpha\beta}$, where $\beta \in [0, 1)$ is an arbitrary parameter we have chosen as $9/10$ for reasons that will be clear later. It is clear from the above equations that **C** and **K** are tridiagonal symmetric positive definite matrices with main diagonal entries as

$$K_{i,i} = s_i + s_{i+1} \quad \text{and} \quad C_{i,i} = c_i + c_{i+1} \quad \text{for} \quad 1 \leq i \leq n-1$$

and

$$K_{n,n} = s_n \quad \text{and} \quad C_{n,n} = c_n.$$

The superdiagonal entries are

$$K_{i,i+1} = -s_{i+1} \quad \text{and} \quad C_{i,i+1} = -c_{i+1} \quad \text{for} \quad 1 \leq i \leq n-1$$

The subdiagonal entries are same as superdiagonal due to the symmetry. After obtaining stiffness and damping matrices, now we present results of numerical simulations.

Numerical Results

We solve Equation (3.1) (a stiff system) numerically using the backward Euler method. We use $n = 3000$, $\alpha = 1/3$ and $2/3$, and $\beta = 9/10$ as mentioned above. We use suitably scaled, zero mean, uniformly distributed, *i.i.d.*, initial conditions. The process of solving

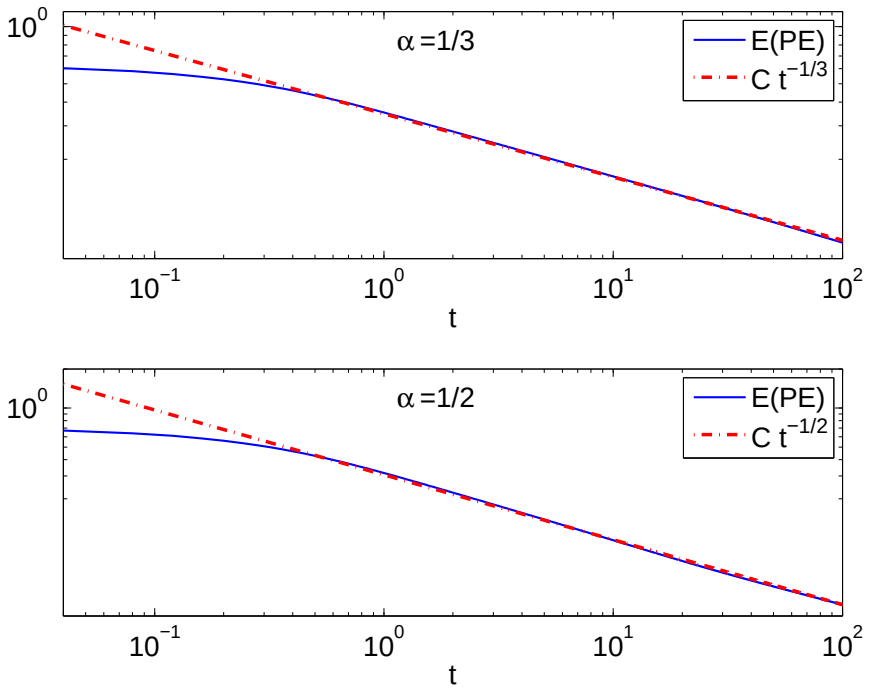

Figure 3.2: Numerical results of potential energy relaxation. Expected value of potential energy $E(PE)$ is compared with $Ct^{-\alpha}$ on the log-log scale, for some constant C; $\alpha = 1/3$ and $1/2$ is used for top and bottom plot respectively.

Equation (3.1) is repeated 50 times for different random initial conditions and the average potential energy as a function of time is computed. Results are shown in Figure 3.2.

It is clear from the above plots that the averaged potential energy of the system follows a power law decay, and a desired exponent of the power law can be obtained by changing the value of the exponent α of the inverse uniform distribution. Observe in both plots that for small values of time, the result of numerical simulation show a flat curve. This is due to the fact that the largest eigenvalues are finite though they may be large numbers, whereas when $t \to 0$, power law decay will require infinite decay rates.

Note that the value of the constant, in the above plots, $C = \dfrac{\Gamma(1+\alpha)}{2^\alpha}$, as will be analytically established later.

3.2 Relaxation of 2-D Network: A Numerical Study

In this section we study a 2-D network consisting of pairs of springs and dashpots. The initial network (mesh) is generated by using Matlab's program "initmesh" and refined afterwords using "refinemesh" (Figure 3.3). We will again construct an equation of the form

$$\mathbf{C}\dot{\mathbf{x}} + \mathbf{K}\,\mathbf{x} = 0, \qquad \mathbf{x}(0) = \mathbf{x}_0,$$

where $\mathbf{C}$ and $\mathbf{K}$ are $n \times n$ damping and stiffness matrices respectively, and $\mathbf{x}$ is $n \times 1$ state vector. The matrices $\mathbf{K}$ and $\mathbf{C}$ are obtained as described below.

Stiffness and Damping Matrices

The mesh used in this numerical study is shown in Figure 3.3. The bottom left node is assumed constrained in both x and y directions, whereas the bottom right node is assumed constrained in the x direction. Lines joining any two nodes of the mesh are assumed to be pairs of springs and dashpots. The stiffness of the spring attached between a particular pair of nodes is assumed to be the inverse of the distance between those two nodes. The value of damping coefficients of dashpots is assumed similar to that explained in Sections 3.1, but now we take $\beta = 0$. The reason for taking $\beta = 0$ is that the smaller eigenvalues (for longer time scales) are now more closely spaced (as observed from numerical results) when compared with 1-D case, and numerical simulations of a manageable size show the power law decay we seek.

The mesh is twice refined using "refinemesh" and matrices $\mathbf{K}$ and $\mathbf{C}$ are obtained as follows. We treat the mesh as a truss and use the standard unit displacement method [40] to obtain the stiffness matrix $\mathbf{K}$. The damping matrix $\mathbf{C}$ is obtained in an analogous method, where we use unit velocity instead of unit displacement. We use $\alpha = 1/3$, $1/2$ and $2/3$ for computing $\mathbf{C}$ (three different cases). After obtaining $\mathbf{K}$ and $\mathbf{C}$, we solve Equation (3.1) numerically, then find the potential energy of the system as a function of time. The initial conditions used here are zero mean uniformly distributed numbers between -0.5 and 0.5.

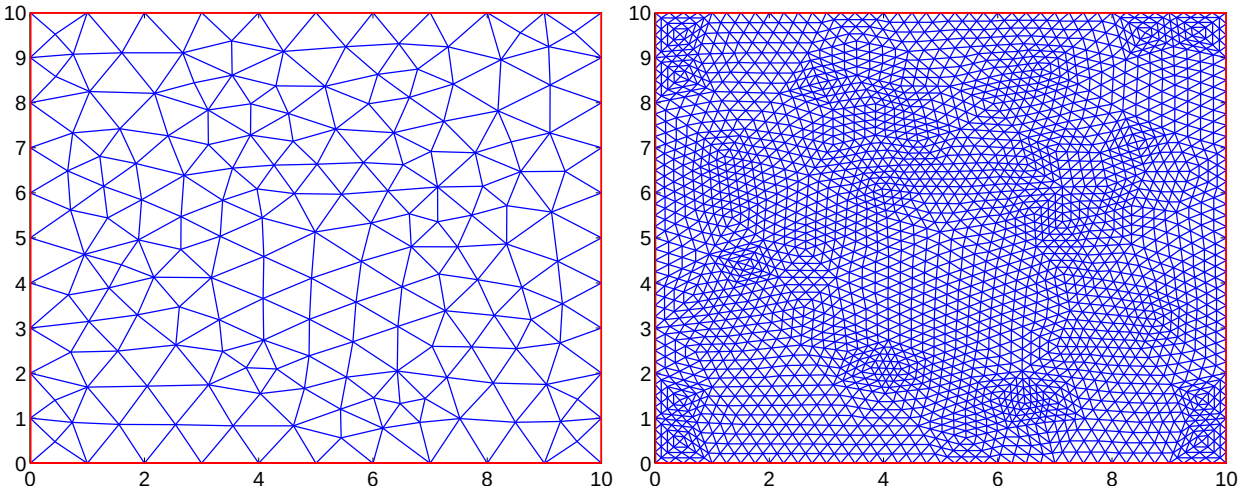

Figure 3.3: Left: A pre-refinement mesh. Right: The refined mesh.

Numerical Results

We solve Equation (3.1) numerically using the backward Euler method as before. We use $\alpha = 1/3$, $1/2$ and $2/3$ in computation of $\mathbf{C}$. The size of the matrix, n, happens to be 5503. The eigenvalues λ_k of the system of Equation (3.1) are computed for these three cases. For each case, the α-order exponent of λ_k (arranged in increasing order) is plotted against k/n, where $k = 1, 2, 3, \ldots n$ and n is the total number of eigenvalues. The results are shown in Figure 3.4. It is clear in each case that the curve is linear at least for the first 80% of the eigenvalues.

Figure 3.5 shows the results of the numerical solution of Equation (3.1). The averaged potential energy of the network is plotted against time on a log-log scale. The numerical results are compared with $C\,t^{-\alpha}$ for $\alpha = 1/3$, $1/2$ and $2/3$, and for some suitable value of C (which has not been analytically obtained). The results match very well for more than two orders of magnitudes of time. Initial flatness in the curves again shows a limitation of the finite approximation.

After presenting the above numerical results, now we present an analytical treatment of the averaged potential energy relaxation of the 1-D chain.

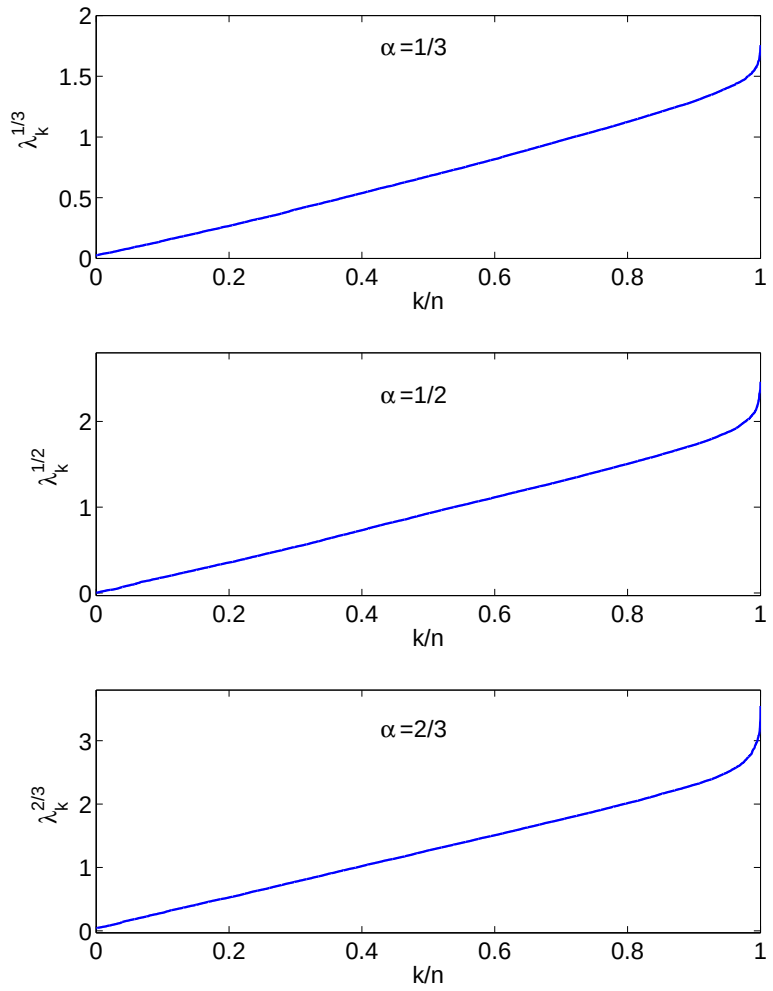

Figure 3.4: ${\lambda_k}^{\alpha}$ is plotted against k/n, where λ_k are eigenvalues of system of Equation (3.1); $\alpha = 1/3$, $1/2$ and $2/3$ is used for top, middle and bottom plot respectively.

3.3 Relaxation of 1-D Chain: A Theoretical Study

It is observed in Figure 3.1 that if a node i (along with all nodes to its right) is moved to the right, while keeping all the nodes on its left side fixed; then node i and all the nodes at the right side of node i relax at the same rate. This rate of relaxation is governed by the stiffness s and damping coefficient c_i of the pair i of spring and dashpot. This is i^{th} mode of relaxation for the chain. It becomes clear that the i^{th} mode is a step function which is zero for all nodes left of the i^{th} and is 1 for the i^{th} node and all nodes to is right. It is also clear that the rate of decay of the i^{th} mode is governed by $\lambda_i = s/c_i$.

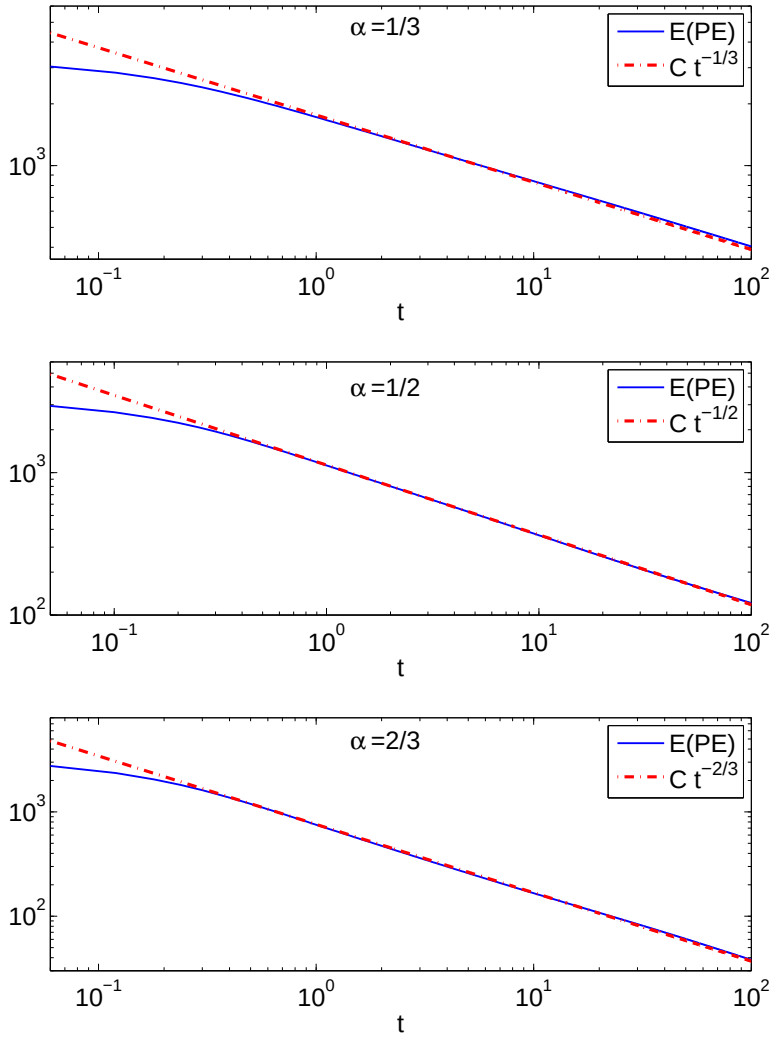

Figure 3.5: Numerical results of potential energy relaxation. Expected value of potential energy $E(PE)$ is compared with $Ct^{-\alpha}$ on the log-log scale, for some constant C; $\alpha = 1/3$, $1/2$ and $2/3$ is used for top, middle and bottom plot respectively.

The solution of Equation (3.1) for a suitably scaled zero mean uniformly distributed *i.i.d.* initial conditions $\mathbf{x}_0$ is given by

$$\mathbf{x}(t) = \mathbf{U} \exp(-\Lambda t)\, \mathbf{U}^{-1}\mathbf{x}_0\,, \tag{3.3}$$

where $\mathbf{U}$ is a matrix of eigenvectors of the system of Equation(3.1) and Λ is a diagonal matrix of corresponding eigenvalues. It follows from a standard result for symmetric positive definite matrices that the columns of $\mathbf{U}$ are orthogonal when weighted by either $\mathbf{K}$ or $\mathbf{C}$. But due to the special structure of $\mathbf{K}$, the matrix product $\mathbf{U}^T\mathbf{K}\mathbf{U}$ becomes $n\mathbf{I}$, where $\mathbf{I}$ is

the identity matrix; this can be shown as follows.

It was explained in the beginning of this section that the eigenvectors of this system are step functions. Hence the matrix $\mathbf{U}$ is lower triangular with all nonzero entries 1. Also, the matrix $\mathbf{K}$ is tridiagonal as well as symmetric in nature. Keeping these two results in mind, the $(j,j)^{th}$ entry of the product $\mathbf{M} = \mathbf{U}^T\mathbf{K}\mathbf{U}$ can be written as

$$M_{j,j} = \sum_{i=1}^{n} K_{i,i}U_{i,j}^2 - 2\sum_{i=1}^{n-1} K_{i,i+1}U_{i,j}U_{i+1,j} = n + \sum_{i=1}^{n-1} 2n - 2\sum_{i=1}^{n-1} n = n, \tag{3.4}$$

where $U_{i,j}$ is the $(i,j)^{th}$ entry of $\mathbf{U}$. So $\mathbf{M} = n\mathbf{I}$.

After obtaining the above preliminary results, now we write an expression for the potential energy of the chain as

$$PE = \frac{1}{2}\mathbf{x}(t)^T\mathbf{K}\,\mathbf{x}(t). \tag{3.5}$$

On substituting $\mathbf{x}(t)$ from Equation (3.3) into Equation (3.5) we get

$$PE = \frac{1}{2}\mathbf{x}_0^T\,\mathbf{U}^{-T}\exp(-\Lambda t)\mathbf{U}^T\mathbf{K}\,\mathbf{U}\,\exp(-\Lambda t)\mathbf{U}^{-1}\mathbf{x}_0 = \frac{n}{2}\,\mathbf{x}_0^T\,\mathbf{U}^{-T}\exp(-2\Lambda t)\mathbf{U}^{-1}\mathbf{x}_0. \tag{3.6}$$

The matrix $\mathbf{U}^{-T}\exp(-2\Lambda t)\mathbf{U}^{-1}$ in the right of the above is a tridiagonal matrix. This can be shown as follows.

Since $\mathbf{U}$ is a lower triangular matrix with all nonzero entries equal to 1, $\mathbf{U}^{-1}$ is a bidiagonal matrix with the diagonal entries 1 and subdiagonal entries -1. This follows from the fact that

$$\sum_{j=1}^{i} U_{i,j}\,L_{j,k} = \delta_{i,k}$$

where $L_{j,k}$ is $(j,k)^{th}$ entry of $\mathbf{U}^{-1}$ and $\delta_{i,k}$ is the Kronecker delta. The summation above is only till $j = i$ since $\mathbf{U}$ is lower triangular. Since all nonzero entries of $\mathbf{U}$ are 1, the above summation becomes

$$\sum_{j=1}^{i} L_{j,k} = \delta_{i,k}.$$

Substituting values for i and k, the above mentioned bidiagonal nature of $\mathbf{U}^{-1}$ is obtained. The basic structure may also be seen easily in the following 4×4 example:

$$\underbrace{\begin{bmatrix} 1 & 0 & 0 & 0 \\ 1 & 1 & 0 & 0 \\ 1 & 1 & 1 & 0 \\ 1 & 1 & 1 & 1 \end{bmatrix}}_{\mathbf{U}} \underbrace{\begin{bmatrix} 1 & 0 & 0 & 0 \\ -1 & 1 & 0 & 0 \\ 0 & -1 & 1 & 0 \\ 0 & 0 & -1 & 1 \end{bmatrix}}_{\mathbf{U}^{-1}} = \begin{bmatrix} 1 & 0 & 0 & 0 \\ 0 & 1 & 0 & 0 \\ 0 & 0 & 1 & 0 \\ 0 & 0 & 0 & 1 \end{bmatrix}$$

Now we consider $\mathbf{U}^{-T} \exp(-2\Lambda t)\mathbf{U}^{-1}$. Expanding this product we get

$$(\mathbf{U}^{-T} \exp(-2\Lambda t)\mathbf{U}^{-1})_{i,k} = \sum_{j=1}^{n} \sum_{m=1}^{n} L_{j,i} D_{j,m} L_{m,k},$$

where, $D_{j,m}$ is the $(j,m)^{th}$ entry of $\exp(-2\Lambda t)$. Since $\exp(-2\Lambda t)$ is diagonal, the above summand is nonzero only when $j = m$, hence it becomes

$$(\mathbf{U}^{-T} \exp(-2\Lambda t)\mathbf{U}^{-1})_{i,k} = \sum_{j=1}^{n} L_{j,i} D_{j,j} L_{j,k}, \tag{3.7}$$

which is clearly a symmetric matrix (as interchanging i and k does not change the sum). Due to the bidiagonal nature of $\mathbf{U}^{-1}$, the above summand is nonzero only if subequations

and

$$\begin{aligned} L_{j,i} \neq 0 \quad &\Longrightarrow \quad j = i \text{ or } i+1 \\ L_{j,k} \neq 0 \quad &\Longrightarrow \quad j = k \text{ or } k+1. \end{aligned}$$

subequations The above two imply that the summation of Equation (3.7) is nonzero only if one of the following conditions holds

$$\begin{aligned} i &= k-1, \\ i &= k, \\ i &= k+1, \end{aligned}$$

which shows that the product is a tridiagonal matrix.

We now return to Equation (3.6). Using the above derived tridiagonal and symmetry properties, and simplifying the expression on the right of Equation (3.6), PE is given by

$$PE = \frac{n}{2} \sum_{i=1}^{n} \sum_{k=1}^{n} L_{k,i}^2 \exp(-2\lambda_k t)\, x_i^2 + n \sum_{i=1}^{n-1} \sum_{k=1}^{n} L_{k,i}\, L_{k,i+1} \exp(-2\lambda_k t)\, x_i\, x_{i+1},$$

where λ_k is the $(k,k)^{th}$ entry of Λ and x_i is the i^{th} entry of $\mathbf{x}_0$. Notice that the sequence in the inner sums of both the terms of the above equation can be suitably rearranged to put the λ's in increasing order. On doing this, we obtain

$$PE = \frac{n}{2}\sum_{i=1}^{n}\sum_{p=1}^{n}\bar{L}_{p,i}^2\,\exp(-2\lambda_p t)\,x_i^2 + n\sum_{i=1}^{n-1}\sum_{p=1}^{n}\bar{L}_{p,i}\,\bar{L}_{p,i+1}\,\exp(-2\lambda_p t)\,x_i\,x_{i+1} \tag{3.8}$$

with λ_p now arranged in ascending order, *i.e.* $\lambda_{p-1} < \lambda_p$ for integers $p \in [2,n]$, and $\bar{L}_{p,i}$ is the $(p,i)^{th}$ entry of the inverse of a permuted version of matrix $\mathbf{U}$, to be defined later.

So far we have not paid attention to the eigenvalues λ_p of the system. It was shown in the beginning of this section that the p^{th} eigenvalue $\lambda_p = s/c_p = n/c_p$ as $s = n$ for all springs. Hence λ_p takes values of the $1/\alpha$ order exponent of uniformly distributed numbers between 0 and $n^{-\alpha\,\beta}$, multiplied by n. In other words,

$$\lambda_p = n(u_p\,n^{-\alpha\,\beta})^{1/\alpha} = n^{1-\beta}(u_p)^{1/\alpha}, \tag{3.9}$$

where u_p is uniformly distributed in (0,1). It should be noted that on arranging numbers u_p in ascending order and letting $n \to \infty$, $u_p \approx p/n$. On replacing u_p with p/n in Equation (3.9) we get

$$\lambda_p = \frac{p^{1/\alpha}}{n^{(1/\alpha)-1+\beta}}. \tag{3.10}$$

Continuing the analysis, on substituting λ_p from above into Equation (3.8), we get

$$PE = \frac{n}{2}\sum_{i=1}^{n}\sum_{p=1}^{n}\bar{L}_{p,i}^2\,\exp\left(-2\frac{p^{1/\alpha}}{n^{(1/\alpha)-1+\beta}}t\right)\,x_i^2 + n\sum_{i=1}^{n-1}\sum_{p=1}^{n}\bar{L}_{p,i}\,\bar{L}_{p,i+1}\,\exp\left(-2\frac{p^{1/\alpha}}{n^{(1/\alpha)-1+\beta}}t\right)\,x_i\,x_{i+1} \tag{3.11}$$

The expected value of PE in the above, assuming independence of x_i and x_{i+1} with respect to each other and also $L_{k,i}$ and $L_{k,i+1}$, is given by

$$E(PE) = \frac{n}{2}\sum_{i=1}^{n}\sum_{p=1}^{n}E(\bar{L}_{p,i}^2)\,\exp\left(-2\frac{p^{1/\alpha}}{n^{(1/\alpha)-1+\beta}}t\right)\,E(x_i^2) + \\ n\sum_{i=1}^{n-1}\sum_{p=1}^{n}E(\bar{L}_{p,i}\,\bar{L}_{p,i+1})\,\exp\left(-2\frac{p^{1/\alpha}}{n^{(1/\alpha)-1+\beta}}t\right)\,E(x_i)\,E(x_{i+1}).$$

The second term above is equal to 0, as $E(x_i) = E(x_{i+1}) = 0$, so that the expected value of PE is given by

$$E(PE) = \frac{n}{2}\sum_{i=1}^{n}\sum_{p=1}^{n}E(\bar{L}_{p,i}^2)\,\exp\left(-2\frac{p^{1/\alpha}}{n^{(1/\alpha)-1+\beta}}t\right)\,E(x_i^2). \tag{3.12}$$

Because of the randomness of c_i values, hence λ_i values, and the renumbering from the k-index to the p-index, $\bar{L}_{p,i}$ is a random quantity.

Now we obtain the probability density for elements $\bar{L}_{p,i}$ of the the matrix $\bar{\mathbf{U}}^{-1}$, to be defined below. A rearrangement of columns of $\mathbf{U}$, in accordance with the rearrangement of λ's in Equation (3.8) can be rewritten as

$$\bar{\mathbf{U}} = \mathbf{U}\,\mathbf{P},$$

where $\mathbf{P}$ is a random permutation matrix (a matrix obtained by a permutation of the columns of the identity matrix), with the property that the probability of the j^{th} entry in the i^{th} column of $\mathbf{P}$ being nonzero is $1/n$. Taking inverse of the above,

$$\bar{\mathbf{U}}^{-1} = \mathbf{P}^{-1}\mathbf{U}^{-1} = \mathbf{P}^{T}\mathbf{U}^{-1},$$

where $\mathbf{P}^{-1} = \mathbf{P}^{T}$ because $\mathbf{P}$ is a permutation matrix. The matrix $\mathbf{P}^{T}$ rearranges the rows of $\mathbf{U}^{-1}$ in such a way that (keeping bidiagonal property of $\mathbf{U}^{-1}$ in mind)

- The probability that the j^{th} entry in the i^{th} column of $\bar{\mathbf{U}}^{-1}$ is nonzero is $2/n$, for $i < n$.
- The probability that the j^{th} entry in the n^{th} column of $\bar{\mathbf{U}}^{-1}$ is nonzero is $1/n$.

The expected value of $\bar{L}^2_{p,i}$ using the above two results and the fact that $\bar{L}^2_{p,i}$ is either 0 or 1, is given by

$$E(\bar{L}^2_{p,i}) = \begin{cases} \dfrac{2}{n}, & \text{for } 1 \le p \le n \text{ and } 1 \le i \le n-1 \\ \dfrac{1}{n}, & \text{for } 1 \le p \le n \text{ and } i = n. \end{cases}$$

On interchanging the order of summation in Equation (3.12), substituting the above result, and assuming elements of $\mathbf{x}_0$ to be *i.i.d.*, we get

$$E(PE) = \frac{n}{2}\,E(x_i^2)\sum_{p=1}^{n}\exp\left(-2\frac{p^{1/\alpha}}{n^{(1/\alpha)-1+\beta}}t\right)\left[\frac{2(n-1)}{n}+\frac{1}{n}\right] = \frac{(2n-1)}{2}\,E(x_i^2)\sum_{p=1}^{n}\exp\left(-2\frac{p^{1/\alpha}}{n^{(1/\alpha)-1+\beta}}t\right) \quad (3.13)$$

By scaling the initial conditions $\mathbf{x}_0$ suitably, we can write

$$E(x_i^2) = \frac{2}{(2n-1)\, n^{1-\alpha+\alpha\beta}}.$$

On substituting the above in Equation (3.13) we get

$$E(PE) = \frac{1}{n^{1-\alpha+\alpha\beta}} \sum_{p=1}^{n} \exp\left(-2\frac{p^{1/\alpha}}{n^{(1/\alpha)-1+\beta}}t\right) = \frac{1}{(2\,t)^{\alpha}} \sum_{p=1}^{n} \frac{(2\,t)^{\alpha}}{n^{1-\alpha+\alpha\beta}} \exp\left(-2\frac{p^{1/\alpha}}{n^{(1/\alpha)-1+\beta}}t\right). \tag{3.14}$$

Define $\xi = \dfrac{(2\,t)^{\alpha}}{n^{1-\alpha+\alpha\beta}}\, p$. Now for $n \gg 1$ and $t \ll n^{(1/\alpha)-1+\beta}$, the sum in the above equation can be replaced by an integral to give

$$E(PE) = \frac{1}{(2\,t)^{\alpha}} \int_{\xi=0}^{\infty} \exp(-\xi^{1/\alpha})\, d\xi = \frac{\Gamma(1+\alpha)}{(2\,t)^{\alpha}}. \tag{3.15}$$

Hence, the expected value of PE follows a power law decay instead of the usual exponential one, explaining the numerical results of Figure 3.2.

From the above analysis of random systems we make the following conclusion. A 1-D disordered viscoelastic material can be considered to be made up of several small segments. These segments may have randomly distributed damping coefficients. For certain choices of the distribution, damping coefficients c_p, when suitably rearranged, may follow $c_p \propto \dfrac{1}{p^{1/\alpha}}$, where $0 < \alpha < 1$ and $p = 1, 2, 3, \ldots$. This type of damping distribution can lead to a fractional power law relaxation. The underlying distribution of damping coefficients may have its origin in the physics of the material, but that is not investigated in this thesis.

3.4 Choice of β

Notice that an arbitrary parameter β was introduced and assumed nonzero in Sections 3.1 and 3.3, whereas it was assumed 0 in Section 3.2. This parameter, however, plays no role in the final analytical result as can be seen from Equation (3.15). The parameter was introduced purely for numerical convenience. The main objective of this chapter is to demonstrate that several closely spaced randomly distributed microscopic processes may manifest themselves as power law decay at the macroscopic level. This is achieved independently of the parameter β.

Nonzero values of β merely serve to decrease the computational effort involved in numerical verification of analytical results. In Section 3.1 the value 9/10 chosen for β, though purely arbitrary, gives the advantage of reduced computational effort and captures the power law behavior faithfully.

Now we come to the reason behind choosing $\beta \in [0, 1)$. It was required (for the numerical simulation of Section 3.1) that the small eigenvalues which correspond to longer time scales remain closely spaced, to get better long time behavior while keeping the size of the problem within reasonable limits (*i.e.* keeping n reasonably small). The numbers $A = n^{-\alpha\beta}$ and $\beta \in [0, 1)$, used to compute damping coefficients in Sections 3.1 and 3.3 ensure this requirement along with satisfying some more conditions, as explained below:

1. For simplicity we desired that for a fixed, but large, n, $\max(\lambda_p)$ remains a function of β alone and this is achieved by taking $A = n^{-\alpha\beta}$ (see Equation (3.10) for $p = n$).

2. In Equation (3.10), as $p \to n$ and $n \to \infty$, we want $\lambda_p \to \infty$. This can only be achieved if $\beta < 1$.

3. It is required, in order to numerically capture the long time power law behavior, that the smaller eigenvalues should be closely spaced. This can be achieved by considering $\beta > 0$, as discussed below.

   Equation (3.10) can be rewritten as

   $$p = \lambda^{\alpha}\, n^{1+(\beta-1)\alpha}.$$

   Letting $\lambda = \epsilon$ in the above, for some small positive ϵ, we get

   $$p = \epsilon^{\alpha}\, n^{1+(\beta-1)\alpha}.$$

   The above suggests that, for a fixed but large n and a small positive ϵ, p eigenvalues will have values less than ϵ. Now p can be made large by assuming larger values of β. Therefore, in the numerical simulations, we have assumed $\beta = 9/10$ which is close to but less than 1 (keeping point 2 in mind).

The above discussion motivates our choice of $A = n^{-\alpha\beta}$ and $\beta \in (0, 1)$. Whereas the analysis is valid for $\beta = 0$ as well, the penalty paid would be that we may not be able to numerically capture the underlying power law behavior while also keeping the size of the problem (for numerical simulation) within reasonable limits.

3.5 Discussion

In this chapter we studied the relaxation of 1-D chains and 2-D networks of springs and dashpots. The damping coefficients of the dashpots were assumed to be randomly distributed. Analytical results were possible for the 1-D chain due to the special structure of stiffness and damping matrices. It was proved that the averaged potential energy of the chain follows a power law relaxation, which means that the closely spaced parallel relaxation processes give rise to a power law relaxation at the macroscopic level. The analytical results were also verified by numerical simulations.

The case of the 2-D network was not analytically tractable, but numerical results show power law relaxation in this case as well.

It should be noted here that the non-zero value of β is used only to ensure that the small eigenvalues which correspond to longer time scales remain closely spaced. This is required to get better long time numerical results while keeping the size of the simulation within reasonable limits (*i.e.* keeping n reasonably small), because only closely spaced parallel decay processes can give power law decay as a net macroscopic effect. Otherwise the above analysis is equally correct for $\beta = 0$ as well.

Chapter 4

Fractional Damping: Statistical Origins

In Chapter 2 we discussed that in rubber like materials, several parallel possibly random microscopic processes add up to give macroscopic stress tensor. It was also mentioned that a power law stress relaxation takes place at a certain time scale. In Chapter 3 we have shown that the networks of springs and dashpots can lead to power law relaxation if the damping coefficients of the dashpots follow certain type of random distribution. Here we discuss a more simplified model, which involves a random system coefficient matrix. A power law relaxation is obtained in this case also. The material of this chapter is taken from [41, 42].

4.1 Fractional Order Power Law: Numerical Results

Consider the model sketched in Fig. 4.1. An elastic rod of length L has a distributed stiffness $b(z) > 0$. Its axial displacement is $u(z,t)$. The internal force at z is $b(z)\,u_z$, and interaction with neighboring material causes viscous forces $c(z)\,u_t$, with $c(z) > 0$ and with z and t subscripts denoting partial derivatives. The free end of the rod is displaced, held for some time, and released. Subsequent motion obeys

$$(b(z)u_z)_z - c(z)u_t = 0, \quad u(0,t) = 0, u_z(L,t) = 0. \tag{4.1}$$

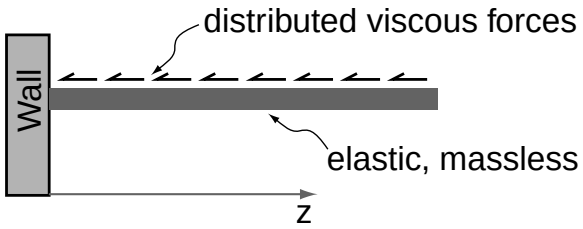

Figure 4.1: One dimensional viscoelastic model.

We will now discuss how sufficient complexity (randomness) in b and c can lead to power law decay.

A solution for the above is sought in the form

$$u(z,t) = \sum_{i=1}^{n} a_i(t)\phi_i(z)$$

where large n gives accuracy, the $a_i(t)$ are to be found, and the chosen basis functions $\phi_i(z)$ satisfy $\phi_i(0) = 0$ and $\phi_i'(L) = 0$, where prime denotes derivative with respect to space variable. We now use the method of weighted residuals [43]. Defining symmetric positive definite matrices $\mathbf{B}$ and $\mathbf{C}$ by $B_{ij} = \int_0^L b\,\phi_{i,z}\,\phi_{j,z}\,dz$ and $C_{ij} = \int_0^L c\,\phi_i\,\phi_j\,dz$, and writing a for the vector of coefficients $a_i(t)$, we obtain

$$\mathbf{C}\dot{a} = -\mathbf{B}\mathbf{a}.$$

On suitable choice of ϕ_i, $\mathbf{C}$ is the identity matrix. Then

$$\dot{\mathbf{a}} = -\mathbf{B}\mathbf{a}.$$

With sufficiently complex microstructural behavior, $\mathbf{B}$ may usefully be treated as random.

Let us study a random $\mathbf{B}$. Begin with $\mathbf{A}$, an $n \times n$ matrix, with n large. Let the elements of $\mathbf{A}$ be random, i.i.d. uniformly in $(-0.5, 0.5)$. Let $\mathbf{B} = \mathbf{A}^T\mathbf{A}$. $\mathbf{B}$ is symmetric positive definite with probability one. We will solve

$$\dot{\mathbf{x}} = -\mathbf{B}\mathbf{x}. \tag{4.2}$$

Solution is done numerically using, for initial conditions, a random $n \times 1$ column matrix $\mathbf{x}_0$ whose elements are i.i.d. uniformly in $(-0.5, 0.5)$. The process is repeated 30 times, with a new $\mathbf{B}$ and $\mathbf{x}_0$ each time. The results, for $n = 400$, are shown in Fig. 4.2.

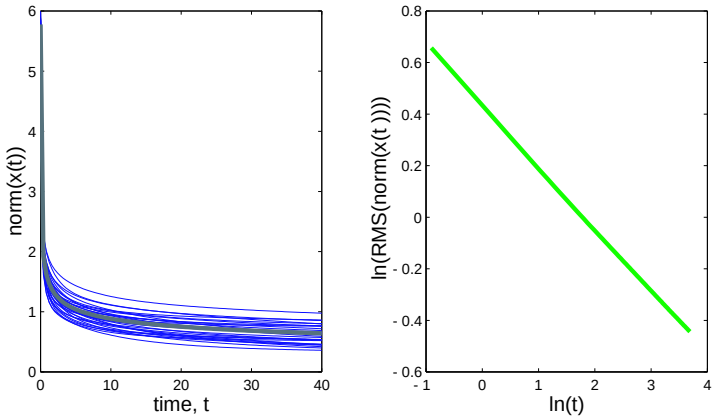

Figure 4.2: Left: $\text{norm}(\mathbf{x}) = \sqrt{\mathbf{x}^T\mathbf{x}}$ against time. 30 individual solutions (thin lines) as well as their RMS values (thick gray). Right: RMS value of $\text{norm}(\mathbf{x})$ against time is a straight line on a log-log scale. A fitted line has slope $-0.24 \approx -1/4$.

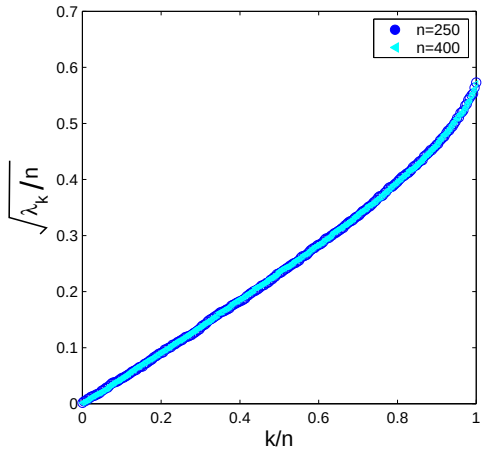

Figure 4.3: Eigenvalues of $\mathbf{B}$ for $n = 250$ and 400.

The solutions, though they are sums of exponentials, decay on average like $t^{-1/4}$. Why? This question will be answered in the following section.

4.2 Fractional Order Power Law: A Theoretical Study

The answer lies in the eigenvalues of $\mathbf{B}$. The spectra of random matrices comprise a subject in their own right. Here, we use numerics to directly obtain a simple fact. Let $n = 250$. Take a random $n \times n$ matrix $\mathbf{B}$ as above. Let λ_k, $k = 1, 2, \cdots, n$, be its eigenvalues in increasing order. Figure 4.3 shows $\sqrt{\dfrac{\lambda_k}{n}}$ plotted against k/n.

Superimposed are the same quantities for $n = 400$. The coincidence between plots indicates a single underlying curve as $n \to \infty$. That curve passes through the origin, and can be taken as linear if we restrict time to values $t \gg \mathcal{O}(1/n)$, by when solution components from the large eigenvalues have decayed to negligible values. Then

$$\sqrt{\frac{\lambda_k}{n}} = \beta \frac{k}{n} \tag{4.3}$$

for some $\beta > 0$. For simplicity, we ignore the variation of eigenvalues around the linear fit.

The solution for the i^{th} element of $\mathbf{x}$ is of the form

$$x_i(t) = \sum_{k=1}^{n} a_{ik}\, e^{-\lambda_k t} = \sum_{k=1}^{n} a_{ik}\, e^{-\beta^2 k^2 t/n}\,, \tag{4.4}$$

where the coefficients a_{ik}, by randomness of $\mathbf{x}_0$ and $\mathbf{B}$ and orthonormality of eigenvectors of the latter, are taken as random, i.i.d., and with zero expected value. The variance is then (upon scaling the initial condition suitably)

$$\text{var}(x_i(t)) = \frac{1}{n\sqrt{2\beta^2 t}} \sum_{k=1}^{n} \sqrt{\frac{2\beta^2 t}{n}}\, e^{-2\beta^2 k^2 t/n}\,.$$

Define $\xi = \sqrt{\dfrac{2\beta^2 t}{n}}\, k$. For $\beta^2 t \ll n$ and $n \gg 1$, the sum is approximated by an integral:

$$\text{var}(x_i(t)) = \frac{1}{n\sqrt{2c^2 t}} \int_0^\infty e^{-\xi^2}\, d\xi = \frac{C^2}{n\sqrt{t}}\,,$$

for some C. Finally, $\text{RMS}\left(\sqrt{\mathbf{x}^T\mathbf{x}}\right)$ is (using independence of the components of $\mathbf{x}$)

$$\text{RMS}\left(\mathbf{x}^T\mathbf{x}\right) = \sqrt{\sum_{i=1}^{n} \text{var}(x_i(t))} = \frac{C}{t^{1/4}}, \tag{4.5}$$

which explains the numerical result. Our point is that no special microstructural damping mechanisms are needed for fractional derivatives to appear, if there is the right sort of disorder or randomness.

After having studied some disordered viscoelastic systems in this chapter and the previous one, now we proceed to develop approximation scheme for fractional derivatives and integrals.

Chapter 5

Galerkin Projections for Fractional Order Derivatives: Global Shape Functions

In this chapter we replace the fractional order derivative with another infinite dimensional system which involves a partial differential equation (PDE). The Galerkin projection is applied to this PDE to obtain a set of ordinary differential equations (ODEs), whereby approximating a fractional derivative with a set of ODEs. We use global shape functions for Galerkin projection. The material of this chapter is taken from [44].

5.1 Introduction

Ordinary differential equations (ODEs) involving fractional order derivatives are used to model a variety of systems, of which an important engineering application lies in viscoelastic damping [6, 7, 8, 9]. Another important application of fractional derivatives lies in control theory (see, e.g., [1, 11, 14, 15]). Linear ODEs with fractional order derivatives or differintegrals are studied using Laplace [6, 7] and Fourier transforms [8]. Linear systems with half order derivatives have also been solved using an eigenvector expansion [45].

Nonlinear ODEs involving fractional order derivatives can be solved numerically.

But the infinite dimensional nature of these systems leads to high computation cost for simulation of long time behaviors, as we will discuss below.

In present and next chapter we present a numerical technique to solve ODEs with fractional order derivatives using a Galerkin projection for reducing the infinite dimensional system to a finite dimensional one. The approximation obtained is specific to the fractional order of the derivative of interest; but it can be used without further change in any system where a derivative of that order appears. This novel method is easy to apply and is computationally more efficient than direct integration based numerical methods for long time simulations. Both global shape functions as well as finite elements are used for the Galerkin projections. The discretization strategy is refined in a few steps to provide motivation for the final strategy adopted. For that final strategy, numerical accuracy obtained is excellent. The method is expected to be most useful for nonlinear ODEs with fractional order derivatives, but can of course be used for linear systems as well. The principal advantage offered by our method, while providing demonstrated accuracy, lies in time savings relative to straightforward numerical integration. Other finite dimensional approximations, as in [19] and [46], will give similar time savings. However, the conceptual basis of our approximation is different and, in our opinion, simpler.

5.2 Background

A fractional derivative of order $n+q$ is given, using the Riemann-Liouville definition [47, 48, 49], as

$$\mathrm{D}_b^{n+q}[x(t)] \equiv \frac{d^{n+q}x(t)}{[d(t-b)]^{n+q}} = \frac{1}{\Gamma(-q)}\frac{d^n}{dt^n}\left[\int_b^t \frac{x(\tau)}{(t-\tau)^{1+q}}d\tau\right], \tag{5.1}$$

where $-1 < q < 0$ and n is a positive integer. For many practical problems it is assumed that the system starts from rest, so that $x(t) \equiv 0$ for $t \leq 0$. In such cases D_b^{n+q} becomes D_0^{n+q}, and we will henceforth drop the b-subscript assuming that the system starts at $b = 0$. Hence the fractional derivative of Equation (5.1) becomes

$$\mathrm{D}^{n+q}[x(t)] = \frac{1}{\Gamma(-q)}\frac{d^n}{dt^n}\left[\int_0^t \frac{x(\tau)}{(t-\tau)^{1+q}}d\tau\right].$$

For many practical problems in dynamics, the order of the fractional derivative lies between 0 and 1, and we will consider fractional values restricted between these limits as

well. Accordingly, substituting $n = 1$ in the above, we get

$$\mathrm{D}^{1+q}[x(t)] = \frac{1}{\Gamma(-q)} \frac{d}{dt} \left[\int_0^t \frac{x(\tau)}{(t-\tau)^{1+q}} d\tau \right] ,$$

which in turn can be rewritten as

$$\mathrm{D}^{\alpha}[x(t)] = \frac{1}{\Gamma(1-\alpha)} \frac{d}{dt} \left[\int_0^t \frac{x(\tau)}{(t-\tau)^{\alpha}} d\tau \right] ,$$

where $0 < \alpha < 1$. Two equivalent forms of the above are given as

$$\mathrm{D}^{\alpha}[x(t)] = \frac{1}{\Gamma(1-\alpha)} \left[\frac{x(0)}{t^{\alpha}} + \int_0^t \frac{\dot{x}(\tau)}{(t-\tau)^{\alpha}} d\tau \right] = \frac{1}{\Gamma(1-\alpha)} \left[\frac{x(0)}{t^{\alpha}} + \int_0^t \frac{\dot{x}(t-\tau)}{\tau^{\alpha}} d\tau \right] . \tag{5.2}$$

In each equivalent expression of Equation (5.2), the first term has a singularity at $t = 0$ but disappears if $x(0) = 0$ (as in, e.g., [18]; we assume the same here), giving

$$\mathrm{D}^{\alpha}[x(t)] = \frac{1}{\Gamma(1-\alpha)} \int_0^t \frac{\dot{x}(t-\tau)}{\tau^{\alpha}} d\tau \, . \tag{5.3}$$

The above integral involves a singular kernel. We mention in passing that substituting $\bar{\tau} = \tau^{(1-\alpha)}$ gives

$$\mathrm{D}^{\alpha}[x(t)] = \frac{1}{\Gamma(2-\alpha)} \int_0^{t^{1-\alpha}} \dot{x}(t - \bar{\tau}^{1/(1-\alpha)}) d\bar{\tau} \, . \tag{5.4}$$

In this way, the singularities can be removed for easier computation; the price paid is that the history of $\dot{x}$, which appears inside the integral, may need to be resampled (using, e.g., splines) before numerical evaluation [22]. However, direct integration of the solution history at each time step is not the subject of this work; our aim is to avoid such integration.

Equation (5.4) shows that the fractional order derivative is non-local. It requires the history of $\dot{x}(\tau)$ from $\tau = 0$ to $\tau = t$. Any ODE involving such a fractional derivative is therefore infinite dimensional.

While numerically solving an ODE with such a fractional derivative through direct evaluation of the integral of Equation (5.4), we face the following problem. Assuming time steps of length Δt, the integral evaluated at instant $t = k\Delta t$ requires $\mathcal{O}(k)$ arithmetic operations. To reach the instant $t = k\Delta t$, therefore, we need

$$\mathcal{O}\left(\sum_{i=1}^{k} i \right) = \mathcal{O}\left(k^2\right)$$

operations. In other words, for a simulation time duration t, we need $\mathcal{O}(t^2)$ calculations. For long times, this is prohibitively high. Yet long times may be unavoidable for, e.g., studying the steady state dynamics of lightly damped or chaotic systems, or nonlinear systems under random forcing using Monte Carlo methods (see, e.g., [50]).

An approximation scheme that does not suffer from this $\mathcal{O}(t^2)$ requirement, but can instead compute solutions in $\mathcal{O}(t)$ time, would be useful. Such schemes may involve finite dimensional and local approximations for the fractional order derivative (the scheme we present below does).

Our scheme is comparable with that of [51] which, though not identical, is quite similar in spirit to ours. In this work, however, we go beyond the treatment of [51] and develop a Galerkin projection as well as finite elements for the dimensional reduction; in this way, we are able to provide a clearer picture of the performance and accuracy of the method. We also mention the work of [52], where there is no finite dimensional approximation *per se*, but the integral required for evaluating the fractional derivative is numerically approximated after subdividing the interval $(0, t)$ into a number of exponentially decreasing contiguous subintervals: the net result is something like $\mathcal{O}(t \ln t)$ time, which is almost as good as $\mathcal{O}(t)$. Unlike [52], our approach *a priori* approximates the fractional derivative operator itself, rather than making approximations while computing the value of the fractional order derivative. Finally, we mention a paper by [53], which critiques [51] and points out asymptotic aspects of the approximation: in particular, short-time and high-frequency asymptotic behavior are *not* captured by Yuan and Agrawal's approximation. Our scheme, too, has this apparent flaw. This flaw may be important from a restricted mathematical viewpoint. However, as we discuss at the end of next chapter, it is insignificant from at least some engineering perspectives.

5.3 Transfer functions and Padé approximants

A way to obtain finite dimensional approximations might be to directly approximate the transfer function (see, e.g., [54]) of the fractional derivative by a rational function, which can then be converted into an equivalent set of ODEs. Considering half-order derivatives, for example, the transfer function of interest is $\sqrt{s}$.

A well known method of obtaining rational approximations is that of Padé approximants, which are rational functions that match the Taylor series expansion of the original function up to a given number of terms. Unfortunately, we have found that Padé approximants for $\sqrt{s}$ give *unstable* transfer functions. Thus, approximating the transfer function directly is nontrivial. Note that considerations of transfer functions can indeed be used to construct very good finite dimensional approximations (see [19] and references therein).

In this work, we do not attempt to directly approximate the transfer function. Following an indirect route, we convert the given infinite dimensional system involving a fractional order derivative into a different infinite dimensional system involving a partial differential equation (PDE) in which α, the fractional order of the derivative (assumed to lie between 0 and 1), appears as a free parameter. We then approximate solutions of the PDE using a Galerkin projection and, finally finite elements.

5.4 An infinite dimensional system

Consider the PDE (which could also be viewed as an ODE in t with a free parameter ξ)

$$\frac{\partial}{\partial t}u(\xi,t) + \xi^{\left(\frac{1}{\alpha}\right)}\, u(\xi,t) = \delta(t)\,, \quad u(\xi,0^-) \equiv 0\,, \tag{5.5}$$

where $\alpha > 0$ and $\delta(t)$ is the Dirac delta function. The solution is

$$u(\xi,t) = h(\xi,t) = \exp(-\xi^{1/\alpha}\, t)\,, \tag{5.6}$$

where the notation $h(\xi,t)$ is used to denote "impulse response function." On integrating h with respect to ξ between 0 and ∞ we get a function only of t, given by

$$g(t) = \int_0^\infty h(\xi,t)\, d\xi = \frac{\Gamma(1+\alpha)}{t^\alpha}\,. \tag{5.7}$$

Abstractly, $g(t)$ is simply the impulse response of a linear, constant coefficient system starting from rest, provided we think of $\displaystyle\int_0^\infty h(\xi,t)\, d\xi$ as the output of the system.

Now if we replace the forcing $\delta(t)$ in Equation (5.5) with some sufficiently well behaved function $\dot{x}(t)$, then the corresponding response $r(t)$ of the same system, again

starting from rest at $t = 0$, is (the last two expressions below are equivalent)

$$r(t) = \int_0^t g(t-\tau)\dot{x}(\tau)\,d\tau = \Gamma(1+\alpha)\int_0^t \frac{\dot{x}(\tau)}{(t-\tau)^\alpha}\,d\tau = \Gamma(1+\alpha)\int_0^t \frac{\dot{x}(t-\tau)}{\tau^\alpha}\,d\tau. \quad (5.8)$$

On comparison with Equation (5.3), we find that

$$r(t) \equiv \Gamma(1+\alpha)\Gamma(1-\alpha)\mathrm{D}^\alpha[x(t)]\,,$$

provided $x(t) \equiv 0$ for $t \leq 0$, and $0 < \alpha < 1$.

In this way, we have replaced an α order derivative by the following operations:

1. Solve
$$\frac{\partial}{\partial t}u(\xi,t) + \xi^{\left(\frac{1}{\alpha}\right)}\,u(\xi,t) = \dot{x}(t)\,, \quad u(\xi,0^-) \equiv 0. \quad (5.9)$$
2. Then integrate to find
$$\mathrm{D}^\alpha x(t) = \frac{1}{\Gamma(1-\alpha)\Gamma(1+\alpha)}\int_0^\infty u(\xi,t)\,d\xi\,. \quad (5.10)$$

There is no approximation so far. The system chosen above was prompted by the studies in Chapters 3 and 4.

Equation (5.9) represents an infinite dimensional system, and so we have replaced one infinite dimensional system (fractional derivative) with another. The advantage gained is that we can use a Galerkin projection to reduce Equation (5.9) to a finite dimensional system of ODEs. In this way, a fractional derivative will be replaced by a finite number of ODEs, and numerical solution up to time t will require $\mathcal{O}(t)$ operations.

Observe here that if we let $\xi = y^{2\alpha}$ and $u(\xi,t) = y^{(1-2\alpha)}\,\phi(y,t)$ in Equation (5.5), then the present formulation becomes equivalent to that of [51]. However, the approximation scheme of [51] is different from ours as it involves the Laguerre integral formula, whereas our approximation scheme is based on Galerkin projection.

5.5 Galerkin projection

For the Galerkin projection, we assume that Equation (5.9) is satisfied by

$$u(\xi,t) \approx \sum_{i=1}^{n} a_i(t)\phi_i(\xi)\,,$$

where n is finite, the ϕ_i are to be chosen by us, and the a_i are to be solved for. The ϕ_i are called shape functions. The choice of shape functions will be discussed in the next section. Below, we outline the Galerkin procedure for Equation (5.9).

Substituting the approximation for $u(\xi,t)$ in Equation (5.9), we define

$$R(\xi,t) = \sum_{i=1}^{n} \left\{ \dot{a}_i(t)\phi_i(\xi) + \xi^{\left(\frac{1}{\alpha}\right)} a_i(t)\phi_i(\xi) \right\} - \dot{x}(t)\,,$$

where $R(\xi,t)$ is called the residual. This residual is made orthogonal to the shape functions, yielding n equations:

$$\int_0^\infty R(\xi,t)\phi_m(\xi)\,d\xi = 0\,, \quad m = 1,2,\cdots,n. \tag{5.11}$$

The integrals above need to exist; this will influence the choice of ϕ_i in the next section. Equations (5.11) constitute n ODEs, which can be written in the form

$$\mathbf{A}\dot{\mathbf{a}} + \mathbf{B}\,\mathbf{a} = \mathbf{c}\,\dot{x}(t)\,, \tag{5.12}$$

where $\mathbf{A}$ and $\mathbf{B}$ are $n \times n$ matrices, $\mathbf{a}$ is an $n \times 1$ vector containing a_i's, and $\mathbf{c}$ is an $n \times 1$ vector. The entries of $\mathbf{A}$, $\mathbf{B}$ and $\mathbf{c}$ are

$$\mathrm{A}_{mi} = \int_0^\infty \phi_m(\xi)\,\phi_i(\xi)\,d\xi\,, \quad \mathrm{B}_{mi} = \int_0^\infty \xi^{1/\alpha}\phi_m(\xi)\,\phi_i(\xi)\,d\xi \quad \text{and } \mathrm{c}_m = \int_0^\infty \phi_m(\xi)\,d\xi\,. \tag{5.13}$$

In this work, we assume that the shape functions are always chosen such that the above integrals exist. The choices of shape functions may therefore depend on α. In all numerical examples that follow, we have used shape functions for which the above integrals are finite.

During numerical solution of (say) a second order system including both $\ddot{x}$ as well as $\mathrm{D}^\alpha[x(t)]$, we will use the quantities x and $\dot{x}$ as parts of the state vector, along with

the a_i above. Having access to $\dot{x}$ at each instant, therefore, we can solve Equation (5.12) numerically to obtain the a_i. Finally

$$\mathrm{D}^{\alpha}[x(t)] \approx \frac{1}{\Gamma(1+\alpha)\Gamma(1-\alpha)}\,\mathbf{c}^{T}\mathbf{a}, \tag{5.14}$$

where the T superscript denotes matrix transpose.

Advantages of the approximation proposed here, as we will demonstrate with examples, are that (i) by suitable choice of shape functions we can hope to obtain somewhat uniform performance over a given frequency range, (ii) systematic refinement of the approximation involves straightforward calculations, and (iii) the approximation depends on α, the fractional order of the derivative, but not on the system where this derivative appears.

5.6 Choice of shape functions

The shape functions are chosen keeping in mind that high frequency behavior (on short time scales) corresponds to large values of ξ, and low frequency behavior (on long time scales) to small values of ξ, due to the role ξ plays in $\exp(-\xi^{1/\alpha}\,t)$ (see Equation (5.6)).

Since the shape functions need to be defined over an infinite domain, we introduce an auxiliary variable z with a bounded domain as:

$$z = \frac{\xi^2 + \dfrac{\xi}{1+\xi^2}}{1+\xi^2}. \tag{5.15}$$

A plot of $z(\xi)$ is given in Figure 5.1. The choice of z as a function of ξ is somewhat arbitrary. It is merely one choice that satisfies the following conditions:

1. z increases monotonically from 0 to 1 as ξ increases from 0 to ∞.

   This condition is needed to inevitably map the infinite interval to the unit interval. Figure 5.1 verifies this condition.

2. z is approximately linear in ξ for small ξ.

   Figure 5.1 verifies this condition as well. This condition is useful for capturing reasonable variations for small ξ, which gives good performance over long times (low frequencies) as mentioned above.

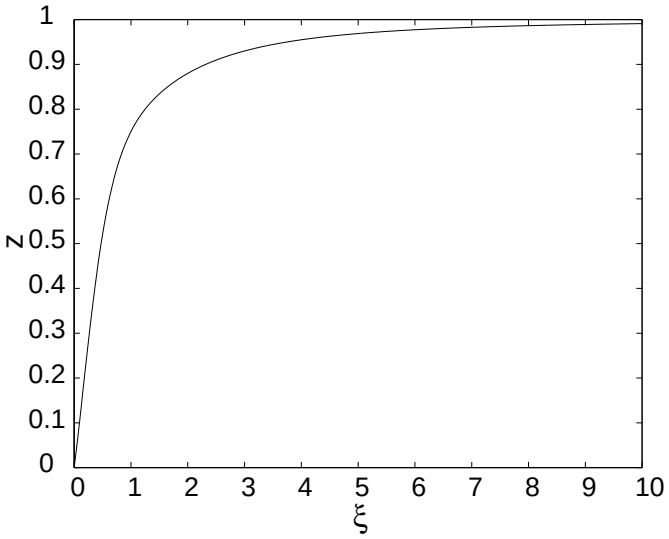

Figure 5.1: Plot of z versus ξ.

For the given choice of $z(\xi)$ and temporarily looking at $\alpha = 1/2$ (we will consider other α values later), we choose the following shape functions:

$$\phi_1(\xi) = 1 - z \quad \text{and} \quad \phi_i(\xi) = \sin\left((i-1)\pi z\right) , \quad \text{for } i = 2, 3, \cdots, n\,.$$

Again, there is arbitrariness in the choice of shape functions. If, for any i,

$$\lim_{z \to 1} \phi_i \neq 0, \tag{5.16}$$

then not all integrals involved in the approximation remain bounded. Thus, we have assumed that the function to be represented is arbitrary on the unit interval except that it is continuous, and zero at the right endpoint. The above choice of shape functions can, for large enough n, accurately match any such function. This is because any function $f(z)$ which satisfies $f(1) = 0$, upon subtraction of $(1 - z)f(0)$, gives a function that is zero at both $z = 0$ as well as $z = 1$; and such functions can be represented using Fourier sine series.

The shape functions chosen above are to be substituted in Equation (5.13), which still includes the free parameter $0 < \alpha < 1$, to obtain matrices $\mathbf{A}$, $\mathbf{B}$ and $\mathbf{c}$. Numerical evaluation of the integrals is required.

The matrices $\mathbf{A}$, $\mathbf{B}$ and $\mathbf{c}$ computed for $\alpha = 1/2$ and $n = 7$ are given in the appendix. Calculations with $\alpha = 1/2$ but other values of n were carried out as well, but only graphical results are presented in Section 5.8 for those cases.

5.7 Accuracy

The above approximation turns out to be reasonably good, but we will eventually do much better (Section 6.4). For now, we check the above approximation by noting from Equation (5.14) that

$$\mathcal{F}(\mathrm{D}^\alpha x(t)) = (i\omega)^\alpha \mathcal{F}(x) \approx \frac{1}{\Gamma(1+\alpha)\Gamma(1-\alpha)}\,\mathbf{c}^T \mathcal{F}(\mathbf{a})\,,\ \text{when } x(t) \equiv 0 \text{ for } t \leq 0,$$

where, $\mathcal{F}(\cdot)$ denotes the Fourier transform. From Equation (5.12)

$$\mathcal{F}(\mathbf{a}) = i\omega\,(i\omega\mathbf{A} + \mathbf{B})^{-1}\mathbf{c}\,\mathcal{F}(x)\,.$$

Combining above two and simplifying we get

$$(i\omega)^\alpha \approx \frac{1}{\Gamma(1+\alpha)\Gamma(1-\alpha)} i\omega\,\mathbf{c}^T (i\omega\mathbf{A} + \mathbf{B})^{-1}\mathbf{c}\,.$$

Right hand side of the above is the frequency response function (FRF) of the α-order fractional derivative, obtained by our Galerkin approximation scheme.

We choose $\alpha = 1/2$ and $n = 10$ for examination. In Figure 5.2, in the first and third plot, we compare the magnitude and phase of the FRF obtained using the above expression with that of $(i\omega)^{1/2}$. The second plot presents relative error of the approximation. The approximation is good for frequencies over about 3 orders of magnitude, and can be refined further. The error is not uniform over the frequency range of interest, but can be made so with suitable choice of shape functions. This will be demonstrated later using finite elements.

5.8 Numerical examples

5.8.1 A linear system

Consider the system

$$\mathrm{D}^2 x(t) + \mathrm{D}^{1/2} x(t) + x(t) = \sin(2\pi t), \tag{5.17}$$

with $x(t) \equiv 0$ for $t \leq 0$ and $\dot{x}(0) = 0$.

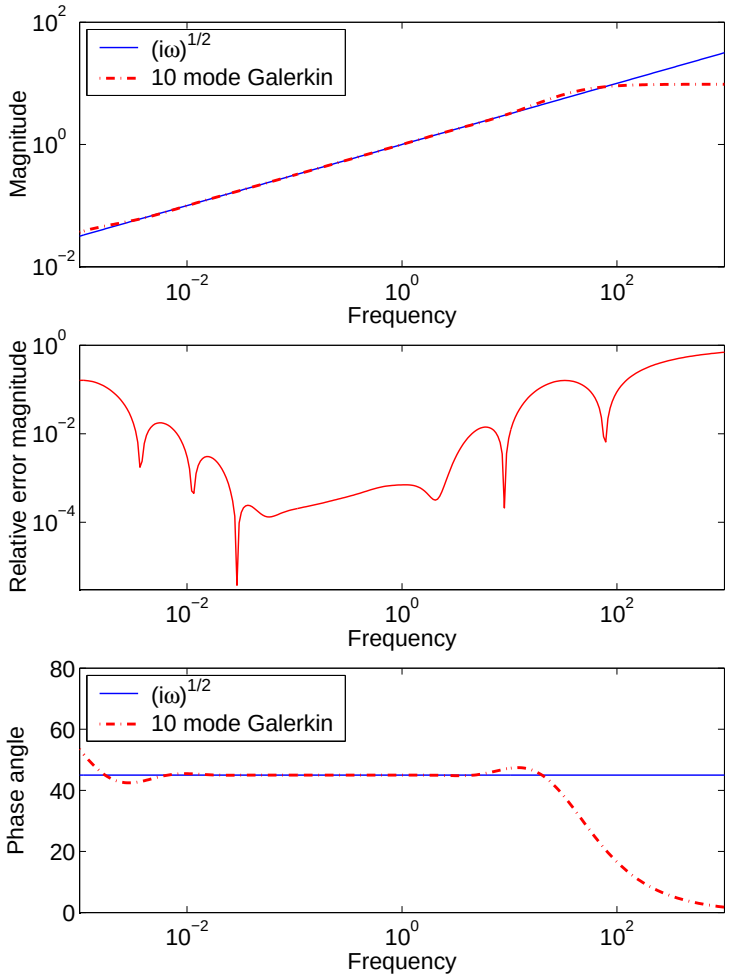

Figure 5.2: Comparison between magnitude and phase angle (given in degrees) of $(i\omega)^{1/2}$, and approximated FRF using 10 mode Galerkin.

We present below the numerical results obtained using our method along with direct numerical solutions where the fractional derivative was calculated by evaluating the integral of Equation (5.4) (this numerical integration was also used in [22]).

For completeness, we outline the numerical procedure followed for $n = 7$. Combining Equations (5.12), (5.14) and (5.17), we now write

$$\ddot{x} + \frac{2}{\pi}\,\mathbf{c}^T\mathbf{a} + x = \sin(2\pi t), \tag{5.18}$$

$$\mathbf{A}\dot{\mathbf{a}} + \mathbf{B}\,\mathbf{a} - \mathbf{c}\,\dot{x} = \mathbf{0}\,, \tag{5.19}$$

with initial conditions $x(0) = 0$, $\dot{x}(0) = 0$, and $\mathbf{a}(0) = \mathbf{0}$, where matrices $\mathbf{A}$, $\mathbf{B}$ and

c are evaluated by numerical integration as described above, and have been provided for reference in the appendix.

Results obtained using the Galerkin approximation for $n = 3$, 5, 7 and 10 are shown first in Figure 5.3, where it is seen that the solutions for $n = 3$ and 5 show some small mismatch, but the solutions for $n = 7$ and 10 are indistinguishable to plotting accuracy. Thus, satisfactory convergence is obtained for reasonable n and $\alpha = 1/2$.

In Figure 5.4 we compare our approximate solutions with direct numerical solutions of the original system (using the technique used by [22]). Both $x(t)$ and $\dot{x}(t)$ plots agree very well with the direct numerical solution. As mentioned earlier, however, the present technique requires $\mathcal{O}(t)$ computations for the solution up to time t, while the direct numerical technique requires $\mathcal{O}(t^2)$ computations.

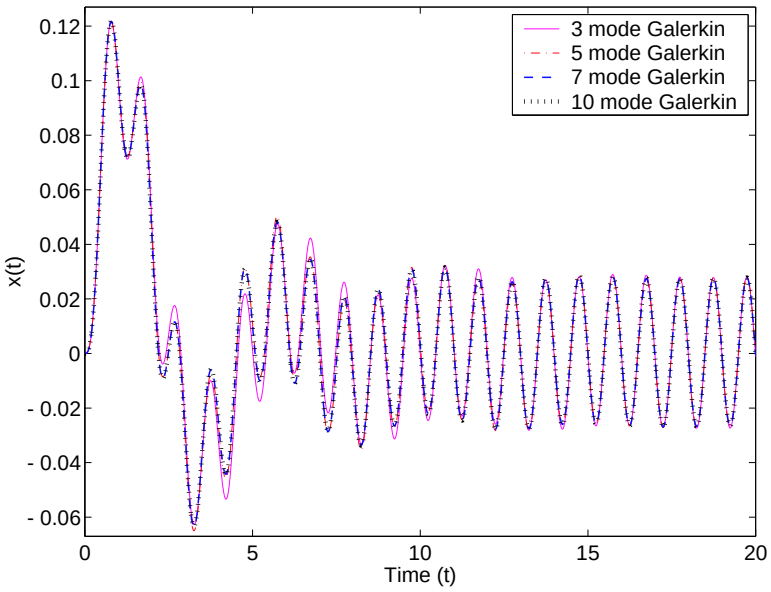

Figure 5.3: $x(t)$ against time, for $n = 3$, 5, 7 and 10.

5.8.2 A nonlinear system

Consider

$$\mathrm{D}^2 x(t) + \mathrm{D}^{1/2} x(t) - x(t) + x(t)^3 = \sin(2\pi t), \tag{5.20}$$

with $x(t) \equiv 0$ for $t \leq 0$ and $\dot{x}(0) = 0$.

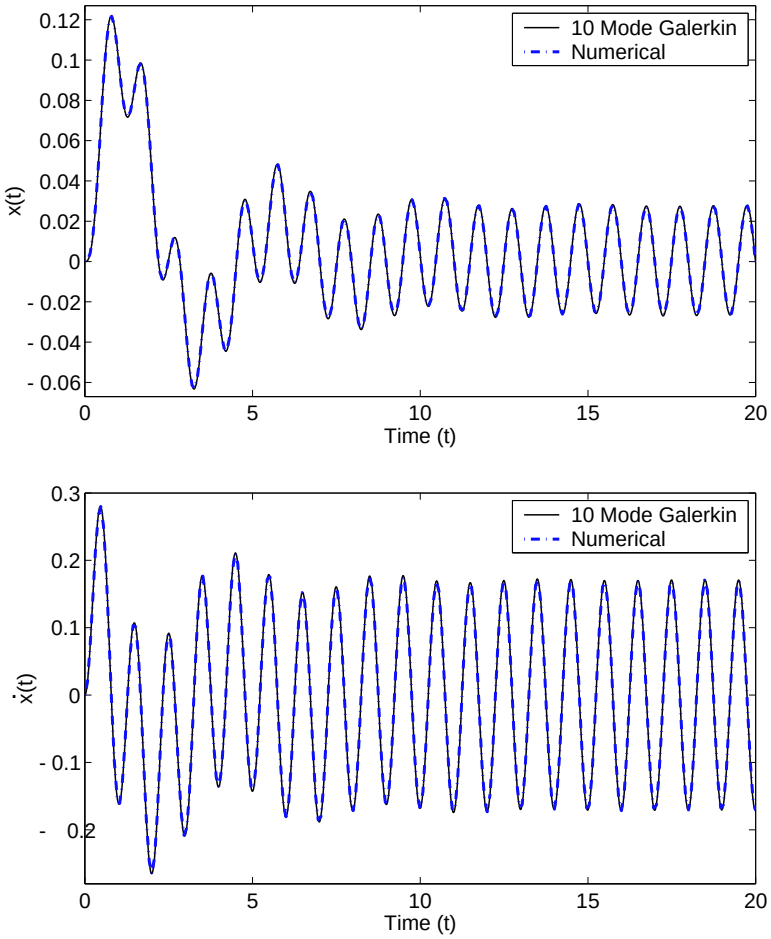

Figure 5.4: $x(t)$ and $\dot{x}(t)$ against time, for Galerkin ($n = 10$) and direct numerical solution.

In Figure 5.5 we compare our approximation with the direct numerical solution. Again, there is very good agreement.

Having described the basic method and noted its apparently promising accuracy, we now move to finite element approximations. The shape functions of Section 5.6 will be replaced with ones defined over finite elements. We will use the two simplest choices of element basis functions: the piecewise constant and the "hat" functions (the shape function for the last element will need to be different, as discussed below). We will also eventually consider values of α other than $1/2$.

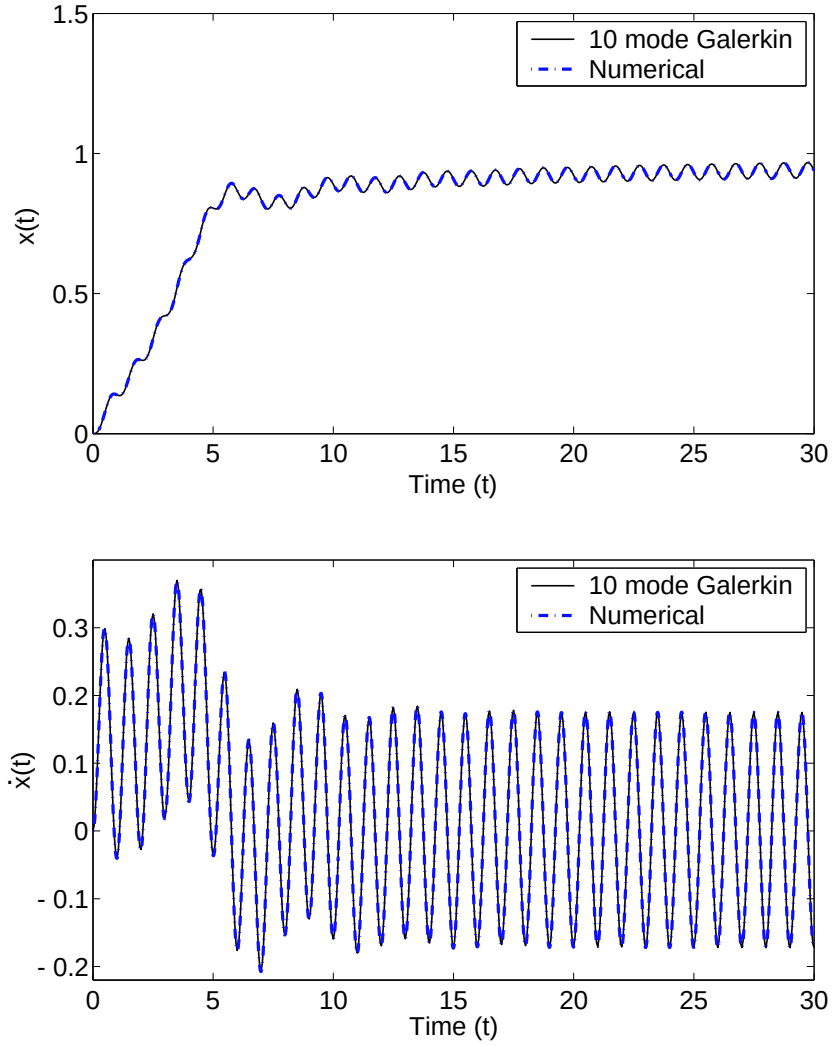

Figure 5.5: Results for Equation (5.20).

In this chapter we have developed the Galerkin approximation scheme using global shape functions. We now proceed to develop the finite element based Galerkin approximation scheme in the next chapter.

Chapter 6

Galerkin Projection for Fractional Order Derivatives: Finite Elements

A Galerkin projection based approximation scheme for fractional order derivatives was proposed in last chapter, where the global shape functions were used for Galerkin projection. In this chapter we use finite elements for Galerkin projection. The finite element based discretization strategy is improved in a few steps until, finally, very good performance is obtained over a user-specifiable frequency range (not including zero). The material of this chapter is taken from [44].

6.1 Finite element formulation: uniform element size

We first develop an approximation using finite elements of uniform length defined on the unit interval. This will help clarify the need for nonuniform elements.

We define the following auxiliary variable $\eta(\xi)$ (note the change from the z used in Equation (5.15))

$$\eta(\xi) = \frac{\xi}{1+\xi} \tag{6.1}$$

which maps the infinite domain to the unit interval [0,1]. Comparing with Equation (5.15), we note that now ξ can be easily solved for in terms of η. A minor price paid is that, for

large ξ, η converges to 1 more slowly than z. This affects the restrictions we must place on the shape function(s) used on last element so as to ensure existence of all integrals involved in the approximation; we will use suitable shape functions for that element below.

Here, again, we temporarily restrict attention to $\alpha = 1/2$.

6.1.1 Piecewise constant case

For the piecewise constant case, the shape functions used are as follows (see Figure 6.1)

$$\phi_i(\eta) = \begin{cases} 1 & p_{i-1} < \eta \le p_i, \\ 0 & \text{elsewhere,} \end{cases} \qquad \text{for } i = 1, 2, \ldots, n-1, \tag{6.2a}$$

$$\phi_n(\eta) = \begin{cases} \left(\dfrac{1-\eta}{1-p_{n-1}}\right)^2 & p_{n-1} < \eta \le 1, \\ 0 & \text{elsewhere}\,, \end{cases} \tag{6.2b}$$

where the element nodal point $p_0 = 0$, and $p_i - p_{i-1} = 1/n$ for each i. Notice that the shape function on the n^{th} subinterval is the only one that needs attention to ensure boundedness of integrals; exponent 2 in the last shape function ensures this requirement (for $\alpha = 1/2$).

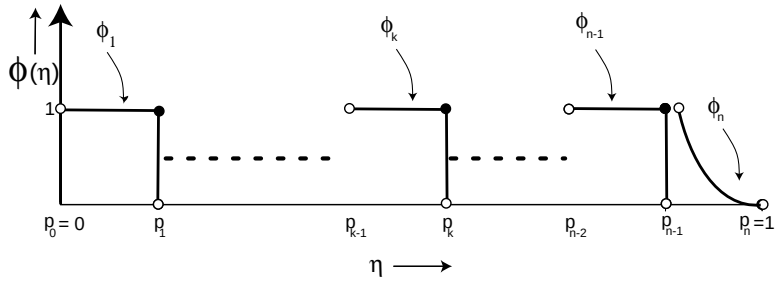

Figure 6.1: Piecewise constant shape functions. The solid and hollow circles at p_{n-1} are shown nearly coincident for visibility alone; in reality, they coincide exactly. The shape function on the last element is chosen to ensure boundedness of integrals.

Now a Galerkin projection similar to Section 5.5 is performed after changing the

integration variable to η, giving

$$\int_0^1 \left(\sum_{i=1}^{n} \left\{ \dot{a}_i(t)\phi_i(\eta) + \left(\frac{\eta}{1-\eta}\right)^{\left(\frac{1}{\alpha}\right)} a_i(t)\phi_i(\eta) \right\} - \dot{x}(t) \right) \phi_m(\eta) \frac{1}{(1-\eta)^2} \, d\eta = 0 \,, \tag{6.3}$$

for $m = 1, 2, \cdots, n$. Equations (6.3) constitute n ODEs, which can be written in the form of Equations (5.12). On combining them with the ODE at hand, we get an initial value problem which can be solved numerically in $\mathcal{O}(t)$ time as before.

6.1.2 Hat functions

For better accuracy, we can increase the smoothness of the shape functions. Here, we use the "hat" shape functions which are defined as follows (see Figure 6.2):

$$\phi_1(\eta) = \begin{cases} \dfrac{p_1 - \eta}{p_1}, & 0 \le \eta \le p_1, \\ \\ 0 \qquad \text{elsewhere}, \end{cases}$$

$$\phi_{i+1}(\eta) = \begin{cases} \dfrac{\eta - p_{i-1}}{p_i - p_{i-1}}, & p_{i-1} \le \eta \le p_i, \\ \\ \dfrac{p_{i+1} - \eta}{p_{i+1} - p_i}, & p_i \le \eta \le p_{i+1}, \\ \\ 0 \qquad \text{elsewhere}, \end{cases} \qquad \text{for } i = 1,\, 2,\, \ldots,\, n-2,$$

and

$$\phi_n(\eta) = \begin{cases} \dfrac{\eta - p_{n-2}}{p_{n-1} - p_{n-2}}, & p_{n-2} \le \eta \le p_{n-1}, \\ \left(\dfrac{1-\eta}{1-p_{n-1}}\right)^2, & p_{n-1} \le \eta \le 1, \\ 0 & \text{elsewhere}, \end{cases} \tag{6.4}$$

where again $p_0 = 0$, and $p_i - p_{i-1} = 1/n$ for each i.

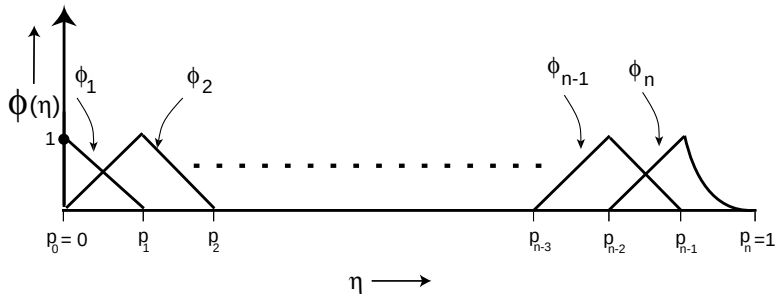

Figure 6.2: Hat shape functions.

Here, we have chosen the last shape function to be identical over the last subinterval to that used with the piecewise constant shape functions (*i.e.,* the quadratic shape function) to ensure the boundedness of all the involved integrals over the last subinterval (valid for $\alpha = 1/2$). Once again, the Galerkin projection gives n ODEs in the matrix form Equation (5.12), which on combining with the ODE at hand reduces to an initial value problem which is solved numerically.

We now check accuracy by comparing FRFs, as described in Section 5.7 (some of these results are also presented in [41]). The FRF for the less accurate piecewise constant case is calculated for 75 elements, whereas only 15 elements are used for the case of hat functions. Results are shown in Figure 6.3. It is clear that both approximations work well over a significant frequency range. Closer examination of relative errors verified (plots not presented here) that the hat functions give superior accuracy within some frequency range, even with far fewer elements.

It should be that the phase angle of the FRF is given in degrees throughout this chapter.

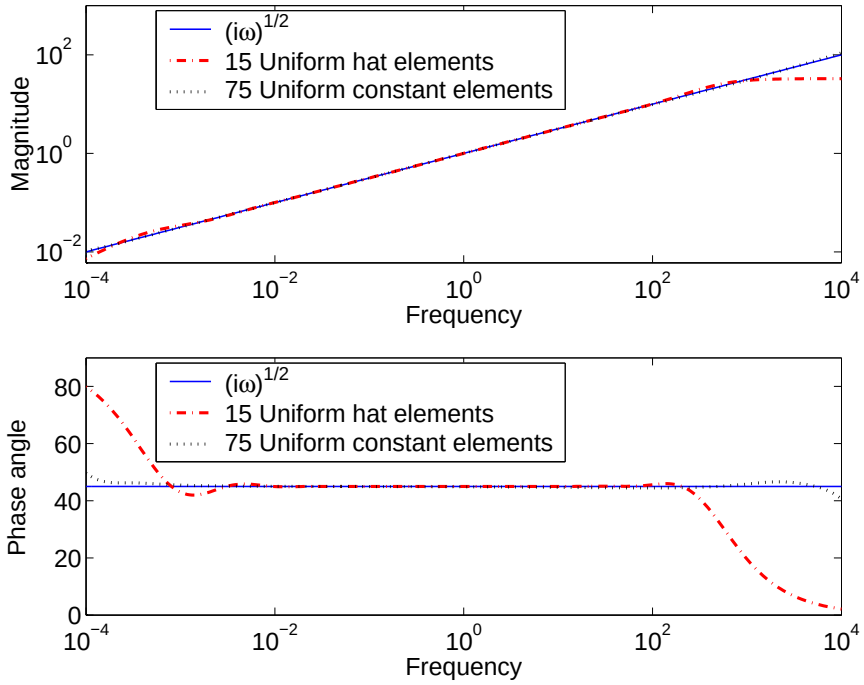

Figure 6.3: Piecewise constant versus hat function elements. Comparison between magnitude and phase angle of $(i\omega)^{1/2}$, and approximated FRFs, using 15 hat functions and 75 piecewise constant functions.

6.2 Nonuniform element sizes

On using uniform element sizes, the relative error in the FRF of the approximation varies significantly with frequency even over the range of good performance. This nonuniformity in the error can be reduced by using nonuniform element sizes (which is the great strength of finite element approximations).

The larger relative error for very low as well as high frequencies is due the lack of refinement of elements for small and large values of η. The approximation can be improved by taking smaller elements near 0 and 1 in the η domain. Here, for demonstration, we have used nodal points that are equally spaced on a logarithmic scale in the ξ domain, as

follows. We first define

$$\mathbf{y} = \text{logspace}(-\beta_1, \beta_2, n-1),$$

where "logspace" is shorthand for $n-1$ points that are logarithmically equally spaced between $10^{-\beta_1}$ and 10^{β_2}. We then set

$$p_i = \frac{y_i}{1+y_i}, \quad i = 1, 2, \cdots, n-1 \tag{6.5}$$

to get an $(n-1) \times 1$ array of nonuniformly spaced points in the interval (0,1). We finally add two more nodes, at 0 and 1, to get an $(n+1) \times 1$ array of nodal locations.

FRFs calculated using the above spacing are shown in Figure 6.4 for 50 piecewise constant and 15 hat functions. It is seen that the relative error is now more uniform over a user-definable frequency range and the phase angle error is very small over that range as well. In particular, relative error in magnitude is less than 1% for frequency varying by seven orders of magnitude; and the phase error over this range of frequencies is also quite small. This example demonstrates the potential for using finite element approximations that can be systematically refined as far as desired in any frequency range of interest (not including exactly zero) in a dynamic simulation. In many mechanical systems, the steady state static behavior is in any case determined by stiffness and not damping, and so large relative errors in approximating the low frequency behavior of the damping term may have negligible effects on the computed response in any case. Similarly, for many mechanical systems, the very high frequency behavior is dominated by inertia and not damping, with similar implications for approximation errors at high frequency.

6.3 Calculations with $\alpha \neq 1/2$

If $\alpha = 2/3$, say, then the shape functions used above for $\alpha = 1/2$ continue to give bounded integrals. However, if $\alpha = 1/3$, say, then they do not. For this case, if we change the shape function on the last element to (compare with Equation (6.4); the exponent 2 there

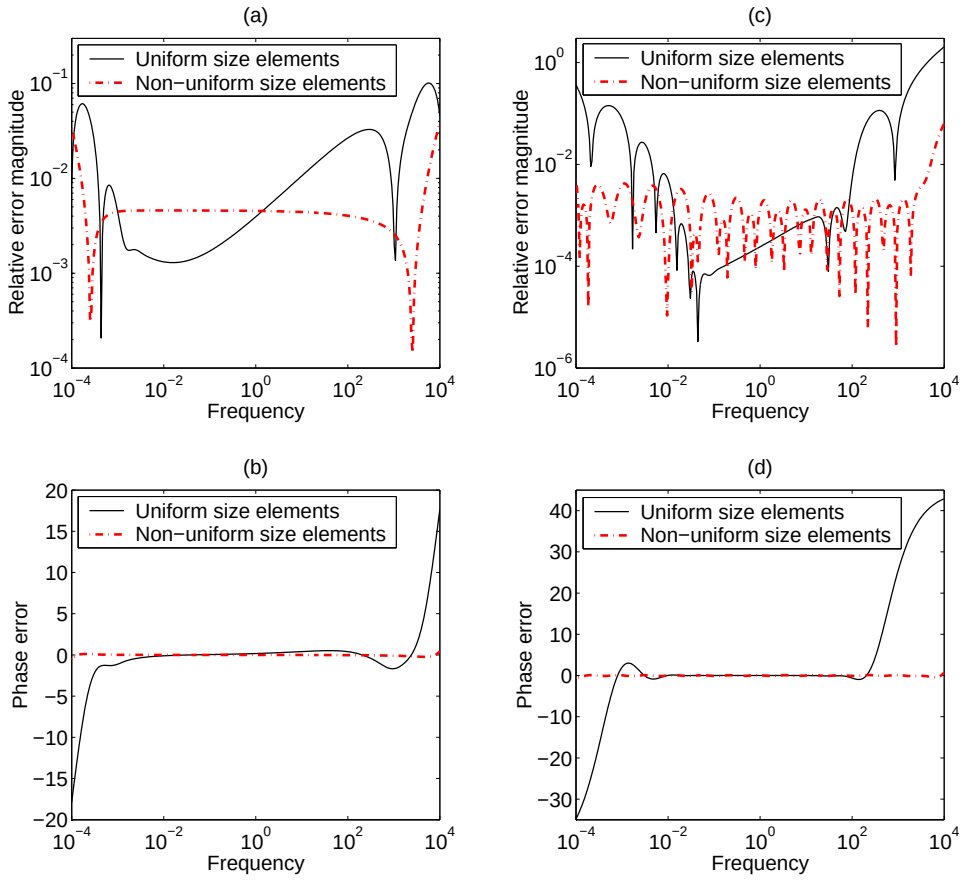

Figure 6.4: Uniformly versus nonuniformly spaced elements. Plots (a) and (b): relative error and phase error (compared with $(i\omega)^{1/2}$) in FRFs using 50 elements (piecewise constant) with uniform element sizes and nonuniform elements with nodes at logspace(-2,2). Plots (c) and (d): relative error and phase error (compared with $(i\omega)^{1/2}$) in FRFs using 15 elements (hat functions) with uniform element sizes and nonuniform elements with nodes at logspace(-2,2).

is changed to 3 here)

$$\phi_n(\eta) = \begin{cases} \dfrac{\eta - p_{n-2}}{p_{n-1} - p_{n-2}}, & p_{n-2} \le \eta \le p_{n-1}, \\ \left(\dfrac{1-\eta}{1-p_{n-1}}\right)^3, & p_{n-1} \le \eta \le 1, \\ 0 & \text{elsewhere}, \end{cases} \tag{6.6}$$

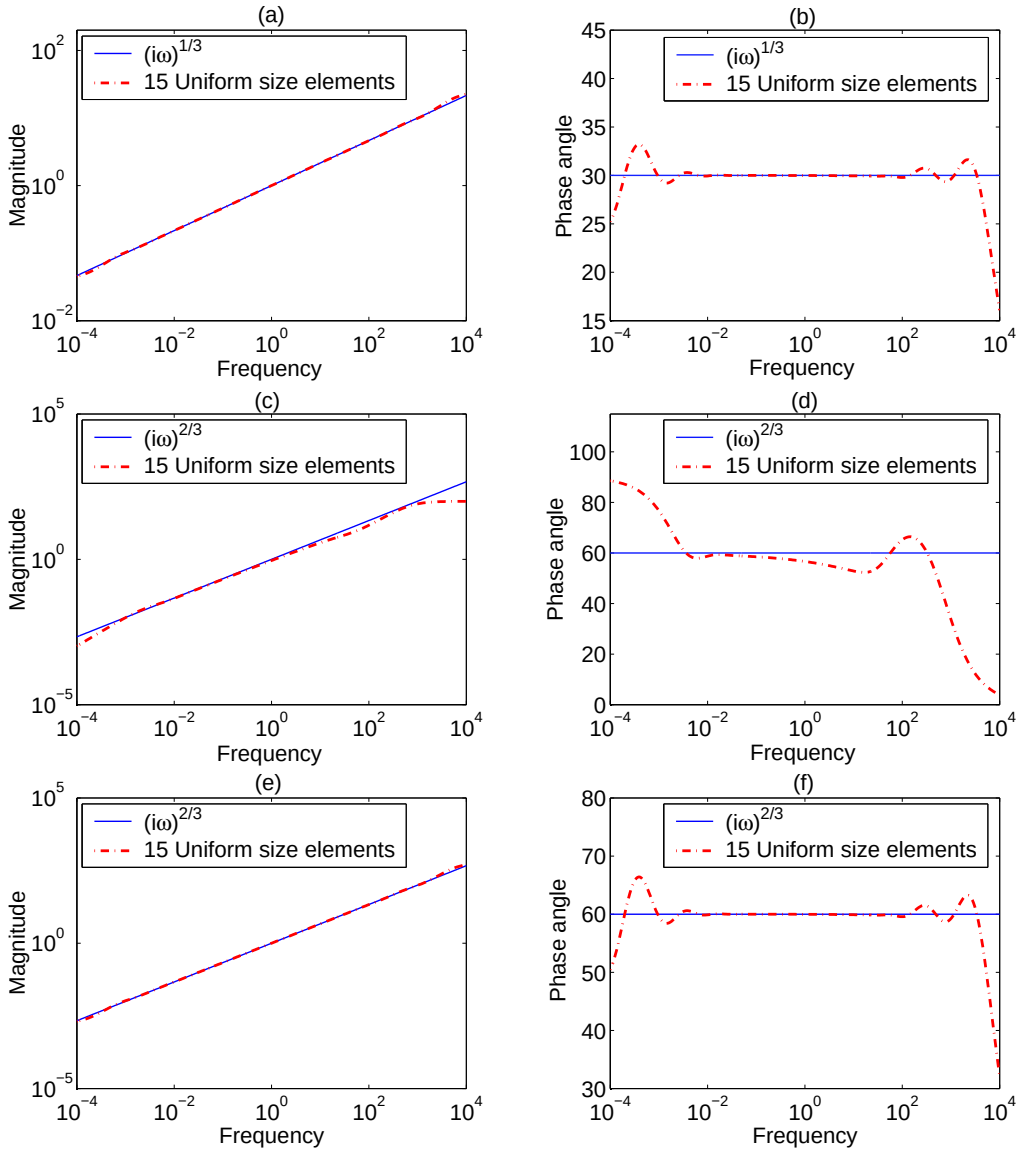

Figure 6.5: Magnitude and phase angle comparison in FRFs. Plots (a) and (b): 15 uniform hat elements and $\alpha = 1/3$. Plots (c) and (d): 15 uniform hat elements and $\alpha = 2/3$. Plots (e) and (f): 15 uniform hat elements and two successive derivatives of order $1/3$ to achieve $\alpha = 2/3$.

then all integrals involved are bounded. This points to an issue which we have not really addressed so far: what is the most suitable choice of shape function for the last element, for a given α? What are the consequences of an inappropriate choice? These issues will be addressed in Section 6.4.

In Figure 6.5, we present the comparisons in FRFs for $\alpha = 1/3$ and $\alpha = 2/3$. We used 15 uniform finite elements and the same hat functions as before, except for the modification of Equation (6.6) in place of (6.4) when $\alpha = 1/3$. The comparison is good for $\alpha = 1/3$. In contrast, the results obtained for $\alpha = 2/3$ are not good. However, on approximating the 2/3 order derivative using two successive 1/3 order derivatives, we obtain good results.

We mention that we obtained similar results with derivatives of order 0.4 and 0.8; of these, the approximation for order 0.4 was much better than that for order 0.8, but the order 0.8 was satisfactorily approximated as two successive derivatives of order 0.4. Similar results, again, were obtained for orders 0.45 and 0.9. The approximations obtained for $\alpha = 0.2$ and 0.25 were also good. All these calculations were done using 15 uniform elements and hat functions. Some of these results are presented in Appendix B.

Based on these studies, it appears that α-order derivatives for relatively higher values of α are not well approximated in the present scheme; but two successive $\alpha/2$-order derivatives, using the same scheme, give better results. The key to this puzzle lies in the α-independence of the mapping from ξ to η in Equation (6.1).

In what follows, we consider an α-dependent mapping. This gives the best performance so far, and all previous calculations may be seen as motivating Section 6.4.

6.4 The final scheme: an α dependent mapping

Here, we replace Equation (6.1) by the following

$$\eta(\xi) = \frac{\xi^{1/\alpha}}{1 + \xi^{1/\alpha}} \tag{6.7}$$

which is again a monotonic mapping of $[0, \infty]$ to [0,1], but now it depends on the order of the fractional derivative α. The advantage gained by using this mapping is that, now, we have more control on the performance of the method for a given frequency range. This is because of the role that ξ and t play in $\exp(-\xi^{1/\alpha} t)$. Here, we can consider $T^* \equiv 1/\xi^{*1/\alpha}$ for some time T^*. It suggests that frequency

$$F^* \equiv \xi^{*1/\alpha} = \frac{\eta^*}{1 - \eta^*} \,. \tag{6.8}$$

Thus, any frequency F^* corresponds to an α-independent point η^* on the unit interval. In other words, a given frequency F^* corresponds to a unique point η^* on the unit interval, independent of α.

We use hat function elements to perform the Galerkin projection (similar to Section 6.1). The only difference in this case is that, the last shape function is also a hat function (compare with Equation (6.3); the exponent of 2 there is changed to 1 here). This choice of last shape function ensures the boundedness of all the involved integrals, as will be clear from the discussion below.

$$\phi_n(\eta) = \begin{cases} \dfrac{\eta - p_{n-2}}{p_{n-1} - p_{n-2}}, & p_{n-2} \leq \eta \leq p_{n-1}, \\ \dfrac{(1-\eta)}{1-p_{n-1}}, & p_{n-1} \leq \eta \leq 1, \\ 0 & \text{elsewhere.} \end{cases}$$

Now a Galerkin projection similar to Section 6.1 is performed after changing the integration variable to η to get the counterpart of Equation (6.3), valid for the last subinterval with the α-dependent mapping, as

$$\int_0^1 \left(\left\{ \dot{a}_i(t)\phi_n(\eta) + \left(\frac{\eta}{1-\eta} \right) a_n(t)\phi_n(\eta) \right\} - \dot{x}(t) \right) \phi_n(\eta) \frac{\alpha}{\eta^{1-\alpha}\,(1-\eta)^{1+\alpha}}\, d\eta \;=\; 0\,. \quad (6.9)$$

It is clear by the choice of shape functions that, integrands corresponding to all but the last shape function are bounded in interval $[0, 1]$. So we focus our attention to the integral corresponding to the last shape function, defined on the last subinterval $[p_{n-1}, 1]$, only. Equation (6.9) consists of summation of integrals of three different integrands. These three integrands after ignoring multiplicative constants, defined on $[p_{n-1}, 1]$ subinterval, are given by

$$I_1 = \frac{1}{\eta^{1-\alpha}\,(1-\eta)^{\alpha-1}}\,, \quad I_2 = \frac{\eta^\alpha}{(1-\eta)^\alpha} \quad \text{and} \quad I_3 = \frac{1}{\eta^{1-\alpha}\,(1-\eta)^\alpha}\,.$$

Clearly integrals of all the above integrands are bounded in subinterval $[p_{n-1}, 1]$ for $0 < \alpha < 1$.

We directly use nonuniform size elements. To this end, we change Equation (6.5) to

$$p_i = \frac{y_i^{1/\alpha}}{1 + y_i^{1/\alpha}}, \quad i = 1, 2, \cdots, n-1\,. \tag{6.10}$$

to get an $(n-1) \times 1$ array of nonuniformly spaced points in the interval (0,1); add two more nodes at 0 and 1; and get an $(n+1) \times 1$ array of nodal locations.

We now come to an interesting point regarding the choice of mesh points in the nonuniform finite element discretization. While the map from ξ to η is now α-dependent, the *choice of mesh points* can be made using

$$p_i = \frac{y_i^2}{1 + y_i^2}, \quad i = 1, 2, \cdots, n-1$$

with no negative consequences (see Equation (6.8) with $\alpha = 1/2$).

In the above, the index 2 in y_i^2 is arbitrary, corresponding to $\alpha = 1/2$, an arbitrary but representative value between 0 and 1. The key point is that p_i lies on the η axis and so the frequency range of the approximation is actually α-independent by Equation 6.8. Another advantage gained is that the frequency range of interest can be specified easily in this way. We have used this in the numerical examples below.

In Figure 6.6, we present the comparisons in FRFs for $\alpha = 1/3$, $\alpha = 1/2$ and $\alpha = 2/3$. 15 nonuniform finite elements were used. The performance is very good in all cases, over a significant frequency range. The percentage error in magnitude and phase angle for $\alpha = 1/3$, $\alpha = 1/2$ and $\alpha = 2/3$ are shown in Figure 6.7. The errors are below 1% for more than seven orders of magnitude of frequency. Calculations for other values of α were also done, and similar results were obtained (not presented here). Similarly, we have also verified that taking more elements gives smaller errors over the same frequency range.

For verification by readers who wish to implement this method, the system matrices for 7 elements are given in the appendix.

6.5 Modeling issues and asymptotics

No matter how many elements we take in the FE mesh, the match in the FRF will be good only over some nonzero finite range of frequencies. The very short time or very high

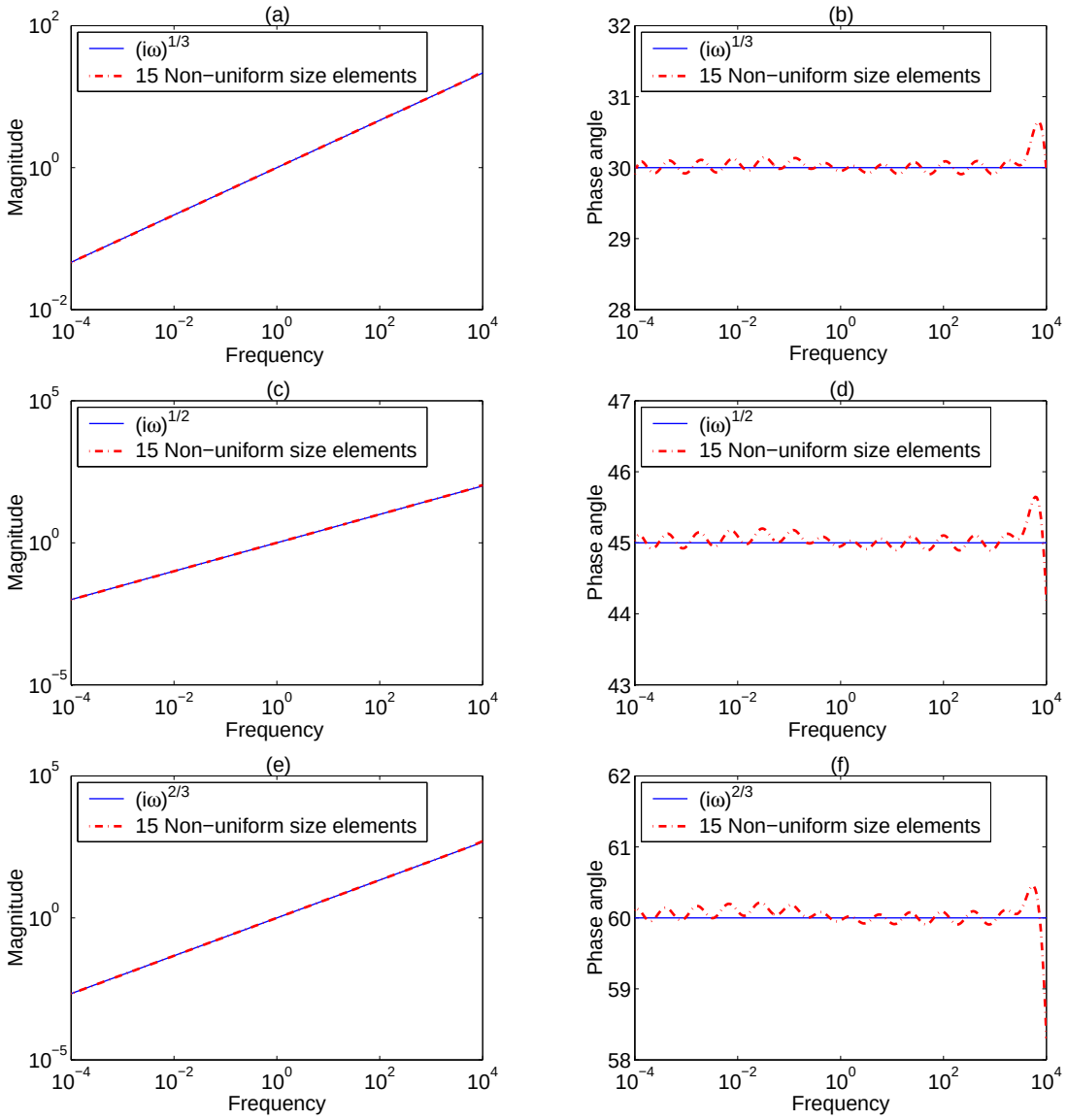

Figure 6.6: Magnitude and phase angle comparison in FRFs. Plots (a) and (b): 15 nonuniform hat elements and $\alpha = 1/3$. Plots (c) and (d): 15 nonuniform hat elements and $\alpha = 1/2$. Plots (e) and (f): 15 nonuniform hat elements and $\alpha = 2/3$.

frequency asymptotic behavior may *always be wrong*. See, e.g., the discussion of [51] in [53]. An anonymous reviewer of this work, who pointed us to these two papers, also raised similar concerns regarding this feature of our approximation.

This unavoidable feature may, however, have acceptably small implications for engineering practice. We do not suggest that Schmidt and Gaul lack understanding of engineer-

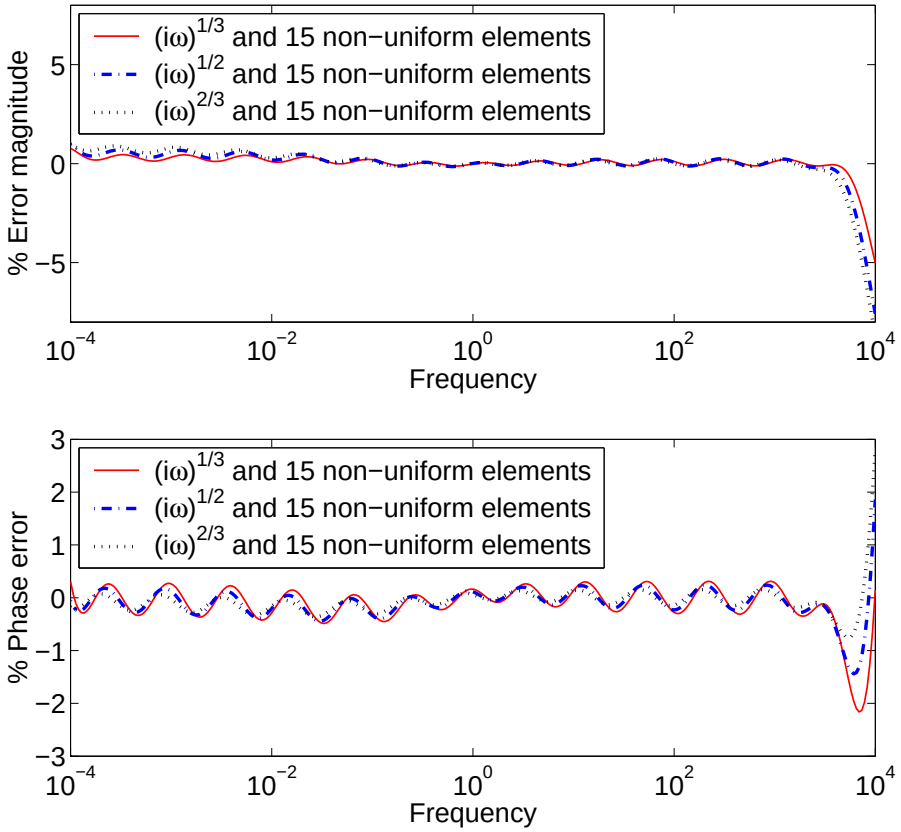

Figure 6.7: % error in magnitude and phase angle for $\alpha = 1/3$, $\alpha = 1/2$ and $\alpha = 2/3$.

ing practice! Rather, their paper is a mathematical one; it raises mathematical concerns and discusses mathematical issues. Here, we present our views on what those issues might or might not imply for actual applications of fractional order derivatives in numerical work with experimentally fitted models for the viscoelastic behavior of physical materials tested in laboratories using imperfect machines with finite frequency ranges and finite measurement precision.

Consider some real material whose experimentally observed damping behavior can be well approximated using fractional order derivatives. We could, of course, also describe this behavior using a large number of (integer order) spring-dashpot combinations (as pointed out by [53]). The parameters of such integer order spring-dashpot combinations may be difficult to estimate robustly in experiments, however.

As seen above, the Galerkin procedure gives very good approximations to fractional order derivatives for many different choices of mesh points. In other words, the same

approximately-fractional-order behavior of the real material can be described by many different combinations of integer-order or classical spring-dashpot combinations; these combinations will do an *experimentally indistinguishable* job of capturing the experimental data, which will *always* span only a finite frequency range. In this way, the classical integer-order approach requires identification of many parameters that cannot really be uniquely determined. The parameter estimation problem is not only bigger, but more ill-posed. In contrast, a model involving fractional order derivatives may match the data over the relevant frequency range; and will also involve identification of fewer parameters in a better-posed problem. For this reason, *description* of damping should be done, wherever indicated, using such fractional order derivatives. This makes parameter identification easier for any individual experimenter; but, more importantly, it allows different experimenters in different laboratories to obtain the *same* parameter estimates, without which material behavior cannot be standardized for widespread engineering use.

However, once a suitable model with fractional order derivatives has been identified and standardized, *simulations* using that model can use different approximation techniques; it matters little what the approximation scheme is, provided it is good enough. The only issue for a given calculation is whether the final computed results are *accurate enough*. But what is accuracy?

For the numerical analyst, accuracy means correspondence with the original and exact fractional order derivative behavior. The approximation should be good over all frequencies and time scales that are important in the calculation. If the results are not reliable for some very high frequency, the analyst notes it, but uses the reliable part of the results anyway. This is the same spirit in which reentrant corners and cracks in elastic bodies are often modeled using ordinary finite element codes: the results are not invalidated simply because even very small finite elements may not exactly capture the singularities in the solution. Rather, a careful analyst keeps a watch on how far from the singularity one must go before the numerical results are reliable.

For the engineer, in addition to the numerical issue, accuracy also means correspondence with the behavior of the original real material we started with. Any difference between exact and approximate mathematical solutions, in behavior regimes where there is no experimental data, are academic curiosities without practical implication in many cases. There is, in the end, no theorem which says that test results for a given piece of

rubber can be extrapolated outside the test range; whether we believe it or not is a matter of individual academic taste.

Do our numerics limit the size of the allowable test range? We think not. As seen above, with merely 15 non-uniform hat function elements, we get errors less than 1% over a frequency range spanning more than 7 orders of magnitude which in a real setup might correspond to a frequency range, e.g., from 0.01 Hz to 100 kHz, or from 0.0001 Hz to 1 kHz. Are there mechanical models for anything at all where the range of validity exceeds this? If there are, we can take (say) 20 elements instead of 15. Note, also, that errors less than 1% in estimating material constants are considered small; for example, the Young's modulus of steel is routinely specified as 210 GPa, i.e., to 2 significant digits only. But, if necessary, the error in our approximation could be made less than 0.1% with more elements.

Finally, if the engineer believes (as discussed in [42]) that the fractional order derivative behavior observed in experiments is actually an artifact of many complex internal dissipation mechanisms, each without memory, then the very-low and very-high (outside the fitting range) frequency behavior of the material may actually *not* match the fitted fractional order behavior. In other words, where the approximation may not match the model, there the model does not match the material anyway.

It is with this viewpoint that we have presented the errors in our numerical approximations above using the frequency domain. While it may well appear in nonlinear differential equations, the fractional derivative itself is very much linear. The error in the approximation of that derivative can therefore be viewed usefully in the frequency domain. A *post facto* study of the spectrum of the computed solution can show whether the solution was in fact confined within the frequency range where the approximation is good; if not, as is clear from our numerical results, the approximation can be improved by the analyst.

6.6 Discussion

A problem with direct numerical simulation of fractionally damped systems is that simulations up to time t require $\mathcal{O}(t^2)$ computations. We have developed a novel Galerkin projection technique for reducing the infinite-dimensional systems associated with fractional

order derivatives to finite dimensional systems. The reduction to a finite dimensional system is accomplished by first transforming the infinite dimensional, fractionally damped ODE to another infinite dimensional system consisting of an ODE coupled with a PDE. The Galerkin projection is then performed on the PDE. The approximation obtained is specific to α, the fractional order of the derivative; it can be used for any system where such a derivative appears.

With the present finite dimensional approximation, simulations up to time t of fractionally damped systems can now be done in $\mathcal{O}(t)$ time. It is emphasized that such time savings are only relative to straightforward numerical integration. Other finite dimensional approximations, such as in [46] and [19], will give similar time savings. However, the conceptual basis of our approximation is both different as well as, in our opinion, simpler.

We have presented calculations with global shape functions, and then with finite elements as well. Use of continuous, piecewise differentiable shape functions and finite elements of nonuniform size, along with an α-dependent mapping of the half line to the unit interval, has been shown, for a relatively small number of elements, to give excellent approximations with fairly uniform and small error over a user-specified frequency range. The present approximation is expected to be useful for long time simulations of nonlinear dynamic systems with fractional order terms.

When compared with Oustaloup *et al.*'s [19] method involving rational function approximation of transfer functions, our method is similar in terms of computational cost. Their method requires higher order derivatives on both input and output side and hence requires extra initial conditions to be supplied. Our method does not require these higher order derivatives and hence is simpler to implement as compared to their method. While they have demonstrated the accuracy of their method by performing detailed error analysis, we have only numerically demonstrated the accuracy of our method. However, our numerical results show that our method can attain high accuracy with suitable mesh refinement and using higher order elements. These issues are further discussed in Chapter 9.

We mention that comments from an anonymous reviewer of [44] led us to develop Section 6.4; and to write Section 6.5, which made us think about many practical issues. These have helped to improve our method.

Chapter 7

Three Classes of FDE's Amenable to Galerkin-based Approximation

In Chapters 5 and 6, we developed a Galerkin approximation scheme for fractional order derivatives, and used it to obtain accurate numerical solutions of second order (mechanical) systems with fractional order damping terms. In this chapter we demonstrate how that approximation can be used to find accurate numerical solutions of three different classes of fractional differential equations (FDEs), where for simplicity we assume that there is a single fractional order derivative, with order between 0 and 1. In the first class of FDEs, the highest derivative has integer order greater than one. An example of a traveling point load on an infinite beam resting on an elastic, fractionally damped, foundation is studied. The second class contains FDEs where the highest derivative has order 1. Examples of the so called generalized Basset's equation are studied. The third class contains FDEs where the highest derivative is the fractional order derivative itself. Two specific examples are considered. In each example studied in this chapter, the Galerkin-based numerical approximation is compared with analytical or semi-analytical solutions obtained by other means. The material of this chapter also appears in [55].

7.1 Introduction

A fractional derivative of order α given using the Riemann-Liouville definition [47, 48] is

$$\mathrm{D}^{\alpha}[x(t)] = \frac{1}{\Gamma(1-\alpha)}\frac{d}{dt}\left[\int_0^t \frac{x(\tau)}{(t-\tau)^{\alpha}}d\tau\right],$$

where $0 < \alpha < 1$. Two equivalent forms of the above with zero initial conditions (as in, e.g., [18]) are given as

$$\mathrm{D}^{\alpha}[x(t)] = \frac{1}{\Gamma(1-\alpha)}\int_0^t \frac{\dot{x}(\tau)}{(t-\tau)^{\alpha}}d\tau = \frac{1}{\Gamma(1-\alpha)}\int_0^t \frac{\dot{x}(t-\tau)}{\tau^{\alpha}}d\tau\,. \tag{7.1}$$

Differential equations with a single independent variable (usually "time") which involve fractional order derivatives of the dependent variable(s) are called fractional differential equations or FDEs. In this work, we consider FDEs where the fractional derivative has order between 0 and 1 only. Such FDEs, for our purposes, are divided into three categories, depending on whether the highest order derivative in the FDE is an integer greater than 1, is exactly equal to 1, or is a fraction between 0 and 1.

In this chapter, we will demonstrate three strategies for these three classes of FDEs, whereby the Galerkin technique presented in Chapters 5 and 6 (also presented in [44]) for fractional derivatives can be used to obtain simple, quick and accurate numerical solutions. The Galerkin approximation scheme of Chapters 5 and 6 ([44]) involves two calculations:

$$\mathbf{A}\dot{\mathbf{a}} + \mathbf{B}\,\mathbf{a} = \mathbf{c}\,\dot{x}(t) \tag{7.2}$$

and

$$\mathrm{D}^{\alpha}[x(t)] \approx \frac{1}{\Gamma(1+\alpha)\Gamma(1-\alpha)}\,\mathbf{c}^T\mathbf{a}, \tag{7.3}$$

where $\mathbf{A}$ and $\mathbf{B}$ are $n \times n$ matrices (specified by the scheme; see Chapters 5 and 6 or [44]), $\mathbf{c}$ is an $n \times 1$ vector also specified by the scheme, and $\mathbf{a}$ is an $n \times 1$ vector of n internal variables that approximate the infinite-dimensional dynamics of the actual fractional order derivative. The T superscript in equation (7.3) denotes matrix transpose.

As will be seen below, the first category of FDEs (section 7.3) poses no real problem over and above the examples already considered in Chapters 5 and 6. That is, in Chapters 5 and 6, the highest derivatives in the examples considered had order 2; while in the example

considered in Section 7.3 below, the highest derivative will be of order 4 (when seeking steady state solution). However, the example of Section 7.3 is a boundary value problem on an infinite domain. Our approximation scheme provides significant advantages for this problem. The second category of FDEs (section 7.4) also leads to numerical solution of ODEs (not FDEs). The specific example considered here is relevant to the physical problem of a sphere falling slowly under gravity through a viscous liquid, but not yet at steady state. Again, the approximation scheme leads to an algorithmically simple, quick and accurate solution. However, the equations are stiff and suitable for a routine that can handle stiff systems, such as Matlab's "ode23t". Finally, the third category of FDEs (section 7.5) leads to a system of differential algebraic equations (DAEs) which can be solved simply and accurately using an index one DAE solver such as Matlab's "ode23t".

We emphasize that we have deliberately chosen linear examples below so that analytical or semi-analytical alternative solutions are available for comparing with our results using the Galerkin approximation. However, it will be clear that the Galerkin approximation will continue to be useful for a variety of nonlinear problems where alternative solution techniques might run into serious difficulties.

7.2 Two Important Observations

1. A fractional integral of order α is given using the Riemann-Liouville definition [47, 48], as
$$\mathrm{I}^{\alpha}[x(t)] = \frac{1}{\Gamma(\alpha)} \int_0^t \frac{x(\tau)}{(t-\tau)^{1-\alpha}} d\tau \,, \tag{7.4}$$
where $0 < \alpha < 1$.

2. Fractional order derivatives in general *do not* hold either the commutative property or the law of exponents. Also in general they do not commute with fractional integrals. However, fractional integrals obey both the commutative property and the law of exponents (see for example [47]).

The above two observations play an important role in the development of solution strategies of Section 7.5.1.

7.3 Traveling Load on an Infinite Beam

The governing equation for an infinite beam on a fractionally damped elastic foundation, and with a moving point load (see Fig. 7.1), is

$$u_{xxxx} + \frac{\bar{m}}{EI}u_{tt} + \frac{c}{EI}\mathrm{D}_t^{1/2}u + \frac{k}{EI}u = -\frac{1}{EI}\delta(x - vt)\,, \tag{7.5}$$

where $\bar{m}$ is mass per unit length, EI flexural rigidity, c damping constant and k is stiffness constant, and $\mathrm{D}^{1/2}$ has a t-subscript to indicate that x is held constant. The boundary conditions of interest are

$$u(\pm\infty, t) \equiv 0.$$

Above problem for damping term $\mathrm{D}_t\, u$ is presented in [56].

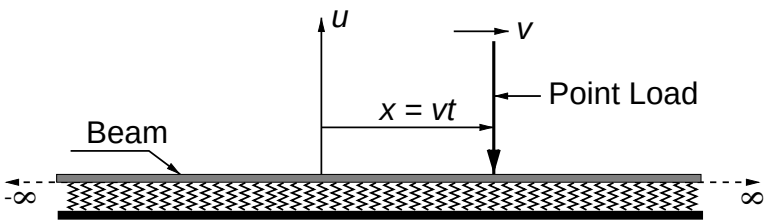

Figure 7.1: Traveling point load on an infinite beam with a fractionally damped elastic foundation.

We seek steady state solutions to this problem in a moving reference frame.

7.3.1 With Galerkin

With the Galerkin approximation of the fractional derivative, we get the new PDEs

$$u_{xxxx} + \frac{\bar{m}}{EI}u_{tt} + \frac{c}{EI\,\Gamma(1/2)\Gamma(3/2)}\mathbf{c}^T\mathbf{a} + \frac{k}{EI}u = -\frac{1}{EI}\delta(x - vt)$$

and

$$\mathbf{A}\dot{\mathbf{a}} + \mathbf{B}\mathbf{a} = \mathbf{c}u_t\,,$$

where $\mathbf{a}$ is now a function of both x and t, and the overdot denotes a partial derivative with respect to t. Changing variables to $\xi = x - vt$ and $\tau = t$ to shift to a steadily moving

coordinate system, we get

$$u_{\xi\xi\xi\xi} + \frac{\bar{m}}{EI}\left(v^2\, u_{\xi\xi} - 2\, v\, u_{\xi\tau} + u_{\tau\tau}\right) + \frac{1}{EI}\left(\frac{c}{\Gamma(1/2)\,\Gamma(3/2)}\mathbf{c}^T\mathbf{a} + k\, u\right) = -\frac{1}{EI}\delta(\xi) \quad (7.6)$$

and

$$\mathbf{A}(\mathbf{a}_\tau - v\,\mathbf{a}_\xi) + \mathbf{B}\mathbf{a} = \mathbf{c}\,(u_\tau - v\,u_\xi)\,. \quad (7.7)$$

Now, seeking a steady state solution in the moving reference frame, Equations (7.6) and (7.7) become

$$u_{\xi\xi\xi\xi} + \frac{\bar{m}}{EI}v^2\, u_{\xi\xi} + \frac{1}{EI}\left(\frac{c}{\Gamma(1/2)\,\Gamma(3/2)}\mathbf{c}^T\mathbf{a} + k\, u\right) = -\frac{1}{EI}\delta(\xi) \quad (7.8)$$

and

$$-v\mathbf{A}\mathbf{a}_\xi + \mathbf{B}\mathbf{a} = -v\,\mathbf{c}\,u_\xi\,. \quad (7.9)$$

That the steady state solution will be stable can, incidentally, be seen by considering the variational equations, which are the same as Equations (7.8) and (7.9) with the $\delta(\xi)$ forcing removed. But this is simply the damped, unforced beam viewed in a moving reference frame. So all solutions must, on physical grounds, eventually approach zero.

The steady state solution will be presented later.

7.3.2 Without Galerkin (Using Fourier Transform)

Without the Galerkin approximation, the fractional term in equation (7.5) can be written as

$$\mathrm{D}_t^{1/2}u(t,x) = \frac{1}{\Gamma(1/2)}\int_0^t \frac{\dot{u}(z,x)}{\sqrt{t-z}}\,dz\,.$$

On letting $w = t - z$ in the above we get

$$\mathrm{D}_t^{1/2}u(t,x) = \frac{1}{\Gamma(1/2)}\int_0^t \frac{\dot{u}(t-w,x)}{\sqrt{w}}\,dw\,. \quad (7.10)$$

After the change of variables $\xi = x - vt$ and $\tau = t$, we get $\dot{u} = -v\,u_\xi + u_\tau$, which gives $\dot{u} = -v\,u_\xi$ for the steady state (τ independent) solution. Hence, $\dot{u}(t-w,x) = -v\,u_\xi(\xi + v\,w)$,

because $\xi = x - vt \Longrightarrow x - v(t-w) = \xi + v\,w$. On substituting in equation (7.10) we get (with incomplete incorporation of steady state conditions)

$$\mathrm{D}_t^{1/2}u(t,x) = \frac{-v}{\Gamma(1/2)}\int_0^\tau \frac{u_\xi(\xi+v\,w)}{\sqrt{w}}\,dw$$
$$= \frac{-v}{\Gamma(1/2)}\left(\int_0^\infty \frac{u_\xi(\xi+v\,w)}{\sqrt{w}}\,dw - \int_\tau^\infty \frac{u_\xi(\xi+v\,w)}{\sqrt{w}}\,dw\right).$$

In the above, steady state is achieved as $\tau \to \infty$, and we get

$$\mathrm{D}_t^{1/2}u(t,x) = \frac{-v}{\Gamma(1/2)}\int_0^\infty \frac{u_\xi(\xi+v\,w)}{\sqrt{w}}\,dw\,.$$

Substituting $y = \xi + v\,w$ above for later convenience, we get

$$\mathrm{D}_t^{1/2}u(t,x) = \frac{-\sqrt{v}}{\Gamma(1/2)}\int_\xi^\infty \frac{u'(y)}{\sqrt{y-\xi}}d\,y = \frac{-\sqrt{v}}{\Gamma(1/2)}\int_{-\infty}^\infty \frac{\mathrm{H}(y-\xi)\,u'(y)}{\sqrt{y-\xi}}d\,y\,,$$

where $\mathrm{H}(y-\xi)$ is the Heaviside step function, with $\mathrm{H}(s) = 1$ if $s > 0$, and 0 otherwise.

Thus, the steady state version of equation (7.5) *without* approximation is

$$u_{\xi\xi\xi\xi} + \frac{\bar{m}v^2}{EI}u_{\xi\xi} - \frac{c\sqrt{v}}{EI\,\Gamma(1/2)}\int_{-\infty}^\infty \frac{\mathrm{H}(y-\xi)\,u'(y)}{\sqrt{y-\xi}}d\,y + \frac{k}{EI}u = -\frac{1}{EI}\delta(\xi)\,. \tag{7.11}$$

Notice that the above equation is an integro-differential equation having only one independent variable namely ξ, which is a *space variable* in the *moving* reference frame.

7.3.3 Solutions, With Galerkin and Without

Solution of equations (7.8) and (7.9) is straightforward and quick. An algebraic eigenvalue problem is solved and a jump condition imposed. The details are as follows. For $\xi \neq 0$, the system reduces to a homogeneous first order system with constant coefficients. The eigenvalues of this system have nonzero real parts, and are found numerically. Those with negative real parts contribute to the solution for $\xi > 0$, while those with positive real parts contribute to the solution for $\xi < 0$. There is a jump in the solution at $\xi = 0$. The jump occurs only in $u_{\xi\xi\xi}$, and equals $-1/EI$, see for example, pages 266–267 of [57]. All other state variables are continuous at $\xi = 0$. These jump/continuity conditions provide as many

equations as there are state variables; and these equations can be used to solve for the same number of unknown coefficients of eigenvectors in the solution. The overall procedure is straightforward, and can be implemented in, say, a few lines of Matlab code. Numerical results obtained will be presented below.

Equation (7.11) cannot, as far as we know, be solved in closed form. It can be solved numerically using Fourier transforms. To this end, first we apply the Fourier transform to Equation (7.11) to get

$$w^4\mathcal{F}(u(\xi)) - \frac{\bar{m}v^2w^2}{EI}\mathcal{F}(u(\xi)) - \frac{c\sqrt{v}}{EI\,\Gamma(1/2)}\left[\mathcal{F}\left(\frac{\mathrm{H}(-\xi)}{\sqrt{-\xi}}\right)\mathcal{F}(u'(\xi))\right] + \frac{k}{EI}\mathcal{F}(u(\xi)) = \frac{-1}{EI}.$$

Notice that the third term in the above is obtained by applying the convolution theorem to the convolution integral of Equation (7.11). On evaluating these Fourier transforms, simplifying and denoting Fourier transform $\mathcal{F}(u(\xi))$ by $U(\omega)$ we get

$$U(\omega)\left(w^4 - \frac{\bar{m}v^2w^2}{EI} - \frac{ic\sqrt{v}w}{EI\,\sqrt{-iw}} + \frac{k}{EI}\right) = \frac{-1}{EI}\,.$$

Hence the Fourier transform of $u(\xi)$ is given by

$$U(\omega) = \frac{\sqrt{-i\omega}}{-EI\omega^4\sqrt{-i\omega} + \bar{m}v^2\omega^2\sqrt{-i\omega} + ic\sqrt{v}\,\omega - k\sqrt{-i\omega}} \tag{7.12}$$

The inverse Fourier transform of the above was calculated numerically, pointwise in ξ. The integral involved in inversion is well behaved and convergent. However, due to the presence of the oscillatory quantity $\exp(i\omega\xi)$ in the integrand, some care is needed. In these calculations, we used numerical observation of antisymmetry in the imaginary part, and symmetry in the real part, to simplify the integrals; and then used MAPLE to evaluate the integrals numerically.

7.3.4 Results

Results for $\bar{m} = 1$, $EI = 1$, $k = 1$ and various values of v and c are shown in Fig. 7.2. The Galerkin approximation is very good.

The agreement between the two solutions (Galerkin and Fourier) provides support for the correctness of both. In a problem with several unequally spaced traveling loads, the Galerkin technique will remain straightforward while the Fourier approach will become more complicated. Our point here is not that the Fourier solution is intellectually inferior (we find it elegant). Rather, straightforward application of the Galerkin technique requires less problem-specific ingenuity and effort.

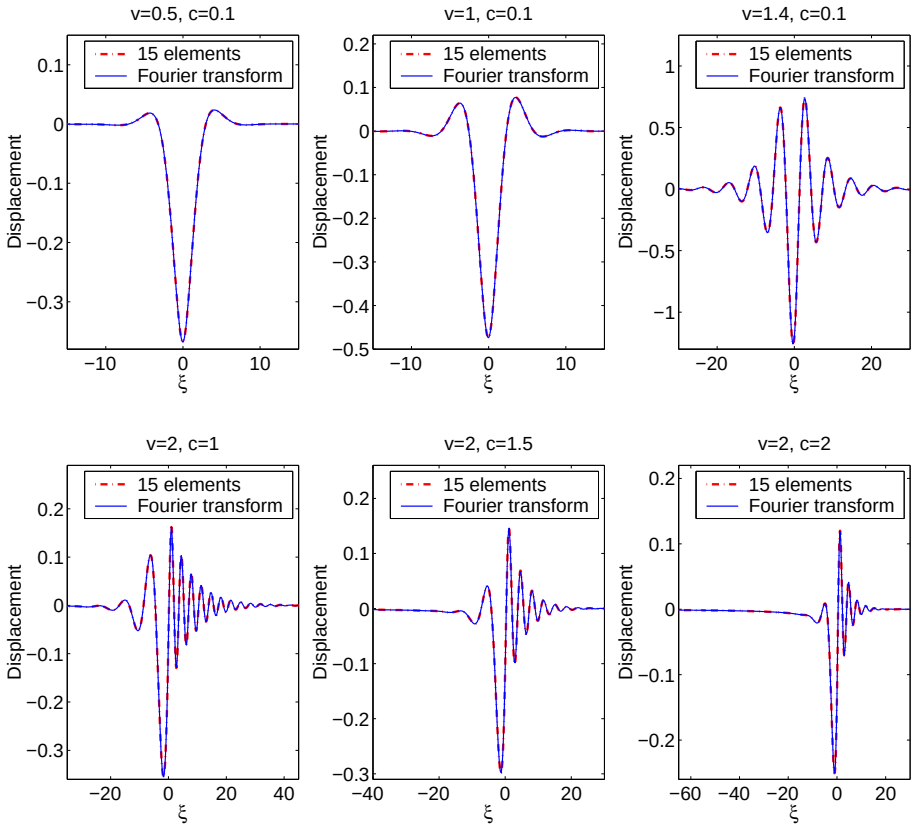

Figure 7.2: Numerical results for a traveling point load on an infinite beam at steady state.

7.4 Off Spheres Falling Through Viscous Liquids

A sphere falling slowly under its own weight through a viscous liquid will approach a steady speed [16]. The approach is described by a FDE where the highest derivative has order 1. Here, we study no fluid mechanics issues. Rather, we consider two such FDEs with, for simplicity, zero initial conditions. Such problems have been referred to as examples of

the generalized Basset's problem [17]. Our aim is to demonstrate the use of our Galerkin approximation for such problems.

Consider

$$\dot{v}(t) + \mathrm{D}^{\alpha} v(t) + v(t) = 1\,, \quad v(0) = 0, \tag{7.13}$$

$0 < \alpha < 1$. Here, for demonstration, we will consider $\alpha = 1/2$ and $1/3$. The solution methods discussed below will work for any reasonable α between 0 and 1. By reasonable values of α we mean those values which are not extremely close to 0 or 1, because the asymptotic behavior of our approximation as $\alpha \to 0$ or 1 has not been investigated.

7.4.1 With Galerkin

The fractional derivative is approximated as before to give

$$\dot{v}(t) + \frac{1}{\Gamma(1-\alpha)\,\Gamma(1+\alpha)} \mathbf{c}^T \mathbf{a} + v(t) = 1 \tag{7.14a}$$

and

$$\mathbf{A}\,\dot{\mathbf{a}} + \mathbf{B}\,\mathbf{a} = \mathbf{c}\,\dot{v}(t)\,, \tag{7.14b}$$

with initial conditions $v(0) = 0$ and $\mathbf{a}(0) = 0$.

Equations (7.14) can be rewritten as a first order system of ODEs, and solved using Matlab's standard ODE solver, "ode45". However, the equations are stiff and the solution takes time. Two or more orders of magnitude less effort seem to be needed if we use Matlab's stiff system and/or index one DAE solver, "ode23t". We will present numerical results later.

7.4.2 Series Solution Using Laplace Transforms

The Laplace transform of the solution to equation (7.13) is given by

$$V(s) = \frac{1}{s(1+s+s^{\alpha})} = \frac{[1-(-s^{-1}-s^{\alpha-1})]^{-1}}{s^2}\,.$$

We can expand the numerator above in a binomial series for $|(s^{-1} + s^{\alpha-1})| < 1$, because $\alpha < 1$ and we are prepared to let s be as large as needed (in particular, suppose we consider s values on a vertical line in the complex plane, we are prepared to choose that line as far into the right half plane as needed). The series we obtain is

$$V(s) = \sum_{n=0}^{\infty}(-1)^n \sum_{r=0}^{n} \binom{n}{r} \frac{1}{s^{n+2-r\alpha}} .$$

Taking the inverse Laplace transform of the above,

$$v(t) = \sum_{n=0}^{\infty}(-1)^n \sum_{r=0}^{n} \binom{n}{r} \frac{t^{n+1-r\alpha}}{\Gamma(n+2-r\alpha)} . \tag{7.15}$$

7.4.3 Results

Results for the above problem are shown in Fig. 7.3. The Galerkin approximation matches well with the series solutions of equation (7.13) for $\alpha = 1/2$ and $1/3$. The sum in equation (7.15) was taken upto the $\mathcal{O}(t^{150})$ term for both cases, using MAPLE (fewer than 150 terms may have worked; more were surely not needed).

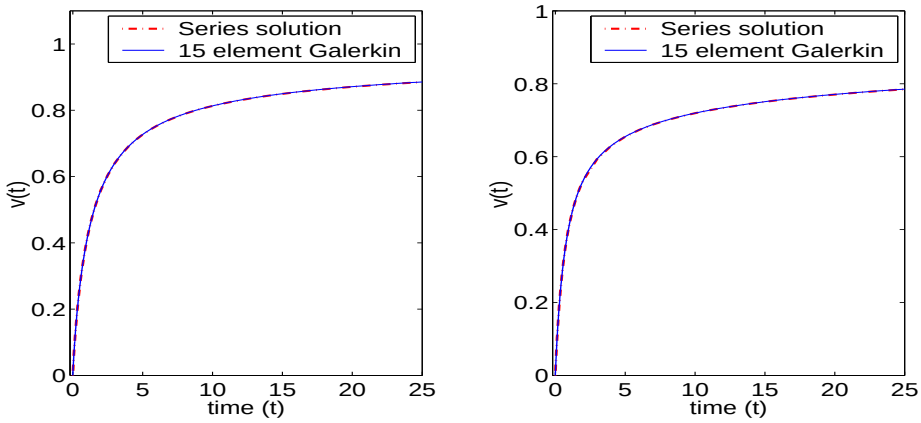

Figure 7.3: Comparison between Laplace transform and 15 element Galerkin approximation solutions: Left: $\alpha = 1/2$ and sum in equation (7.15) upto $\mathcal{O}(t^{150})$ term. Right: $\alpha = 1/3$ and sum in equation (7.15) upto $\mathcal{O}(t^{150})$ term.

A comment on passing is that the above series as well as others to be encountered in the rest of this thesis involve operations like addition and multiplication of very large

numbers, which may lead to numerical instabilities and hence wrong results. But such errors can be avoided by using Maple's inbuilt function "Digits", which specifies how many number of digits to be used while numerically evaluating a function.

7.5 FDEs With Highest Derivative Fractional

Consider

$$\mathrm{D}^{\alpha}x(t) + x(t) = f(t)\,, \quad x(0) = 0. \tag{7.16}$$

Equations of this form are called relaxation fractional equations [10]. These equations have relevance to, e.g., mechanical systems with fractional order damping and under slow loading (where inertia plays a negligible role), such as in creep tests. Here, we concentrate on demonstrating the use of our Galerkin technique for this class of problems.

7.5.1 Adaptation of the Galerkin Approximation

Our usual Galerkin approximation strategy will not work here directly, because it requires $\dot{x}(t)$ as an input (see equations (7.2) and (7.3)). We could introduce $\dot{x}(t)$ by taking a $1-\alpha$ order derivative, but such differentiation requires the forcing function $f(t)$ to have such a derivative, and we avoid such differentiation here. Instead, we adopt the Galerkin approximation through constraints that lead to differential algebraic equations (DAEs), which are then easily solved using standard available routines.

The detailed steps that follow in our solution strategy below are required because of the properties of fractional derivatives and integrals noted in Section 7.2. These steps, although may appear redundant, are required in developing mathematically accurate solution strategy.

Observe that $\dot{x}(t)$ forcing in equation (7.2) results in an α order derivative of $x(t)$ in equation (7.3). We interpret the above as follows. If the forcing was some general function $h(t)$ instead of $\dot{x}(t)$; and if $h(t)$ was integrable, i.e., $h(t) = \dot{g}(t)$ for some function $g(t)$; and if, in addition, $g(t)$ was continuous at $t = 0$, then by adding a constant to $g(t)$ we could

ensure that $g(0) = 0$ while still satisfying $h(t) = \dot{g}(t)$. Further, the forcing of $h(t)$ (in place of $\dot{x}(t)$) in equation (7.2) would result in an α order derivative of $g(t)$ (in place of $x(t)$) in equation (7.3). In other words, if

$$h(t) = \dot{g}(t)\,,\ g(0) = 0 \tag{7.17a}$$

and

$$\mathbf{A}\,\dot{\mathbf{a}} + \mathbf{B}\,\mathbf{a} = \mathbf{c}\,\dot{g}(t) \tag{7.17b}$$

then (within our Galerkin approximation)

$$\mathrm{D}^{\alpha}[g(t)] = \frac{1}{\Gamma(1+\alpha)\Gamma(1-\alpha)}\,\mathbf{c}^{T}\mathbf{a}\,.$$

But, by definitions of fractional integral and derivative,

$$\mathrm{D}^{\alpha}[g(t)] = \frac{1}{\Gamma(1-\alpha)}\int_0^t \frac{\dot{g}(\tau)}{(t-\tau)^{\alpha}}d\tau = \frac{1}{\Gamma(1-\alpha)}\int_0^t \frac{h(\tau)}{(t-\tau)^{\alpha}}d\tau = \mathrm{I}^{1-\alpha}[h(t)]\,,$$

hence

$$\mathrm{I}^{1-\alpha}[h(t)] = \frac{1}{\Gamma(1+\alpha)\Gamma(1-\alpha)}\,\mathbf{c}^{T}\mathbf{a}\,. \tag{7.18}$$

Keeping this in mind along with the fact that fractional derivatives in general do not follow either the law of exponents or the commutative property, as mentioned in Section 7.2, we adopt the following strategy:

1. Compute matrices $\mathbf{A}$, $\mathbf{B}$ and $\mathbf{c}$ for $1-\alpha$ order derivatives instead of α order derivatives. To emphasize this crucial distinction, we write $\mathbf{A}_{1-\alpha}$, $\mathbf{B}_{1-\alpha}$ and $\mathbf{c}_{1-\alpha}$ respectively.

2. Replace equation (7.16) by the following system:

$$x(t) + y(t) = f(t)\,, \tag{7.19a}$$

$$\mathbf{A}_{1-\alpha}\dot{\mathbf{a}} + \mathbf{B}_{1-\alpha}\mathbf{a} = \mathbf{c}_{1-\alpha}\,y(t) \tag{7.19b}$$

and

$$x(t) - \frac{1}{\Gamma(\alpha)\,\Gamma(2-\alpha)}\mathbf{c}_{1-\alpha}^{T}\mathbf{a} = 0\,. \tag{7.19c}$$

Here, equation (7.19) is a set of differential algebraic equations (DAEs) [58]. By equations (7.17) and (7.18), equation (7.19c) can be rewritten as

$$x(t) - \mathrm{I}^{\alpha} y(t) = 0$$

or

$$\mathrm{D}^{\alpha} x(t) = y(t)\,, \quad \text{provided} \quad \mathrm{D}^{\alpha}\mathrm{I}^{\alpha} y(t) = y(t)\,. \tag{7.20}$$

It happens that $\mathrm{D}^{\alpha}\mathrm{I}^{\alpha} y(t) = y(t)$ (see Section 8.4.1 or [47] for details). On substituting Equation (7.20) into Equation (7.19a), we get Equation (7.16). Thus in totality Equation (7.19) within the accuracy of Galerkin approximation is equivalent to Equation (7.16).

We used $\alpha = 1/2$ and $1/3$ for numerical simulations. The index of the DAEs here (see [58] for details) is one. For both values of α, DAEs (7.19) are solved using Matlab's built in function "ode23t" for $f(t) = 1$. Consistent initial conditions are calculated as $x(0) = 0\,,\ \mathbf{a}(0) = \mathbf{0}$ and $y(0) = 1$; a guess for corresponding initial slopes, which is an optional input to "ode23t," is $\dot{x}(0) = 0\,,\ \dot{\mathbf{a}}(0) = \mathbf{A}_{1-\alpha}^{-1}\mathbf{c}_{1-\alpha}$ and $\dot{y}(0) = 0$. Results obtained will be presented later.

7.5.2 Analytical Solutions

The solution of equation (7.16) can be obtained using Laplace transforms. For $\alpha = 1/2$, MAPLE gives

$$x(t) = -e^{t}\left(\mathrm{erfc}\left(\sqrt{t}\right) - e^{-t}\right)\,. \tag{7.21}$$

Since we were unable to analytically invert the Laplace transform using MAPLE for $\alpha = 1/3$, we present a series solution below, along the lines of our previous series solutions (this solution is not new, and will be familiar to readers who know about Mittag-Leffler functions).

The Laplace transform of the solution to equation (7.16) for $\alpha = 1/3$ is given by

$$X(s) = \frac{1}{s(1 + s^{1/3})} = \frac{[1 - (-s^{-1/3})]^{-1}}{s^{4/3}}\,. \tag{7.22}$$

On expanding the numerator above (assuming $|s| > 1$) and simplifying, we get

$$X(s) = \sum_{n=4}^{\infty} \frac{(-1)^n}{s^{n/3}} \,. \tag{7.23}$$

The above series is absolutely convergent for $|s| > 1$. Inverting gives

$$x(t) = \sum_{n=4}^{\infty} \frac{(-1)^n \, t^{n/3-1}}{\Gamma(n/3)} \,. \tag{7.24}$$

7.5.3 Results

Numerical results are shown in Fig. 7.4. The Galerkin approximation matches the exact solutions well in both cases. The sum in equation (7.24) is taken upto the $\mathcal{O}(t^{150})$ term (fewer may have sufficed).

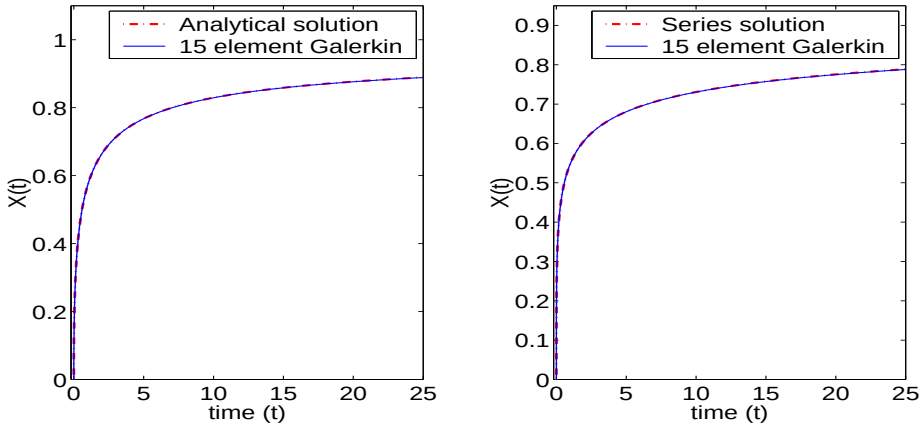

Figure 7.4: Comparison between analytical and 15 element Galerkin approximation solutions. Left: $\alpha = 1/2$. Right: $\alpha = 1/3$. For $\alpha = 1/3$, the series is summed up to $\mathcal{O}(t^{150})$.

7.6 Discussion

We have identified three classes of FDEs that are amenable to solution using a new Galerkin approximation for the fractional order derivative, that was developed in Chapters 5 and

6. To showcase the effectiveness of the approximation technique, we have used linear FDEs which could also be solved analytically (if only in the form of fractional power series). However, more general linear and nonlinear problems which are impossible to solve analytically are also expected to be equally effectively solved using this approximation technique.

The approximation technique used here, as discussed in Chapters 5 and 6, involves numerical evaluation of certain matrices. For approximation of a derivative of a given fractional order between 0 and 1, and with a given number of shape functions in the Galerkin approximation, these matrices need be calculated only once. They can then be used in any problem where a derivative of the same order appears. We hope that this technique will serve to provide a simple, reliable, and routine method of numerically solving FDEs in a wide range of applications.

Chapter 8

DAE-based Solution of Nonlinear Multiterm FIEs

In this chapter, we extend applications of our Galerkin technique to solve fractional differential equations (FDEs). The technique has previously (Chapters 5 and 7) been used to solve FDEs involving derivatives of order between 0 and 1 only, and with zero initial conditions. Here we show how the method can be used for a broader class of possibly-nonlinear multiterm fractional integrodifferential equations with nonzero initial conditions. In particular, we develop a set of differential algebraic equations (DAEs) that can be used to obtain useful solutions for such problems. Numerical solutions using Matlab demonstrate the effectiveness of the proposed approach.

8.1 Introduction

Fractional differential and integral operators have been used in many problems of science and engineering [2, 10]. For an introduction to the fundamental ideas, see [47, 48, 49]. Exact analytical solution of such equations tends to be difficult, if not impossible, especially in the presence of nonlinearities and multiple terms involving fractional order derivatives or integrals of various, possibly incommensurate, orders. Numerical solution of nonlinear multiterm fractional integrodifferential equations (FIEs) has also been considered difficult. In what seems to be the first serious attack on this problem, Diethelm and Ford [59] present

a numerical scheme that involves approximating incommensurate orders (if any) with commensurate ones; and constructing a system of equations that may be very large. The system of [59] *will* be large if orders are incommensurate and high accuracy is desired; note that the incommensurate nature of the orders of derivatives involved causes the largeness of the system due to the nature of their approximation scheme. Momani [60] obtains series solutions for FIEs using the Adomian decomposition. We also mention the accurate Laplace-domain approximations to fractional order operators developed in [19], whose rational transfer functions imply multiple derivatives on both input and output sides, leading to somewhat different issues than ours regarding initial conditions in explicit time domain calculations.

In this work, we bring an entirely different approach to this problem. Our approach has two key elements in the present context. The first key element is the use of a Galerkin procedure to accurately compute fractional order derivatives of a numerically known function $x(t)$ (actually, the method computes fractional order integrals of $\dot{x}(t)$). This Galerkin procedure, with some preliminary examples, is presented in detail in Chapter 5. The second key element is the use of differential algebraic equations (DAEs) within the solution strategy. DAEs can now be solved routinely using widely available packages like Matlab, and the use of DAEs lets us easily solve some useful problems using the Galerkin procedure (see [55]). Here, we continue to develop the approach further and extend the range of problems that can be tackled using this approach to include nonlinear multiterm fractional integrodifferential equations.

Our approach does not, in principle, rely on approximation of incommensurate orders with commensurate ones (unlike [59]). It does rely, through the Galerkin procedure, on approximating the fractional order integrals and derivatives through the introduction of a finite number of additional (internal) state variables; as shown and discussed in Chapters 5 and 6, excellent numerical solutions can be obtained. The main contribution of the present work lies in extending the range of problems that can be tackled, in particular including some nonlinear multiterm equations which, as discussed in [59], are difficult to solve numerically.

For motivation, we put down here an example of the sort of equations we have in mind:

$$\mathrm{D}^{\alpha}x(t) + f(x,t)\mathrm{D}^{\beta}x(t) + g(x,t)\mathrm{I}^{\gamma}x(t) + h(x,t) = 0,$$

with, say, $0 < \{\alpha, \beta, \gamma\} < 1$ and $x(0) = x_0$; and where D represents a fractional order derivative, and I represents a fractional order integral. The demonstration that a set of DAEs that we will develop below can be used to obtain a solution of this problem is the main contribution of this work.

For completeness, we first present the definitions of a fractional integral and derivative related to this work, followed by a brief introduction to the Galerkin technique.

8.2 Definitions

The fractional integral of order α is given using the Riemann-Liouville definition [47, 48], as

$$\mathrm{I}^{\alpha} x(t) = \frac{1}{\Gamma(\alpha)} \int_0^t \frac{x(\tau)}{(t-\tau)^{1-\alpha}}\, d\tau\,, \tag{8.1}$$

where $\alpha > 0$. Similarly, the Riemann-Liouville fractional derivative of order α is given as

$$\mathrm{D}^{\alpha} x(t) = \frac{1}{\Gamma(n-\alpha)} \frac{d^n}{dt^n} \left[\int_0^t \frac{x(\tau)}{(t-\tau)^{\alpha-n+1}} d\tau \right]\,, \tag{8.2}$$

where $n-1 < \alpha < n$ and n is a positive integer, notice that the above definition is similar to that given in Equation (5.1) for $\alpha = n + q$ and $b = 0$. The Riemann-Liouville fractional derivatives are used frequently in the mathematical literature, but their applications in science and engineering encounter difficulties associated with nonzero initial conditions.

Another definition for a fractional derivative was proposed by Caputo [61]. According to this definition, a fractional derivative of order α is given by

$$\mathrm{D}_*^{\alpha} x(t) = \frac{1}{\Gamma(n-\alpha)} \int_0^t \frac{x^{(n)}(\tau)}{(t-\tau)^{\alpha-n+1}} d\tau\,, \tag{8.3}$$

where $n-1 < \alpha < n$; n is a positive integer; and $x^{(n)}(t)$ denotes the n^{th} derivative of $x(t)$. The above definition of the fractional derivative is more popular in science and engineering problems modeled by fractional differential equations (FDEs), because an FDE involving a Caputo derivative can be initialized like a routine initial value ODE. This is the definition that we will adopt in this chapter.

To avoid confusion below, we emphasize the notation adopted here: D_* refers to the Caputo derivative, while D refers to the Riemann-Liouville derivative. A point in the

passing may be noted that Riemann-Liouville as well as Caputo definitions of fractional derivatives are same for *zero* initial conditions.

Systems with fractional integrals or derivatives are in general difficult to solve analytically; also, due to the non-local nature of the operators involved, long-time numerical solutions are computationally expensive. The Galerkin technique of Chapters 5 and 6 reduces the fractional derivative to a set of first order ODEs, which can be easily yet accurately solved at low computational cost. For completeness, we now briefly present the Galerkin technique.

8.3 Development of the Galerkin procedure

8.3.1 An Infinite Dimensional System

Consider the PDE (or ODE in t with a free parameter ξ)

$$\frac{\partial}{\partial t}u(\xi,t) + \xi^{\left(\frac{1}{\alpha}\right)} u(\xi,t) = \delta(t)\,, \quad u(\xi,0^-) \equiv 0\,, \tag{8.4}$$

where $\alpha > 0$ and $\delta(t)$ is the Dirac delta function. The solution is

$$u(\xi,t) = h(\xi,t) = \exp(-\xi^{1/\alpha}\, t)\,,$$

where the notation $h(\xi,t)$ is used to denote "impulse response function." On integrating h with respect to ξ between 0 and ∞ we get a function only of t, given by

$$g(t) = \int_0^\infty h(\xi,t)\, d\xi = \frac{\Gamma(1+\alpha)}{t^\alpha}\,. \tag{8.5}$$

Abstractly, $g(t)$ is simply the impulse response of a linear, constant coefficient system starting from rest.

Now if we replace the forcing $\delta(t)$ in Equation (8.4) with some sufficiently well behaved function $x(t)$, then the corresponding response $r(t)$ of the same system again starting from rest at $t = 0$, is

$$r(t) = \int_0^t g(t-\tau)x(\tau)\, d\tau = \Gamma(1+\alpha)\int_0^t \frac{x(\tau)}{(t-\tau)^\alpha}\, d\tau\,. \tag{8.6}$$

8.3.1.1 An Equivalent of the Fractional Integral

Here we propose an equivalent of a fractional integral of order $0 < \alpha < 1$. Suppose we replace α in Equation (8.4) by $1 - \alpha$ and $\delta(t)$ by a well behaved function $x(t)$ then $r(t)$ of Equation (8.6) becomes

$$r(t) = \Gamma(2-\alpha) \int_0^t \frac{x(\tau)}{(t-\tau)^{1-\alpha}}\, d\tau\,.$$

Now, by the definition of the fractional integral (Equation (8.1))

$$\mathrm{I}^{\alpha} x(t) = \frac{1}{\Gamma(\alpha)} \int_0^t \frac{x(\tau)}{(t-\tau)^{1-\alpha}}\, d\tau = \frac{r(t)}{\Gamma(\alpha)\Gamma(2-\alpha)}\,, \tag{8.7}$$

where $\mathrm{I}^{\alpha} x(t)$ is an α order integral of $x(t)$.

8.3.1.2 An Equivalent of the Caputo Fractional Derivative

Here we propose an equivalent of a Caputo type fractional derivative of an arbitrary order α such that $n-1 < \alpha < n$, where n is a positive integer. Now, replacing α in Equation (8.4) by $\alpha - n + 1$ and $\delta(t)$ by a well behaved function $x^{(n)}(t)$, $r(t)$ in Equation (8.6) becomes

$$r(t) = \Gamma(\alpha - n + 2) \int_0^t \frac{x^{(n)}(\tau)}{(t-\tau)^{\alpha-n+1}} d\tau\,.$$

Now, by the definition of the Caputo fractional derivative (Equation (8.3))

$$\mathrm{D}_*^{\alpha} x(t) = \frac{1}{\Gamma(n-\alpha)} \int_0^t \frac{x^{(n)}(\tau)}{(t-\tau)^{\alpha-n+1}} d\tau = \frac{r(t)}{\Gamma(n-\alpha)\Gamma(\alpha-n+2)}\,, \tag{8.8}$$

where $\mathrm{D}_*^{\alpha} x(t)$ is an α order derivative of $x(t)$.

There is no approximation so far. Equation (8.4) represents an infinite dimensional system, and hence we have replaced one infinite dimensional system (fractional integral/derivative) with another. But we can use a Galerkin projection to reduce Equation (8.4) to a finite system of ODEs. In this way, a fractional integral or derivative will also be replaced by a finite set of ODEs using a Galerkin projection, as described below.

8.3.2 Galerkin Scheme

The Galerkin procedure used here is explained in detail in Chapters 5 and 6. The Galerkin procedure requires computation of system matrices $\mathbf{A}\,, \mathbf{B}$ and $\mathbf{c}$. These matrices are functions of a single parameter α. The matrices $\mathbf{A}$ and $\mathbf{B}$ are $m \times m$, and $\mathbf{c}$ is $m \times 1$, where the positive integer m is the order of the approximation (for the numerical results presented in this work, $m = 15$). We have used nonuniform finite elements with "hat" functions for the discretization (see, Chapter 6).

Definition: In this work we introduce subscripts for clarity and define $\mathbf{A}_\alpha\,, \mathbf{B}_\alpha$ and $\mathbf{c}_\alpha$ as the system matrices[1] of Chapter 6 computed for a given value of α.

8.3.2.1 Case I: Fractional Integral

A fractional integral of order α between 0 and 1 is approximated as follows:

1. Compute system matrices $\mathbf{A}_{1-\alpha}\,, \mathbf{B}_{1-\alpha}$ and $\mathbf{c}_{1-\alpha}$ as described in Chapter 6,
2. Numerically integrate the ODEs

$$\mathbf{A_{1-\alpha}}\dot{\mathbf{a}} + \mathbf{B_{1-\alpha}}\,\mathbf{a} = \mathbf{c_{1-\alpha}}\,x(t) \tag{8.9}$$

with initial conditions to be described below, and obtain the approximation

$$\mathrm{I}^\alpha x(t) \approx \frac{1}{\Gamma(\alpha)\Gamma(2-\alpha)}\,\mathbf{c}_{1-\alpha}^T\mathbf{a}\,. \tag{8.10}$$

8.3.2.2 Case II: Fractional Derivative

A Caputo type fractional derivative of order α between non-negative integers $n-1$ and n is approximated as follows:

1. Compute system matrices $\mathbf{A}_{\alpha-n+1}\,, \mathbf{B}_{\alpha-n+1}$ and $\mathbf{c}_{\alpha-n+1}$ as described in Chapter 6.

[1] A Maple-8 worksheet to compute the matrices $\mathbf{A}_\alpha$, $\mathbf{B}_\alpha$ and $\mathbf{c}_\alpha$ is available on request: (email: sjsingh@mecheng.iisc.ernet.in, anindya100@gmail.com).

2. Numerically integrate the ODEs in

$$\mathbf{A}_{\alpha-\mathbf{n}+\mathbf{1}}\dot{\mathbf{a}} + \mathbf{B}_{\alpha-\mathbf{n}+\mathbf{1}}\,\mathbf{a} = \mathbf{c}_{\alpha-\mathbf{n}+\mathbf{1}}\,x^{(n)}(t) \tag{8.11}$$

with initial conditions to be described below, and obtain the approximation

$$\mathrm{D}_*^{\alpha}x(t) \approx \frac{1}{\Gamma(n-\alpha)\Gamma(\alpha-n+2)}\,\mathbf{c}_{\alpha-n+1}^{T}\mathbf{a}\,. \tag{8.12}$$

In both cases above, $\mathbf{a}$ is an $m \times 1$ vector of m internal variables that approximate the infinite-dimensional dynamics of the actual fractional order integral and derivative respectively. Note that $x(t)$ above is generally unknown in advance, and is computed in parallel with $\mathbf{a}$ using the integrodifferential equation we have set out to solve in the first place, wherein we insert the approximation for $\mathrm{I}^{\alpha}x(t)$ and/or $\mathrm{D}_*^{\alpha}x(t)$ (see examples in [55] in addition to those given below).

8.3.3 A Preliminary Example

Consider the following integral equation

$$g(x,t) + h(x,t)\,\mathrm{I}^{\alpha}x(t) = 0, \quad 0 < \alpha < 1. \tag{8.13}$$

8.3.3.1 DAE-based Method

The fractional integral of Equation (8.13) is approximated as explained in Section 8.3.2.1 to give

$$g(x,t) + h(x,t)\,\frac{1}{\Gamma(\alpha)\Gamma(2-\alpha)}\mathbf{c}_{1-\alpha}^{T}\mathbf{a} = 0 \tag{8.14a}$$

and

$$\mathbf{A}_{\mathbf{1}-\alpha}\dot{\mathbf{a}} + \mathbf{B}_{\mathbf{1}-\alpha}\,\mathbf{a} = \mathbf{c}_{1-\alpha}\,x(t)\,, \tag{8.14b}$$

where $\mathbf{A}_{\mathbf{1}-\alpha}\,,\mathbf{B}_{\mathbf{1}-\alpha}$ and $\mathbf{c}_{1-\alpha}$ are as explained in Section 8.3.2.1. Equations (8.14) are a set of differential algebraic equations (DAEs) of index 1 (see [58] for more details about DAEs).

Here, for comparison with analytical/series solution we solve a linear example of Equation (8.13) by assuming $g(x,t) = x(t) - f(t)$ and $h(x,t) = 1$. The resulting DAEs

(8.14) are solved using the Matlab function "ode15" for $\alpha = 1/2$ as well as $2/3$, and for $f(t) = \sin(t) + \cos(t)$. It may be noted here that with the above mentioned choice of $g(x,t)$, Equation (8.13) becomes an Abel's integral equation.

The consistent initial condition used for $x(t)$ is $x(0) = f(0) = 1$, for reasons discussed next. Initial conditions for $\mathbf{a}$ require some attention as well.

It is clear from the definition of the fractional integral (see Equation (8.1)) that, if $x(\tau)$ is bounded for $\tau \in [0,t]$, then $\mathrm{I}^{\alpha}x(t) \to 0$ as $t \to 0$. This leads to the initial condition $x(0) = f(0) = 1$. Further, $\mathbf{a}(0) = \mathbf{0}$ (using Equation (8.10)) is the choice of initial conditions for $\mathbf{a}$ which is consistent with the requirement that the system starts from rest in the PDE of Equation (8.4).

Numerical results obtained are presented below. We note first the analytical solution of Equation (8.13) is given by

$$x(t) = \int_0^t f(t-\tau)\, e'_{\alpha}(\tau)\, d\tau + f(t),$$

where the prime denotes a derivative, and $e_{\alpha}(t) = E_{\alpha}(-t^{\alpha})$, the Mittag-Leffler function [10] of order α; the above solution can be found using term by term integration from a power series solution (details omitted).

8.3.3.2 Numerical Results

The results of numerical solution are compared with the analytical solution in Figure 8.1. The DAE-based approximation scheme matches the exact analytical solution very well for $\alpha = 1/2$ and $2/3$.

8.4 Multiterm Fractional Integrodifferential Equations

Consider the nonlinear multiterm fractional integrodifferential equation

$$\mathrm{D}_*^{\alpha}x(t) + f(x,t)\,\mathrm{D}_*^{\beta}x(t) + g(x,t)\,\mathrm{I}^{\gamma}x(t) + h(x,t) = 0\,, \quad x(0) = x_0\,, \text{ and } \alpha\,,\beta\,,\gamma \in (0,1). \tag{8.15}$$

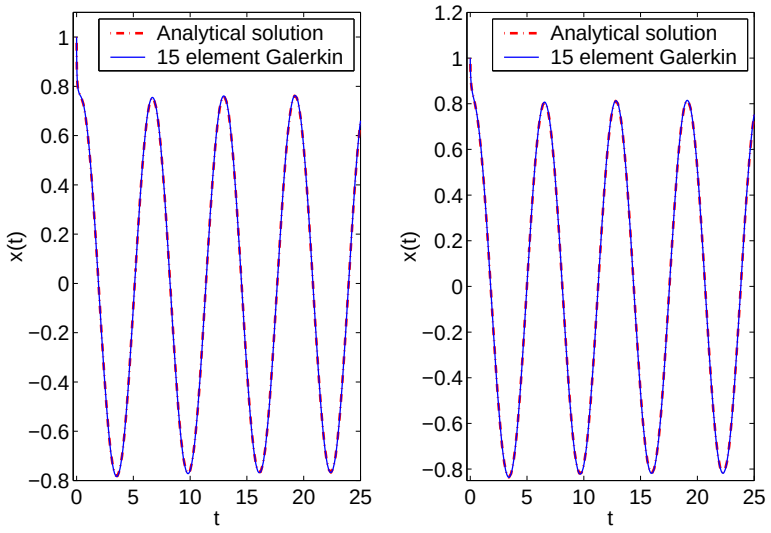

Figure 8.1: Comparison between analytical and DAE-based approximation solutions. Left: $\alpha = 1/2$. Right: $\alpha = 2/3$.

Analytical solution is impossible in general; some linear constant coefficient cases can be tackled using the Laplace transform. Here, we develop a numerical solution.

8.4.1 Development of DAE-based Numerical Solution

Our Galerkin procedure requires $\dot{x}(t)$ as an input (see Equations (8.11) and (8.12) with $n = 1$ and $0 < \alpha < 1$), which is not available here. Observe that $x(t)$ forcing in Equation (8.9) results in an α order integral of $x(t)$ in Equation (8.10). Keeping this in mind, we replace Equation (8.15) by the following system:

$$\mathbf{A}_{1-\alpha}\dot{\mathbf{a}} + \mathbf{B}_{1-\alpha}\mathbf{a} = \mathbf{c}_{1-\alpha}\, y(t), \tag{8.16a}$$

$$x(t) - \frac{1}{\Gamma(\alpha)\,\Gamma(2-\alpha)}\mathbf{c}_{1-\alpha}^T\mathbf{a} = x(0), \tag{8.16b}$$

$$\mathbf{A}_{1-\beta}\dot{\mathbf{b}} + \mathbf{B}_{1-\beta}\mathbf{b} = \mathbf{c}_{1-\beta}\, z(t), \tag{8.16c}$$

$$x(t) - \frac{1}{\Gamma(\beta)\,\Gamma(2-\beta)}\mathbf{c}_{1-\beta}^T\mathbf{b} = x(0), \tag{8.16d}$$

$$\mathbf{A}_{1-\gamma}\dot{\mathbf{d}} + \mathbf{B}_{1-\gamma}\mathbf{d} = \mathbf{c}_{1-\gamma}\, x(t), \tag{8.16e}$$

$$y(t) + f(x,t)\, z(t) + g(x,t)\, \frac{\mathbf{c}_{1-\gamma}^T\mathbf{d}}{\Gamma(\gamma)\,\Gamma(2-\gamma)} + h(x,t) = 0\,. \tag{8.16f}$$

Equation (8.16a-f) is a set of DAEs, whose choice will now be justified. The following demonstration that this set of DAEs effectively also gives the solution for Equation (8.15) is the main contribution of this work.

By Equations (8.9), (8.10), and (8.16a), Equation (8.16b) can be rewritten as (up to the accuracy of the Galerkin procedure)

$$x(t) - \mathrm{I}^{\alpha} y(t) = x(0)\,.$$

On taking an α order Caputo derivative of the above, we get

$$\mathrm{D}_{*}^{\alpha} x(t) - \mathrm{D}_{*}^{\alpha}\mathrm{I}^{\alpha} y(t) = 0\,. \tag{8.17}$$

Now, the second term in the left side of the above can be rewritten, by direct application of the definitions of Caputo and Riemann-Liouville derivatives, as

$$\mathrm{D}_{*}^{\alpha}\mathrm{I}^{\alpha} y(t) = \mathrm{I}^{1-\alpha}\mathrm{D}\,\mathrm{I}^{\alpha} y(t) = \mathrm{I}^{1-\alpha}\mathrm{D}^{1-\alpha} y(t).$$

On noting the identity $\mathrm{I}^{\alpha}\mathrm{I}^{\beta} f(t) = \mathrm{I}^{\alpha+\beta} f(t)$, we can simplify

$$\begin{aligned}\mathrm{I}^{1-\alpha}\mathrm{D}^{1-\alpha} y(t) = \mathrm{I}^{1-\alpha}\left[y(0)t^{\alpha-1}/\Gamma(\alpha) + \mathrm{D}_{*}^{1-\alpha} y(t)\right] &= y(0) + \mathrm{I}^{1-\alpha}\mathrm{I}^{\alpha}\mathrm{D}_{*} y(t) \\ &= y(0) + \mathrm{I}\,\mathrm{D}_{*} y(t) = y(0) + y(t) - y(0) = y(t).\end{aligned}$$

Hence, by Equation (8.17) and the above result, we reach the important conclusion:

$$\mathrm{D}_{*}^{\alpha} x(t) = y(t)\,. \tag{8.18}$$

By similar analysis of Equation (8.16d), we reach another important conclusion:

$$\mathrm{D}_{*}^{\beta} x(t) = z(t)\,. \tag{8.19}$$

Finally, it is clear by Equations (8.9), (8.10), and (8.16e) that $\dfrac{\mathbf{c}_{1-\gamma}^{T}\mathbf{d}}{\Gamma(\gamma)\,\Gamma(2-\gamma)}$ in the third term of Equation (8.16f) represents $\mathrm{I}^{\gamma} x(t)$.

Therefore, Equation (8.16a-f) in totality ensures that Equation (8.16f), within the accuracy of the Galerkin approximation, is identical to Equation (8.15). It is also clear that nonlinear multiterm fractional integrodifferential equations of more general forms can easily be handled using this same strategy; however, for simplicity, we restrict our explicit discussion to the form used here. Initial conditions to be used for the DAEs will be discussed below.

8.4.2 Numerical Examples

8.4.2.1 Linear Constant Coefficient Multiterm FIE

As a linear constant coefficient example of Equation (8.15), we use

$$f(x,t) = g(x,t) = 1\,, h(x,t) = x - 1;\ \alpha = 2/3\,, \beta = 1/3\,, \gamma = 1/2;\ \text{ and } x(0) = 2. \quad (8.20)$$

Index one DAEs (see [58]) such as Equation (8.16) can be solved using Matlab's built in function "ode15i". Initial conditions for $\mathbf{a}\,, \mathbf{b}\,, \mathbf{d}\,, y$ and z are obtained as follows.

As discussed above, the second term on the left hand side of Equation (8.16b) is an α-order integral of $y(t)$. Therefore, for a well behaved function $y(t)$ the initial conditions for $\mathbf{a}$ used here are the same as in Section 8.3.3.1, i.e., $\mathbf{a}(0) = \mathbf{0}$. Using similar arguments for Equations (8.16d) and (8.16e), we get $\mathbf{b}(0) = \mathbf{d}(0) = \mathbf{0}$. Variables $y(t)$ and $z(t)$ of DAEs (8.16) are α and β order derivatives of $x(t)$ respectively, and their initialization follows the discussion in [62], where the relevant conclusion is that, for $t \to 0$, only the highest order derivative is allowed to be nonzero. By this criterion, using initial values of x and $\mathbf{d}$, in Equation (8.16f), we get $y(0) = -1$ and $z(0) = 0$. After obtaining initial conditions for the full state vector, use of $x(0)$ in the right sides of Equation (8.16b) or (8.16d) is now seen to be consistent and correct (the $x(0)$ there may be viewed as an integration constant chosen to match initial conditions).

Series Solution using Laplace Transform

For comparison with numerics, we need an analytical (series) solution. The Laplace transform (see, e.g., [63]) of the solution to Equation (8.15), with Equation (8.20), is given by

$$X(s) = \left[x(0)\left(\frac{1}{s} + \frac{1}{s^{1+\alpha-\beta}}\right) + \frac{1}{s^{1+\alpha}}\right]\left[1 + s^{\beta-\alpha} + s^{-\alpha} + s^{-\gamma-\alpha}\right]^{-1}$$

We expand $[1+s^{\beta-\alpha}+s^{-\alpha}+s^{-\gamma-\alpha}]^{-1}$ above in a series for $|s^{\beta-\alpha}+s^{-\alpha}+s^{-\gamma-\alpha}| < 1$, because $\alpha, \beta, \gamma > 0$ and $\beta < \alpha$ and we are prepared to let s be large (in particular, on a vertical line as far into the complex right half-plane as needed). The series we obtain is

$$X(s) = \sum_{n=0}^{\infty}\sum_{k=0}^{n}\sum_{l=0}^{k}\binom{n}{k}\binom{k}{l}(-1)^n\left[\frac{x(0)}{s^{1+n/3+k/3+l/2}} + \frac{x(0)}{s^{4/3+n/3+k/3+l/2}} + \frac{1}{s^{5/3+n/3+k/3+l/2}}\right].$$

Taking the inverse Laplace transform of the above,

$$x(t) = \sum_{n=0}^{\infty} \sum_{k=0}^{n} \sum_{l=0}^{k} \binom{n}{k} \binom{k}{l} (-1)^n \left[\frac{x(0)\, t^{n/3+k/3+l/2}}{\Gamma\left(1+n/3+k/3+l/2\right)} + \frac{x(0)\, t^{1/3+n/3+k/3+l/2}}{\Gamma\left(4/3+n/3+k/3+l/2\right)} + \frac{t^{2/3+n/3+k/3+l/2}}{\Gamma\left(5/3+n/3+k/3+l/2\right)} \right] \quad (8.21)$$

In the results presented below, we compare the numerical solution obtained using our DAE-based method with the numerical sum of the series of Equation (8.21) truncated at some suitably large value of n. In particular, truncation at $n = 3p$ (say) gives terms correct upto $\mathcal{O}(t^p)$.

Results

Numerical results are shown in Figure 8.2. The DAE-based solution matches the series solution (truncated at $n = 600$) in Equation (8.21) very well. Absolute error, over a fairly long time interval, is less than 0.0015 and relative error is less than 1%. We emphasize that the Galerkin procedure used in the background of the simulation had only 15 finite elements; increasing the number of elements will reduce the error. However, even at this level of refinement, there is no doubt that our DAE-based method works well.

8.4.2.2 Nonlinear Multiterm FIEs

Consider the following multiterm nonlinear FIE

$$\mathrm{D}_*^{\alpha} x(t) + x(t)\, \mathrm{D}_*^{\beta} x(t) + x(t)\, \Gamma^{\gamma} x(t) + x(t)^3 = p(t)\,, \quad x(0) = 1, \quad \alpha = 2/3,\ \beta = 1/3 \ \text{ and } \ \gamma = 1/2. \quad (8.22)$$

The above FIE is difficult to solve analytically. For the particular case (artificially

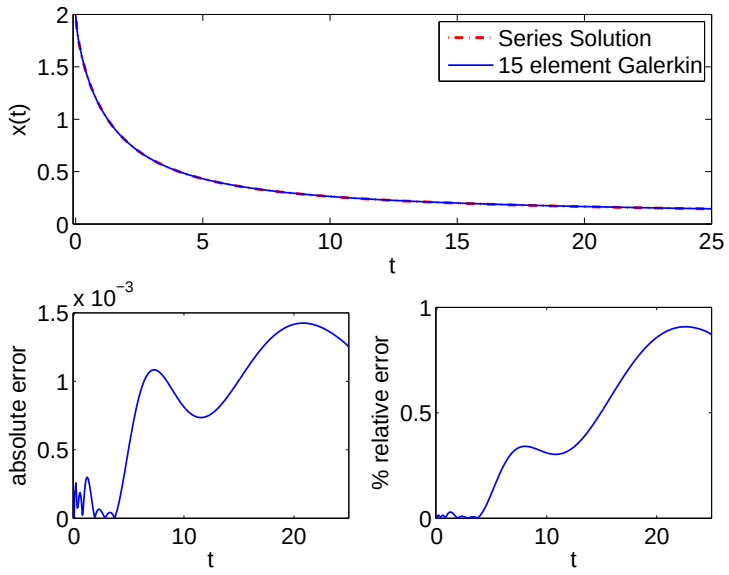

Figure 8.2: Top: numerical solution of Equation (8.15) for Equation (8.20). Bottom: error.

constructed, like an example in [59]) of

$$p(t) = 1/4\,\frac{\sqrt{3}\Gamma\left(2/3\right)\sqrt[3]{t}\left(-12+9\,\ln\left(3\right)+6\,\ln\left(t\right)+\sqrt{3}\pi\right)}{\pi}+ \\ \left(1+t\,\ln\left(t\right)\right)\left(1/4\,\frac{t^{2/3}\left(-3+9\,\ln\left(3\right)+6\,\ln\left(t\right)-\sqrt{3}\pi\right)}{\Gamma\left(2/3\right)}+ \right. \\ \left. 2/9\,\frac{\sqrt{t}\left(9-10\,t+12\,t\,\ln\left(2\right)+6\,t\,\ln\left(t\right)\right)}{\sqrt{\pi}}+\left(1+t\,\ln\left(t\right)\right)^2\right) \quad (8.23)$$

and $x(0) = 1$, this equation has the solution

$$x(t) = 1 + t\,\ln(t).$$

We solve the above FIE using our DAE-based technique. The procedure is similar to that explained in Section 8.4.2.1; replace in Equation (8.15) $f(x,t)$ and $g(x,t)$ by $x(t)$; replace $h(x,t)$ by $x(t)^3 - p(t)$; and thus obtain DAE (8.16), to be solved using Matlab's DAE solver "ode15i". Initial conditions for x, y and z are now $x(0) = 1$, $y(0) = 0$ and $z(0) = 0$; the remaining initial conditions remain the same as Section 8.4.2.1.

Results

Numerical results are shown in Figure 8.3. It is clear, as in the previous case, that the DAE-based solution procedure works well. Errors are small, and may be made smaller by using more elements in the underlying Galerkin projection, as demonstrated by the convergence study of Figure 8.4, performed on the numerical solutions of Equation (8.22) with Equation (8.23). A very good convergence is obtained; the absolute error reduces by a factor of more than 20 when the the number of finite elements used in Galerkin approximation are increased from 15 to 30.

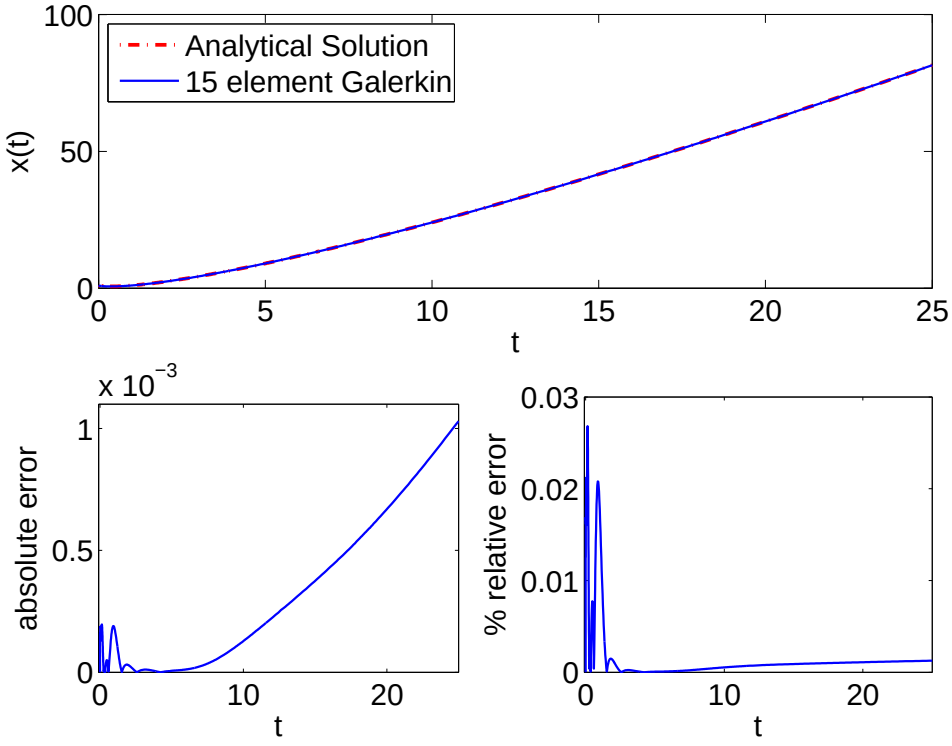

Figure 8.3: Top: numerical solution of Equation (8.22) with Equation (8.23). Bottom: error.

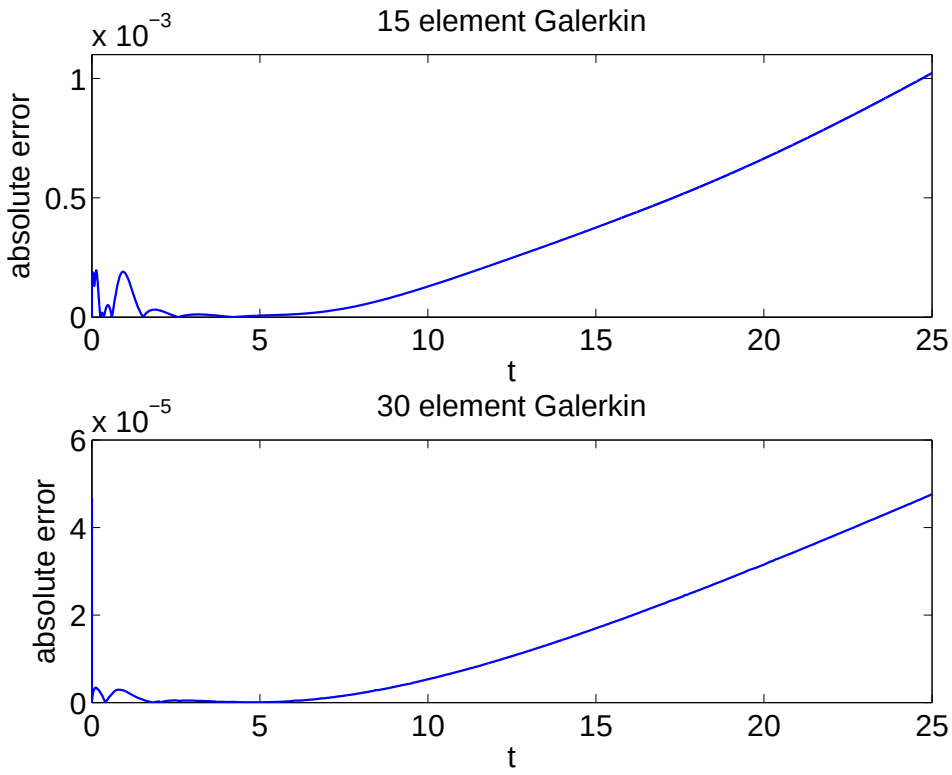

Figure 8.4: Convergence study for Equation (8.22) with Equation (8.23). Top: 15 element Galerkin. Bottom 30 element Galerkin.

We have successfully solved some multiterm FIEs using our approach. We now move on to derivatives of higher order.

Chapter 9

Solving Higher Order FDEs and FIEs

In Chapter 8, we have solved multiterm, possibly nonlinear, FIEs with nonzero initial conditions. The order of the fractional derivative and integral was assumed between 0 and 1. In this chapter, we extend applications of our Galerkin technique by solving FDEs and FIEs of higher order. The order of fractional derivative can now take any positive real values, whereas the value of fractional integral is between 0 and 1; nonzero initial conditions are allowed. A nonlinear multiterm FIE is also solved below to show the effectiveness of our method. Again, we develop a set of differential algebraic equations (DAEs) that can be used to obtain useful solutions for such problems. Numerical solutions using Matlab demonstrate the effectiveness of the proposed approach.

9.1 Elementary Example: Bagley-Torvik Equation

Consider the following equation

$$\ddot{x}(t) + \mathrm{D}_*^{\alpha} x(t) + x(t) = 0\,, \quad 1 < \alpha < 2 \quad \text{and} \quad x(0) = 1\,,\ \dot{x}(0) = 1\,. \tag{9.1}$$

This is known as the Bagley-Torvik equation. It arises in the modeling of the motion of a rigid plate immersed in a Newtonian fluid. It was originally proposed in [2] and is thoroughly discussed in [49].

We will consider $\alpha = 5/3$ here. But the method discussed below should work for all reasonable values of α between 1 and 2.

9.1.1 Galerkin Method

The fractional derivative of Equation (9.1) is approximated as explained in Section 8.3.2.2. Here, we take $n = 2$ and $\alpha = 5/3$. After approximation, Equation (9.1) is replaced by the following set of ODEs

$$\ddot{x}(t) + \frac{1}{\Gamma(n-\alpha)\Gamma(\alpha-n+2)}\mathbf{c}^T_{\alpha-n+1}\mathbf{a} + x(t) = 0 \tag{9.2a}$$

and

$$\mathbf{A}_{\alpha-n+1}\dot{\mathbf{a}} + \mathbf{B}_{\alpha-n+1}\,\mathbf{a} = \mathbf{c}_{\alpha-n+1}\,\ddot{x}(t)\,, \tag{9.2b}$$

where $\mathbf{A}_{\alpha-n+1}\,, \mathbf{B}_{\alpha-n+1}$ and $\mathbf{c}_{\alpha-n+1}$ are as explained in Section 8.3.2.2. Equations (9.2) are a set of ODEs. These ODEs are stiff in nature and are solved using the "Matlab" function "ode23t" for $x(0) = 1\,,\ \dot{x}(0) = 1$. Initial conditions for $\mathbf{a}$ are assumed to be $\mathbf{a}(0) = \mathbf{0}$ (by reasoning similar to Sections 8.3.3.1 and 8.4.2.1) because from Equation (8.3), $\mathrm{D}^{5/3}_*[x(t)] \to 0$ as $t \to 0$ when $\ddot{x}(\tau)$ is bounded for $\tau \in [0, t]$. The results obtained will be presented later.

9.1.2 Series Solution using Laplace Transform

The Laplace transform of the solution to Equation (9.1) is given by

$$X(s) = \left[x(0)\left(\frac{1}{s} + \frac{1}{s^{3-\alpha}}\right) + \dot{x}(0)\left(\frac{1}{s^2} + \frac{1}{s^{4-\alpha}}\right)\right][1 + s^{\alpha-2} + s^{-2}]^{-1}$$

We can expand $[1 + s^{\alpha-2} + s^{-2}]^{-1}$ above in a binomial series for $|(s^{\alpha-2} + s^{-2})| < 1$, because $1 < \alpha < 2$ and we are prepared to let s be as large needed (in particular, suppose we consider s values on a vertical line in the complex plane, we are prepared to choose that line as far into the right half plane as needed). The series we obtain (after substituting $x(0) = 1$ and $\dot{x}(0) = 1$ in the above) is

$$X(s) = \sum_{n=0}^{\infty}\sum_{r=0}^{n}(-1)^n\binom{n}{r}\left(\frac{1}{s^{2n-\alpha r+1}} + \frac{1}{s^{2n-\alpha(1+r)+3}} + \frac{1}{s^{2n-\alpha r+2}} + \frac{1}{s^{2n-\alpha(1+r)+4}}\right).$$

Taking the inverse Laplace transform of the above,

$$x(t) = \sum_{n=0}^{\infty}\sum_{r=0}^{n}(-1)^n\binom{n}{r}\left(\frac{t^{2n-\alpha r}}{\Gamma(2n-\alpha r+1)} + \frac{t^{2n-\alpha(1+r)+2}}{\Gamma(2n-\alpha(1+r)+3)} + \frac{t^{2n-\alpha r+1}}{\Gamma(2n-\alpha r+2)} + \frac{t^{2n-\alpha(1+r)+3}}{\Gamma(2n-\alpha(1+r)+4)}\right). \tag{9.3}$$

9.1.3 Results

Results for the above problem are shown in Figure 9.1. The Galerkin approximation matches well with the series solutions of Equation (9.1). The series of Equation (9.3) is truncated at some suitably large value of n. In particular, truncation at $n = p/2$ (say) gives terms correct upto $\mathcal{O}(t^p)$.

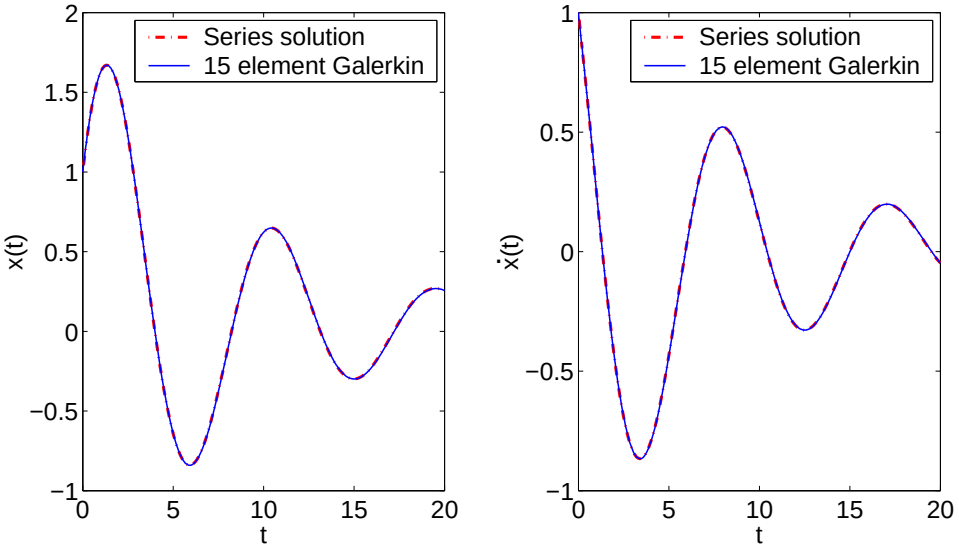

Figure 9.1: Comparison between Laplace transform and 15 element Galerkin approximation solutions, sum in Equation (9.3) upto $\mathcal{O}(t^{200})$: Left: displacement *vs* time. Right: velocity *vs* time.

9.2 Higher Order Multiterm FIEs

Consider the nonlinear multiterm fractional integrodifferential equation

$$\mathrm{D}_*^{\alpha} x(t) + f(x,t)\,\mathrm{D}_*^{\beta} x(t) + g(x,t)\,\mathrm{I}^{\gamma} x(t) + h(x,t) = 0\,, \quad \mathbf{x}(0) = \mathbf{x}_0, \tag{9.4}$$

where $n-1 < \alpha < n$, $m-1 < \beta < m$, $0 < \gamma < 1$ and $m < n$. Analytical solution of such FIEs is impossible in general; some linear constant coefficient cases can be tackled using the Laplace transform, but obtaining series solutions becomes very difficult if the order of

the FIE is large, and initial conditions are nonzero. Here, we develop a numerical solution similar to Section 8.4.1.

9.2.1 Development of DAE-based Numerical Solution

Our Galerkin procedure requires $x^{(n)}(t)$ as an input (see Equations (8.11) and (8.12)), which is not available here. To this end we use the definition of the Caputo derivative to obtain the following identity

$$\mathrm{D}_*^{\alpha} x(t) = \mathrm{D}_*^{\bar{\alpha}} x^{(n-1)}(t), \tag{9.5}$$

where $n-1 < \alpha < n$, $\bar{\alpha} = \alpha - n + 1$ and $x^{(n-1)}(t)$ denotes the $(n-1)^{th}$ derivative of $x(t)$. Substituting the above in Equation (9.4), we get

$$\mathrm{D}_*^{\bar{\alpha}} x^{(n-1)}(t) + f(x,t)\,\mathrm{D}_*^{\bar{\beta}} x^{(m-1)}(t) + g(x,t)\,\Gamma^{\gamma} x(t) + h(x,t) = 0\,, \quad \mathbf{x}(0) = \mathbf{x}_0, \tag{9.6}$$

where $0 < \{\bar{\alpha},\, \bar{\beta}\} < 1$, and $x^{(n-1)}(t)$ and $x^{(m-1)}(t)$ are known as a part of the state vector. Thus we can develop a solution strategy similar to Section 8.4.1. Replace Equation (9.6) by the following system:

$$\mathbf{A}_{1-\bar{\alpha}}\dot{\mathbf{a}} + \mathbf{B}_{1-\bar{\alpha}}\mathbf{a} = \mathbf{c}_{1-\bar{\alpha}}\, y(t), \tag{9.7a}$$

$$x^{(n-1)}(t) - \frac{1}{\Gamma(\bar{\alpha})\,\Gamma(2-\bar{\alpha})}\mathbf{c}_{1-\bar{\alpha}}^T\mathbf{a} = x^{(n-1)}(0), \tag{9.7b}$$

$$\mathbf{A}_{1-\bar{\beta}}\dot{\mathbf{b}} + \mathbf{B}_{1-\bar{\beta}}\mathbf{b} = \mathbf{c}_{1-\bar{\beta}}\, z(t), \tag{9.7c}$$

$$x^{(m-1)}(t) - \frac{1}{\Gamma(\bar{\beta})\,\Gamma(2-\bar{\beta})}\mathbf{c}_{1-\bar{\beta}}^T\mathbf{b} = x^{(m-1)}(0), \tag{9.7d}$$

$$\mathbf{A}_{1-\gamma}\dot{\mathbf{d}} + \mathbf{B}_{1-\gamma}\mathbf{d} = \mathbf{c}_{1-\gamma}\, x(t), \tag{9.7e}$$

$$y(t) + f(x,t)\, z(t) + g(x,t)\,\frac{\mathbf{c}_{1-\gamma}^T\mathbf{d}}{\Gamma(\gamma)\,\Gamma(2-\gamma)} + h(x,t) = 0\,. \tag{9.7f}$$

Note in the above that Equations (9.7b) and (9.7d) are treated as algebraic equations (*not* as differential equations) because $x^{(n-1)}(t)$ and $x^{(m-1)}(t)$ are available as part of the input state vector. Analysis of Equation (9.7b) similar to that done in Section 8.4.1 for Equation (8.16b) and the use of identity (9.5) implies that

$$\mathrm{D}_*^{\alpha} x(t) = \mathrm{D}_*^{\bar{\alpha}} x^{(n-1)}(t) = y(t),$$

similarly Equation (9.7d) gives

$$\mathrm{D}_*^{\beta} x(t) = \mathrm{D}_*^{\bar{\beta}} x^{(m-1)}(t) = z(t).$$

Keeping the above two results in mind, by the discussion of Section 8.4.1, Equation (9.7a-f) in totality ensures that Equation (9.7f), within the accuracy of the Galerkin approximation, is identical to Equation (9.4). It is also clear that nonlinear multiterm fractional integrodifferential equations of more general forms can easily be handled using this same strategy; however, for simplicity, we restrict our explicit discussion to the form used here.

9.2.2 Numerical Example

As a linear constant coefficient example of Equation (9.4), we use

$$f(x,t) = g(x,t) = 1\,, h(x,t) = x - 1;\ \alpha = 8/3\,, \beta = 4/3\,, \gamma = 1/2;\ \text{ and}$$
$$x(0) = 2,\ \dot{x}(0) = 0\ \text{ and }\ \ddot{x}(0) = 0. \quad (9.8)$$

Index one DAEs (see [58]) such as Equation (9.7) can be solved using Matlab's built in function "ode15i". Initial conditions for $\mathbf{a}\,, \mathbf{b}\,, \mathbf{d}\,, y$ and z are similar to that explained in Section 8.4.2.1. The zero initial conditions obtained for $\mathbf{a}$ and $\mathbf{b}$ (as explained in Section 8.4.2.1) justify the use of $x^{(n-1)}(0)$ and $x^{(m-1)}(0)$ on the right hand sides of Equations (9.7b) and (9.7d) respectively.

Notice here that the initial conditions for first and second derivative of $x(t)$ in Equation (9.8) are chosen zero only to reduce the complexity of the series solution to be obtained in the following; our method will work for any other nonzero initial conditions also.

Series Solution using Laplace Transform

For comparison with numerics, we need an analytical (series) solution. The Laplace transform (see, e.g., [63]) of the solution to Equation (9.4), with Equation (9.8), is given by

$$X(s) = \left[x(0)\left(\frac{1}{s} + \frac{1}{s^{1+\alpha-\beta}}\right) + \frac{1}{s^{1+\alpha}}\right]\left[1 + s^{\beta-\alpha} + s^{-\alpha} + s^{-\gamma-\alpha}\right]^{-1}$$

Due to the special choice of initial conditions in Equation (9.8), the above expression for the Laplace transform is similar to that obtained in Section 8.4.2.1. Therefore by a procedure similar to that in Section 8.4.2.1, the series solution of Equation 9.4 is given by

$$x(t) = \sum_{n=0}^{\infty} \sum_{k=0}^{n} \sum_{l=0}^{k} \binom{n}{k} \binom{k}{l} (-1)^n \left[\frac{x(0)\, t^{\alpha\, n - \beta\, n + \beta\, k + l\, \gamma}}{\Gamma\left(1 + \alpha\, n - \beta\, n + \beta\, k + l\, \gamma\right)} \right.$$
$$\left. \frac{x(0)\, t^{-\beta + \alpha + \alpha\, n - \beta\, n + \beta\, k + l\, \gamma}}{\Gamma\left(1 - \beta + \alpha + \alpha\, n - \beta\, n + \beta\, k + l\, \gamma\right)} + \frac{t^{\alpha + \alpha\, n - \beta\, n + \beta\, k + l\, \gamma}}{\Gamma\left(1 + \alpha + \alpha\, n - \beta\, n + \beta\, k + l\, \gamma\right)} \right] \quad (9.9)$$

In the results presented below, we compare the numerical solution obtained using our DAE-based method with the numerical sum of the series of Equation (9.9), correctly truncated (as explained in Section 8.4.2.1) at some suitably large value.

Results

Numerical results are shown in Figure 9.2. The DAE-based solution matches the series solution (truncated at $n = 110$) in Equation (9.9) very well. Absolute error for $x(t)$ and $\dot{x}(t)$, over a fairly long time interval, is less than 0.2.

Figure 9.3 shows the results of the convergence study performed on the numerical solutions of Equation (9.4) with Equation (9.8). In Figure 9.3, top left plot is absolute error in $x(t)$ with 15 element Galerkin and top right with 30 element Galerkin, and bottom left plot is absolute error in $\dot{x}(t)$ with 15 element Galerkin and bottom right with 30 element Galerkin. A very good convergence is obtained for both $x(t)$ as well as $\dot{x}(t)$; the absolute error reduces by a factor of more than 20 when the number of finite elements used in Galerkin approximation are increased from 15 to 30.

We mention here that we also solved a nonlinear higher order multiterm FIE (results not presented here). The results of numerical solutions in this case were not as accurate as the linear case. Also, we did not obtain good convergence on increasing the refinement. We are not sure whether this is due to the nature of our formulation or an artifact of the DAE solver. We leave this question as the subject of future work.

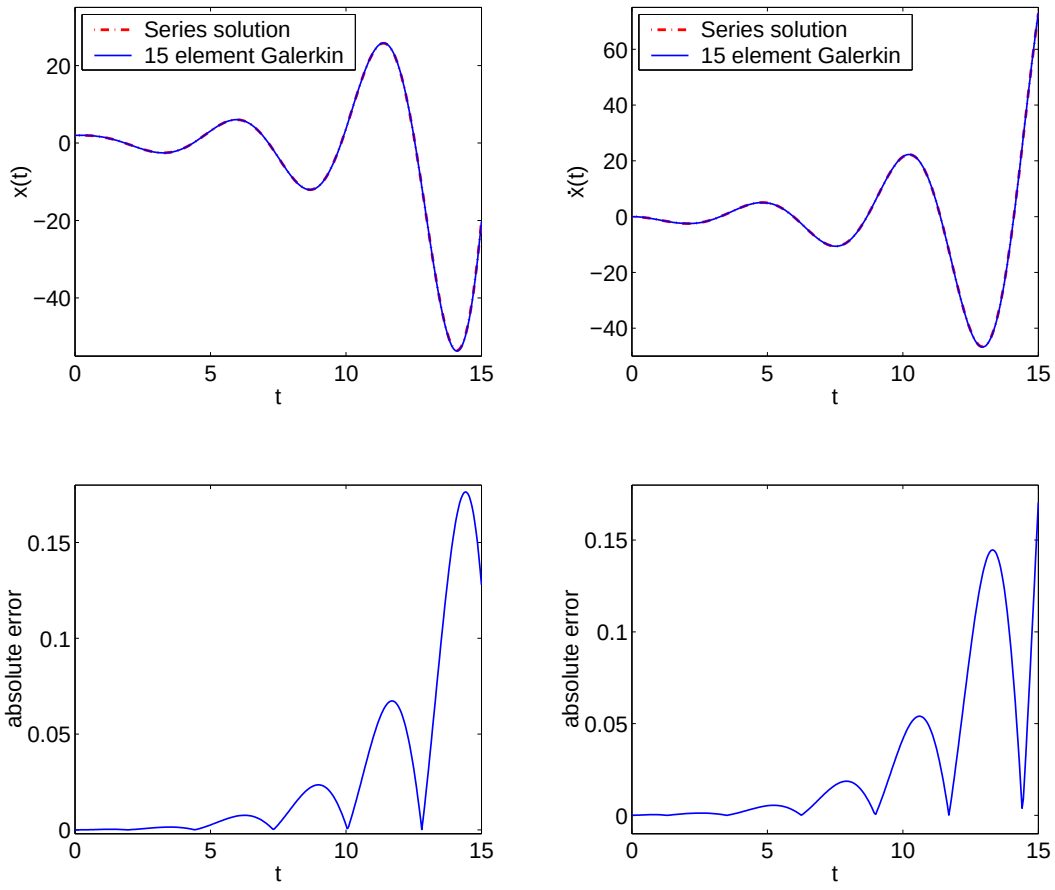

Figure 9.2: Top: numerical solution of Equation (9.4) for Equation (9.8). Bottom: error.

9.3 Discussion

The Galerkin approximation technique in the background of our DAE-based solution uses three matrices (**A**, **B** and **c**), as described in Chapters 6. For approximation of a fractional integral/derivative of a given order, using a given number of shape functions or finite elements (in our numerical work we used 15 elements), these matrices need be calculated only once. A MAPLE file for calculating these matrices is available on request (email: sjsingh@mecheng.iisc.ernet.in, anindya100@gmail.com).

When compared with the method of [59], our DAE-based method has the advantage of not requiring large systems of equations to be constructed when the derivative orders are incommensurate. We emphasize that, although the examples presented here use derivative orders that are simple rational numbers, our underlying Galerkin projection does *not* as-

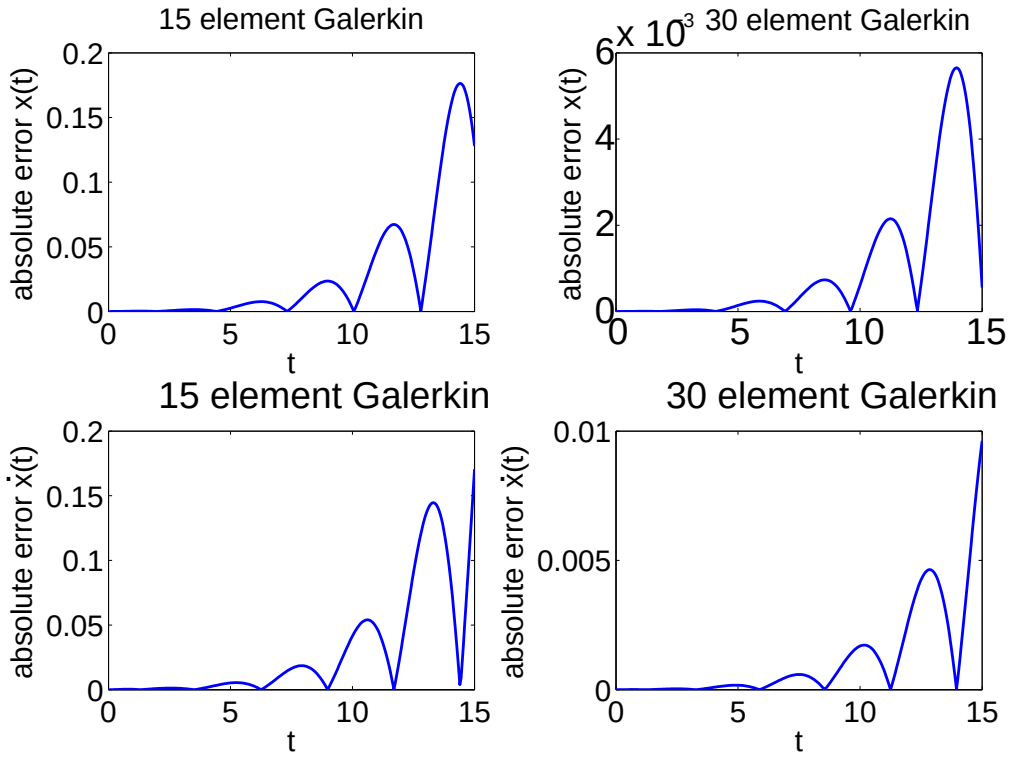

Figure 9.3: Convergence study for Equation (9.4) with Equation (9.8). Top: for $x(t)$. Bottom: for $\dot{x}(t)$.

sume that they are so, and so our method is indifferent to the question of whether or not the different orders of derivatives present have simple commensurate approximations. Also compared to [59], our method may be said to have the procedural advantage of constructing simple DAEs of manageable size; the fact that numerical solution of DAEs requires some sophistication is, from a user's point of view, peripheral because commercial packages like Matlab can handle such systems of equations. Our method works well for long times while series solutions [60] require more and more terms.

Finally, compared with the approximation of Oustaloup *et al.* [19], whose rational transfer function approximations imply multiple derivatives on both input and output sides, all our additional state variables are contained within the Galerkin approximation, with no higher integer order derivatives required (in time domain calculations) of the function whose fractional-order derivative is sought. We mention, however, that the approximation of [19] seems ideal for use in Matlab's SIMULINK, provided initial conditions are suitably

worked out (this aspect was pointed out by an anonymous reviewer).

In conclusion, we have presented a DAE-based method for numerically solving linear or nonlinear multiterm fractional integrodifferential equations with nonzero initial conditions. While we have numerically solved equations of a specific form in this work, it is clear that other, more general, forms can be tackled similarly. The level of error in the numerical solutions obtained has been seen to be small; moreover, refinement of the Galerkin projection based finite element calculation in the background can give larger sized matrices ($\mathbf{A}$, $\mathbf{B}$ and $\mathbf{c}$) but more accurate results, if desired.

Chapter 10

Conclusions

In this thesis we have studied the origin of fractional damping in disordered viscoelastic materials and developed a Galerkin based approximation technique for solving FDEs and FIEs.

We began by summarizing some of the theoretical treatments focused on understanding rubber viscoelasticity in Chapter 2. In particular, we aimed to understand the reasons behind the power law relaxation behavior of such materials.

In Chapter 3, we performed relaxation studies of disordered systems consisting of 1-D chains and 2-D networks of springs and dashpots. The damping coefficients of the dashpots were assumed to be randomly distributed. The special structure of stiffness and damping matrices allowed us to obtain analytical results for the 1-D chain. It was proved that the averaged potential energy of the chain follows a power law relaxation, which means that the closely spaced parallel relaxation processes give rise to a power law relaxation at the macroscopic level. The numerical simulations were also in agreement with the analytical results. Although analytical results were not possible for the 2-D case, numerical simulations show the power law relaxation in this case also.

In Chapter 4, we made a further simplification in the system by assuming a random system coefficient matrix. Numerical results of the relaxation study of this system also showed a power law decay. The analytical solution obtained in this case also showed a power law relaxation, giving further support to the numerical results.

In Chapter 5, we identified an infinite dimensional system which is equivalent to the fractional order derivative or integral. We then developed a Galerkin projection based finite dimensional approximation scheme for fractional order derivatives. We used global shape functions for the Galerkin projections. This resulted in significant reduction in computational costs. For demonstration of the working of this scheme, we solved a linear as well as nonlinear fractional differential equation of order two.

In Chapter 6, we used finite elements for the Galerkin approximation scheme developed in the previous chapter. The finite element based discretization strategy is improved in a few steps until, finally, very good performance is obtained over a user-specifiable frequency range (not including zero).

In Chapter 7, we have identified three classes of FDEs that are amenable to solution using a new Galerkin approximation for the fractional order derivative, that was developed in Chapters 5 and 6. To showcase the effectiveness of the approximation technique, we have used linear FDEs which could also be solved analytically (if only in the form of power series). However, more general and nonlinear problems which are impossible to solve analytically are also expected to be equally effectively solved using this approximation technique.

In Chapter 8, we have presented a DAE-based method for numerically solving linear or nonlinear multiterm fractional integrodifferential equations with nonzero initial conditions. The order of the fractional derivatives and integrals was chosen between 0 and 1. The level of error in the numerical solutions obtained has been seen to be small. A convergence study for the nonlinear case was also performed. A very significant reduction in the absolute error was obtained; the error reduced by a factor of 20 upon doubling the number of elements used in the underlying Galerkin projections.

In Chapter 9, we have extended the applicability of our DAE-based method to include multiterm fractional integrodifferential equations and fractional differential equations with fractional derivatives of higher orders. The system was assumed to start from nonzero initial conditions. The magnitude of the error in the numerical solutions obtained has been seen to be small for the linear case. A convergence study performed for the linear case showed a significant reduction in the absolute error; again the error reduced by a factor of more than 20 upon doubling the number of elements used in the underlying Galerkin projections. However, similar accuracy and convergence was not obtained for a nonlinear

problem. We do not understand whether this is due to the nature of our formulation or it is an artifact of the DAE solver. We leave answering this question for future work.

Appendix A

System Matrices

The matrices described in Section 5.5 are given below for $n = 7$. We present these for verification by readers implementing the calculation, not direct use. Users are advised to calculate the elements of these matrices to more digits of precision.

$$\mathbf{A} = \begin{bmatrix} 0.3836 & 0.5094 & -0.1495 & 0.3400 & -0.1403 & 0.2400 & -0.1048 \\ 0.5094 & 1.0663 & -0.8553 & 0.7806 & -0.6667 & 0.5728 & -0.4899 \\ -0.1495 & -0.8553 & 1.8469 & -1.5220 & 1.3534 & -1.1565 & 1.0063 \\ 0.3400 & 0.7806 & -1.5220 & 2.4197 & -2.0119 & 1.7869 & -1.5487 \\ -0.1403 & -0.6667 & 1.3534 & -2.0119 & 2.8532 & -2.4040 & 2.1533 \\ 0.2400 & 0.5728 & -1.1565 & 1.7869 & -2.4040 & 3.2196 & -2.7512 \\ -0.1048 & -0.4899 & 1.0063 & -1.5487 & 2.1533 & -2.7512 & 3.5533 \end{bmatrix},$$

$$\mathbf{B} = \begin{bmatrix} 0.3836 & 1.1486 & -2.0856 & 2.8635 & -3.5233 & 4.0857 & -4.5792 \\ 1.1486 & 3.4909 & -6.4706 & 8.9340 & -11.0176 & 12.7999 & -14.3592 \\ -2.0856 & -6.4706 & 12.4249 & -17.4881 & 21.7339 & -25.3767 & 28.5574 \\ 2.8635 & 8.9340 & -17.4881 & 25.2248 & -31.8473 & 37.4914 & -42.4180 \\ -3.5233 & -11.0176 & 21.7339 & -31.8473 & 40.9823 & -48.8886 & 55.7325 \\ 4.0857 & 12.7999 & -25.3767 & 37.4914 & -48.8886 & 59.2233 & -68.2649 \\ -4.5792 & -14.3592 & 28.5574 & -42.4180 & 55.7325 & -68.2649 & 79.6822 \end{bmatrix},$$

and

$$\mathbf{c} = \begin{bmatrix} 1.0708 \\ 2.4137 \\ -3.1911 \\ 4.2328 \\ -4.6777 \\ 5.3009 \\ -5.6135 \end{bmatrix}.$$

The system matrices obtained using α-dependent mapping in Section 6.4 are given below for $n = 7$.

$$\mathbf{A} = \begin{bmatrix} 1.3822\text{e}{-1} & 2.3129\text{e}{-2} & 0 & 0 & 0 & 0 & 0 \\ 2.3129\text{e}{-2} & 1.0951\text{e}{-1} & 2.8911\text{e}{-2} & 0 & 0 & 0 & 0 \\ 0 & 2.8911\text{e}{-2} & 1.7846\text{e}{-1} & 5.4390\text{e}{-2} & 0 & 0 & 0 \\ 0 & 0 & 5.4390\text{e}{-2} & 2.7544\text{e}{-1} & 1.0044\text{e}{-1} & 0 & 0 \\ 0 & 0 & 0 & 1.0044\text{e}{-1} & 4.7224\text{e}{-1} & 1.7158\text{e}{-1} & 0 \\ 0 & 0 & 0 & 0 & 1.7158\text{e}{-1} & 9.4760\text{e}{-1} & 3.0324\text{e}{-1} \\ 0 & 0 & 0 & 0 & 0 & 3.0324\text{e}{-1} & 2.0920 \end{bmatrix},$$

$$\mathbf{B} = \begin{bmatrix} 1.3765\text{e}{-4} & 9.2261\text{e}{-5} & 0 & 0 & 0 & 0 & 0 \\ 9.2261\text{e}{-5} & 1.8197\text{e}{-3} & 9.6345\text{e}{-4} & 0 & 0 & 0 & 0 \\ 0 & 9.6345\text{e}{-4} & 1.8634\text{e}{-2} & 1.1022\text{e}{-2} & 0 & 0 & 0 \\ 0 & 0 & 1.1022\text{e}{-2} & 1.5438\text{e}{-1} & 1.1486\text{e}{-1} & 0 & 0 \\ 0 & 0 & 0 & 1.1486\text{e}{-1} & 1.3348 & 1.1040 & 0 \\ 0 & 0 & 0 & 0 & 1.1040 & 1.4873\text{e}1 & 1.1838\text{e}1 \\ 0 & 0 & 0 & 0 & 0 & 1.1838\text{e}1 & 3.0839\text{e}2 \end{bmatrix},$$

and

$$\mathbf{c} = \begin{bmatrix} 1.6135\text{e}{-1} \\ 1.6155\text{e}{-1} \\ 2.6176\text{e}{-1} \\ 4.3027\text{e}{-1} \\ 7.4426\text{e}{-1} \\ 1.4224 \\ 3.7947 \end{bmatrix}.$$

Appendix B

Further Results from Section 6.3

Some of the results following the discussion of Section 6.3 are presented below.

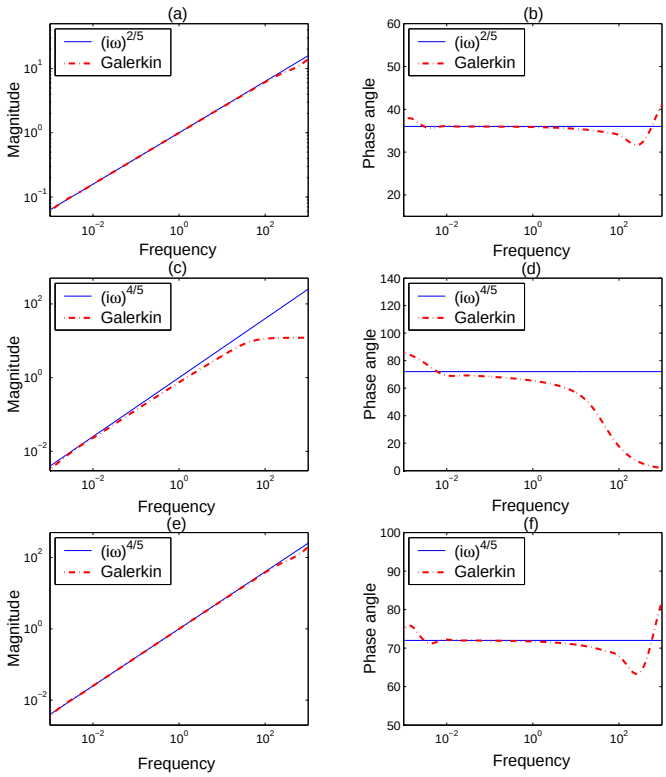

Figure B.1: Magnitude and phase angle comparison in FRFs. Plots (a) and (b): 15 hat elements and $\alpha = 2/5$. Plots (c) and (d): 15 hat elements and $\alpha = 4/5$. Plots (e) and (f): 15 hat elements and two successive derivatives of order 2/5 to achieve $\alpha = 4/5$.

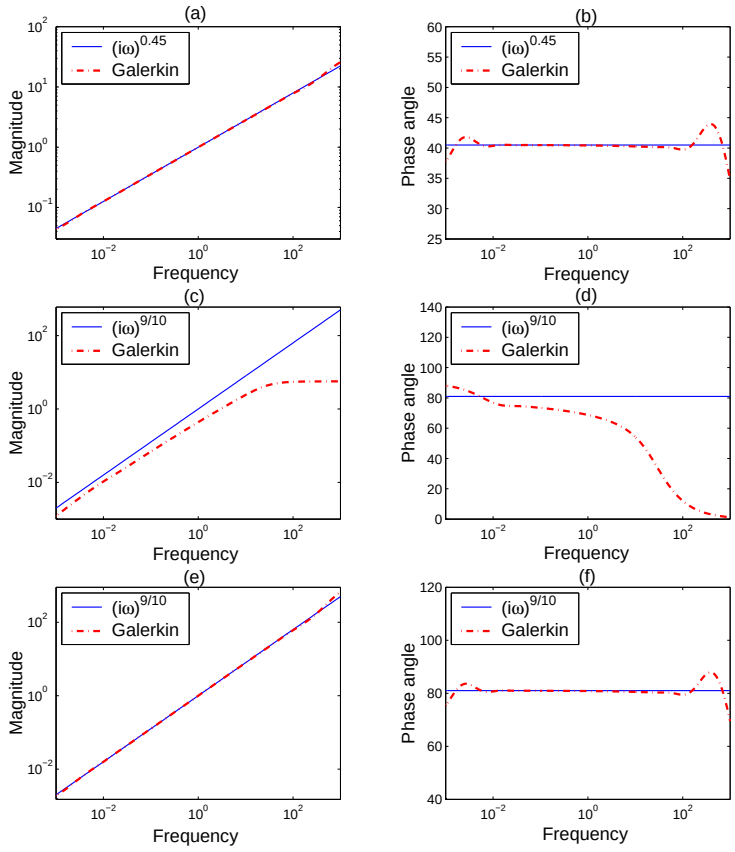

Figure B.2: Magnitude and phase angle comparison in FRFs. Plots (a) and (b): 15 hat elements and $\alpha = 0.45$. Plots (c) and (d): 15 hat elements and $\alpha = 0.9$. Plots (e) and (f): 15 hat elements and two successive derivatives of order 0.45 to achieve $\alpha = 0.9$.

References

[1] Debnath L (2003) Recent Applications of Fractional Calculus to Science and Engineering. International Journal of Mathematics and Mathematical Sciences, 2003(54):3413–3442.

[2] Torvik PJ, Bagley RL (1984) On the Appearance of the Fractional Derivative in the Behavior of Real Materials. Journal of Applied Mechanics, 51:294–298.

[3] Bagley RL, Torvik PJ (1983) A Theoretical Basis for the Application of Fractional Calculus to Viscoelasticity. Journal of Rheology, 27(3):201–210.

[4] Bagley RL, Torvik PJ (1986) On the Fractional Calculus Model of Viscoelastic Behavior. Journal of Rheology, 30(1):133–155.

[5] Bagley RL (1988) Power Law and Fractional Calculus Model of Viscoelasticity. AIAA Journal, 27(10):1412–1417.

[6] Bagley RL, Torvik PJ (1983) Fractional Calculus: A Different Approach to the Analysis of Viscoelastically Damped Structures. AIAA Journal, 21(5):741–748.

[7] Bagley RL, Torvik PJ (1985) Fractional Calculus in the Transient Analysis of Viscoelastically Damped Structures. AIAA Journal, 23(6):918–925.

[8] Gaul L, Klein P, Kempfle S (1989) Impulse Response Function of an Oscillator with Fractional Derivative in Damping Description. Mechanics Research Communications, 16(5):297–305.

[9] Makris N (1991) Fractional Derivative Model for Viscous Damper. ASCE Journal of Structural Engineering, 117:2708–2724.

[10] Mainardi F (1996) Fractional Relaxation-oscillation and Fractional Diffusion-wave Phenomena. Chaos, Solitons & Fractals, 7(9):1461–1477.

[11] Moreau X, Ramus-Serment C, Oustaloup A (2002) Fractional Differentiation in Passive Vibration Control. Nonlinear Dynamics, 29(1-4):343–362.

[12] Agrawal OP (2006) Fractional Variational Calculus and the Transversality Conditions. Journal of Physics A: Mathematical and General, 39:10375–10384.

[13] Agrawal OP (2007) Fractional Variational Calculus in Terms of Riesz Fractional Derivatives. Journal of Physics A: Mathematical and General, 40:6287–6303.

[14] Podlubny I, Petras I, Vinagre BM, Chen Y, O'Leary P, Dorcak L (2003) Realization of Fractional Order Controllers. Acta Montanistica Slovaca, 8(4):233–235.

[15] Chen Y, Moore KL (2001) On D^{α}-type Iterative Learning Control. In Proceedings of the 40th IEEE Conference on Decision and Control, 4451–4456.

[16] Basset AB (1910) On the Descent of a Sphere in a Viscous Liquid. Quarterly Journal of Pure and Applied Math, 41:369–381.

[17] Mainardi F, Pironi P, Tampieri F (1995) On a Generalization of Basset Problem via Fractional Calculus. In: Proceedings CANCAM 95.

[18] Koh CG, Kelly JM (1990) Application of Fractional Derivative to Seismic Analysis of Base-isolated Models. Earthquake Engineering and Structural Dynamics 19:229–241.

[19] Oustaloup A, Levron F, Mathieu B, Nanot FM (2000) Frequency-Band Complex Non-integer Differentiator: Characterization and Synthesis. IEEE Transactions on Circuits and Systems I: Fundamental Theory and Applications, 47(1):25–39.

[20] Grigolini P, Rocco A, West BJ (1999) Fractional Calculus as a Macroscopic Manifestation of Randomness. Physical Review E, 59(3):2603–2613.

[21] Kalmykov YP, Coffey WT, Crothers DSF, Titov SV (2004) Microscopic Models for Dielectric Relaxation in Disordered Systems. Physical Review E, 70(041103):1–11.

[22] Wahi P, Chatterjee A (2004) Averaging Oscillations with Small Fractional Damping and Delay Terms. Nonlinear Dynamics, 38(1-2):3–22.

[23] Mirevskiu SP, Boyadjiev L, Scherer R (2007) On the Riemann-Liouville Fractional Calculus, g-Jacobi Functions and F-Gauss Functions. Applied Mathematics and Computation, 187:315–325.

[24] Surguladze TA (2002) On Certain Applications of Fractional Calculus to Viscoelasticity Journal of Mathematical Sciences, 112(5):4517–4557.

[25] Carpinteri A, Mainardi F (1997) *Fractals and Fractional Calculus in Continuum Mechanics.* Springer Verlag, New York.

[26] Treloar LRG (1975) *The Physics of Rubber Elasticity.* Clarendon, Oxford.

[27] Green MS, Tobolsky Av (1946) A New Approach to the Theory of Relaxing Polymeric Media. The Journal of Chemical Physics, 14(2):80–92.

[28] Bird RB, Armstrong RC, Hassager O (1988) *Dynamics of Polymeric Liquids Volume 2: Kinetic Theory.* John Wiley and Sons, New York.

[29] Jongschaap RJJ (1990) Microscopic Modelling of the Flow Properties of Polymers. Reports on Progress in Physics, 53:1–55.

[30] Doi M, Edwards SF (1986) *The Theory of Polymer Dynamics.* Oxford University Press, New York.

[31] De Gennes PG (1971) Reptation of a Polymer Chain in the Presence of Fixed Obstacles. The Journal of Chemical Physics, 55(2):572–579

[32] Doi M, Edwards SF (1978) Dynamics of Rod-like Macromolecules in Concentrated Solution. Part 1 Journal of the Chemical Society, Faraday Transactions 2, 74:560–570.

[33] Doi M, Edwards SF (1978) Dynamics of Concentrated Polymer Systems. Part 2—Molecular Motion Under Flow Journal of the Chemical Society, Faraday Transactions 2, 74:1802–1817.

[34] Rouse EP (1953) A Theory of the Linear Viscoelastic Properties of Dilute Solutions of Coiling Polymers. The Journal of Chemical Physics, 21(7):1272–1280.

[35] Thirion P, Chasset R (1970) Recent Observations on the Mechanical Properties of Polymer Networks. Pure and Applied Chemistry, 23:183–199.

[36] Huber DL (1985) Statistical Model for Stretched Sxponential Relaxation in Macroscopic Systems. Physical Review B, 31(9):6070–6071.

[37] Huber DL (1996) Dynamical Model for Stretched Exponential Relaxation in Solids. Physical Review E (53):6544–6546.

[38] Vlad MO, Schönfisch B, Mackey MC (1996) Fluctuation-dissipation Relations and Universal Behavior for Relaxation Processes in Systems with Static Disorder and in the Theory of Mortality. Physical Review E, 53(5):4703–4710.

[39] Vlad MO, Metzler R, Ross J (1998) Generalized Huber Kinetics for Nonlinear Rate Processes in Disordered Systems: Nonlinear Analogs of Stretched Exponentials. Physical Review E, 57(6):6497–6505.

[40] Cook RD (1994) *Finite Element Modeling for Stress Analysis.* John Wiley & Sons New York.

[41] Singh SJ, Chatterjee A (2007) Fractional Damping: Statistical Origins and Galerkin Projections. Advances in Fractional Calculus: Theoretical Developments and Applications in Physics and Engineering 389–402. Springer, Dordrecht, The Netherlands.

[42] Chatterjee A (2005) Statistical Origins of Fractional Derivatives in Viscoelasticity. Journal of Sound and Vibration, 284:1239–1245, 2005.

[43] Finlayson BA (1972) *The Method of Weighted Residuals and Variational Principles.* Academic Press.

[44] Singh SJ, Chatterjee A (2006) Galerkin Projections and Finite Elements for Fractional Order Derivatives. Nonlinear Dynamics, 45(1-2):183–206.

[45] Suarez LE, Shokooh A (1997) An Eigenvector Expansion Method for the Solution of Motion Containing Fractional Derivatives. ASME Journal of Applied Mechanics, 64(3):629–635.

[46] Chen Y, Vinagre MB, Podlubny I (2004) Continued Fraction Expansion Approaches to Discretizing Fractional Order Derivatives–An Expository Review. Nonlinear Dynamics, 38(1-2):155–170.

[47] Samko SG, Kilbas AA, Marichev OI (1993) *Fractional Integrals and Derivatives: Theory and Applications.* Gordon and Breach, Amsterdam.

[48] Oldham KB (1974) *The Fractional Calculus.* Academic Press, New York.

[49] Podlubny I (1999) *Fractional Differential Equations.* Academic Press, San Diego, CA.

[50] Shinozuka M (1972) Monte Carlo Solution of Structural Dynamics. Computers and Structures, 2(5-6):855–874.

[51] Yuan L, Agrawal OP (2002) Numerical Scheme for Dynamic Systems Containing Fractional Derivatives. Journal of Vibration and Acoustics, 124:321-324.

[52] Ford NJ, Simpson AC (2001) The Numerical Solution of Fractional Differential Equations: Speed Versus Accuracy. Numerical Algorithms, 26:333–346.

[53] Schmidt A, Gaul L (2006) On a Critique of a Numerical Scheme for the Calculation of Fractionally Damped Dynamical Systems. Mechanics Research Communications, 33(1):99–107.

[54] Ogata K (1998) *System Dynamics.* Prentice Hall, New Jersey.

[55] Singh SJ, Chatterjee A (2007) Three Classes of FDE's Amenable to Approximation Using a Galerkin Technique. Advances in Fractional Calculus: Theoretical Developments and Applications in Physics and Engineering 3–14. Springer, Dordrecht, The Netherlands.

[56] Fryba L (1970) *Vibration of Solids and Structures Under Moving Loads.* Noordhoff International Publishing, The Netherlands.

[57] Zemanian AH (1965) *Distribution Theory And Transform Analysis.* McGraw Hill, New York.

[58] Hairer E, Wanner G (1991) *Solving Ordinary Differential Equations II: Stiff and Differential Algebraic Problems.* Springer, Berlin.

[59] Diethelm K, Ford NJ (2004) Multi-order Fractional Differential Equations and their Numerical Solution. Applied Mathematics and Computations, 154:621–640.

[60] Momani S (2006) A Numerical Scheme for the Solution of Multi-order Fractional Differential Equations. Applied Mathematics and Computation, 182:761–770.

[61] Caputo M (1967) Linear Models of Dissipation Whose Q is Almost Frequency Independent, Part II. Geophys. J. R. Astr. Soc., 13:529–539.

[62] Ortigueira MD (2003) On the Initial Conditions in Continuous-time Fractional Linear Systems. Signal Processing, 83:2301–2309.

[63] Doetsch G (1974) *Introduction to the Theory and Application of the Laplace Transformation.* Springer Verlag, New York.